New aspects of star cluster physics

Dissertation

zur

Erlangung des Doktorgrades (Dr. rer. nat)

der

Mathematisch-Naturwissenschaftlichen Fakultät

der

Rheinischen Friedrich-Wilhelms-Universität Bonn

vorgelegt von
Jan Pflamm-Altenburg
aus
Kiel

Bonn
November, 2009

Angefertigt mit Genehmigung der Mathematisch-Naturwissenschaftlichen Fakultät der
Rheinischen Friedrich-Wilhelms-Universität Bonn

1. Gutachter Prof. Dr. Pavel Kroupa
2. Gutachter Prof. Dr. Norbert Langer

Tag der Promotion: 09. Juni 2010
Erscheinungsjahr 2010

Summary

Star clusters are the birth-sites of both low- and high-mass stars and can be considered to be the building blocks of galaxies. Therefore, the understanding of the formation, evolution, and death of star clusters is of fundamental importance for the understanding of galaxy evolution. This thesis focuses on several new aspects of star cluster physics: For a long time the stellar populations of star clusters were believed to be single aged populations. But recent observations have cast a doubt on this simple picture. Based on these observations this thesis shows that i) the capture of older field stars during star cluster formation can mimic apparently prolonged star formation, and that ii) gas accretion by massive star clusters can account for multiple stellar populations. Because massive stars are, despite their short life times of only a few Myr, the driving engines for galactic evolution, the process which releases them from the star clusters to the galactic field must be understood. This is problem iii) addressed in this thesis: iiia) The decay of few-body groups of massive stars formed in star clusters, iiib) a new ejection process combining the dynamical and the supernova ejection process of massive stars, and iiic) the large scale dispersion of massive stars.

Preface

The individual topics covered by my recent work can be broadly divided into two classes, both related to star clusters: i) aspects which deal with single star clusters, and ii) problems which consider the galaxy-wide stellar population composed of all stars in all star clusters. The PhD project started originally with the analysis of the dynamical evolution of compact few-body groups of massive stars in individual star clusters. This work then lead me directly to related problems of single star clusters. Therefore only these topics are part of my thesis which deal with dynamical and individual star cluster issues. Parallely I contributed to the IGIMF-theory which describes the galaxy-wide population of young stars being born in star clusters in a whole galaxy. My IGIMF work is, however, not part of this thesis.

The thesis is organised as follows: In Chapter 1 an introduction and overview is provided on the topics covered by this thesis as well as their relation to my IGIMF work.

Chapters 2–5 present my work which is already published (Chapter 2–4) or submitted (Chapter 5). These Chapters consist of published or submitted papers and therefore some parts may be redundant.

Chapter 2 is based on Pflamm-Altenburg & Kroupa, "*A highly abnormal massive star mass function in the Orion Nebula cluster and the dynamical decay of trapezium systems*", (2006, MNRAS, 373, 295) and analyses the OB-star content of the ONC and the dynamical stability of the ONC-Trapezium.

Chapter 3 is based on Pflamm-Altenburg & Kroupa, "*Captured older stars as the reason for apparently prolonged star formation in young star clusters*", (2007, MNRAS, 375, 855) and shows that the observed fraction of much older low-mass stars in the ONC must not necessarily imply a long star formation time scale in young star clusters, but may be due to captured older stars.

Chapter 4 is based on Pflamm-Altenburg & Kroupa, "*Recurrent gas accretion by massive star clusters, multiple stellar populations and mass thresholds for spheroidal stellar systems*", (2009, MNRAS, 397, 488) and reveals, for the first time, a mass threshold of 10^6 $M_\odot$ above which star clusters may be able to accrete gas from the surrounding interstellar medium.

Chapter 5 is based on Pflamm-Altenburg & Kroupa, "*Two step ejection of massive stars and the issue of their formation in isolation*", (2009, MNRAS, submitted) in which

the combination of the dynamical and supernova ejection scenario of massive stars is investigated for the first time to my knowledge.

Chapters 6–8 deal with started work which is not yet submitted to any journal. These are collected in the outlook part:

Chapter 6 describes the application of the field-star capture process of Chapter 3 to the most massive young star cluster in the Local Group, R136 in the LMC.

Chapter 7 introduces a formalism to describe primordial mass segregation and how to analyse its effect on the evolution of an apparent IMF in young massive star clusters during gas expulsion.

Chapter 8 extends the work on the ejection mechanism of massive stars from star clusters and emphasises its importance for galaxy evolution.

The papers have been edited by merging their list of references with the references of the outlook chapters.

The work covered in this thesis has been published in three papers. One additional paper is submitted. My IGIMF work has been published in four papers in three different journals (MNRAS, ApJ, and Nature), while one further paper has been submitted. In total, seven first-author papers have been published during the PhD phase and two others have been submitted and are being reviewed. A list of all published and submitted papers as well as papers which are in preparation can be found on p. 115.

A list of all my national and international conference participations with oral and poster contributions and press releases that have resulted from my work are presented on p. 117.

The appendix summarises the practical numerical formulation of the IMF and the man-pages of the IMF-library and the CATENA code developed by me and published in Pflamm-Altenburg & Kroupa (2006).

Bonn, November 2009 Jan Pflamm-Altenburg

Contents

List of Figures

List of Tables

Chapter 1

Overview and introduction

Stars do not form uniformly distributed over the entire star forming galaxy, but are confined to small regions within galaxies building more or less compact spheroidal configurations, which we call star clusters. They are the birth places of massive stars which are, despite their short life times, the driving engines of the chemical and energetic evolution of the inter-stellar medium (ISM). In order to understand the evolution of the ISM of galaxies we therefore need to understand how the massive stars are distributed.

Star clusters exist with quite different masses ranging from a few solar masses (the solar mass is 1 $M_{\odot}$=1.989 $\times$ 10^{30} kg), like the very young Taurus Auriga systems which contain only low-mass stars ($\leq$1 $M_{\odot}$), up to 10^5 $M_{\odot}$ such as the most massive star-forming young star cluster in the Local Group, R136 in the LMC, or even exceeding 10^6 $M_{\odot}$ in the case of a few Galactic or extra-galactic Globular star clusters which are believed to be the remnants of ancient star burst phases.

Massive star-forming star clusters are rare but as they are the most luminous types of star clusters they are observationally accessible up to large distances. Low-mass star clusters like Taurus Auriga type systems are by far dominating in number, but because they do not host luminous O- and B-type stars they can only be observed easily in the solar neighourhood. However, observational data of the formation of low-mass and high-mass stars are required to obtain a complete understanding of the star formation process on local sub-parsec scales (1 pc = 3.086 $\times$ 10^{16} m) and its importance for the evolution of whole galaxies.

THE ONC

One of the best objects to study the process and the conditions of low-mass and high-mass star formation is the Orion Nebula cluster (ONC), a young star cluster with an age of about 1 Myr which is only $\approx$470$\pm$90 pc away from us (Hillenbrand, 1997). The observed total stellar mass within a radius of $\approx$2 pc around its centre is about 1800 $M_{\odot}$ (Hillenbrand, 1997; Hillenbrand & Hartmann, 1998). This is roughly 40 per cent of its

viral mass of 4500 $M_\odot$. The presence of both high- and low-mass stars and its close vicinity makes it an ideal object for testing theoretical results and predictions.

For example, pioneering theoretical work on the process of early gas expulsion due to the feedback by massive stars and the subsequent expansion of a star cluster has been successfully tested by comparing the ONC with the 150 Myr old and dynamically evolved open star cluster, the Pleiades, on the basis of extensive numerical simulations (Kroupa, Aarseth, & Hurley, 2001). The theoretically expected influence of the external destruction of protoplanetary discs and the observed properties of protoplanetary discs can be well compared in the ONC (Olczak et al., 2008).

Furthermore, as the ONC is still a compact young star cluster with massive stars it is an ideal test object to study the dynamics of OB-star groups, which are not observed in the Galactic field but in young star clusters.

THE TRAPEZIUM SYSTEM AND ITS STABILITY (CHAP. 2)

Four massive OB-stars are found at the centre of the ONC. They form a trapezium-like, non-hierarchical four-body system, thus it is called the ONC-Trapezium. Its total mass is about 90 $M_\odot$ (Pflamm-Altenburg & Kroupa, 2006) and has a diameter of approximately 10000 AU (1 AU = earth–sun distance) in projection (Hillenbrand, 1997).

Given a spherically symmetric mass distribution of the ONC, the dynamical behaviour of the central Trapezium is not influenced by the gravitational forces of those parts of the ONC outside the Trapezium. Thus the Trapezium forms a compact few-body subsystem consisting of massive stars at the ONC centre. Assuming that the Trapezium is in local viral equilibrium then the corresponding crossing-time of the Trapezium is about 13000 yr (Pflamm-Altenburg & Kroupa, 2006).

Extensive calculations have shown that *a non-hierarchical few-body system decays in a few crossing-times* (e.g. Sterzik & Durisen, 1998). It follows that for an assumed age of a about 1 Myr the ONC Trapezium should have totally decayed by now (Kroupa, 2004). The implication of this is that to understand the distribution of massive stars in galaxies, we need to not only know how the star clusters are distributed, but we also need to understand the dynamical processes in their birth clusters.

N-BODY SIMULATIONS - TWO APPROACHES

In order to explore theoretically the expected instability of the ONC-Trapezium Monte-Carlo simulations of few-body systems have to be carried out. For dynamical simulations of N-body systems which consist of single stars, many different algorithms have been developed. Despite of the variety and manifoldness of available methods, the set of algorithms can be divided into two main classes:

i) The first class of algorithms are based on a *spatial stellar field* approximation. The stars are treated to constitute a smooth matter distribution. The forces on individual

stars are calculated by the gradient of the smooth overall gravitational potential derived from the Poisson equation. The advantage of this method is that it saves computational time especially for very large N-systems. On the other hand the discretisation of the gravitational potential is lost and processes as for example the deflections of stars during close fly-bys and sling-shots of stars can not be treated.

ii) The second class of N-body-algorithms are based on the direct integration of the Newtonian equations of motion, in which the total force on individual stars is the sum of all gravitational forces exerted by all other stars. Thus the number of force evaluations increases quadratically with the number of stars. Although this is the most accurate method it can only be applied to large N-systems (e.g. N=10^5 for Globular clusters) with enormous computational effort, requiring not only special software but also special hardware.

To decide whether the accurate direct N-body approach has to be applied to a particular N-body problem or whether instead the more efficient field approach can be used, the two-body relaxation time scale, $t_{\rm relax}$, can be estimated to determine whether the particular N-body system evolves collisionally or collisionless over the physical time scale considered. Following Binney & Tremaine (1987, p. 190) the two-body relaxation time of an N-body system can be roughly calculated by

$$t_{\rm relax} = \frac{N}{8\ \ln N}\ t_{\rm cross}\ , \tag{1.1}$$

where $t_{\rm cross}$ is the crossing time of the N-body system. The two-body relaxation time is, basically, the time-scale on which energy-equipartition significantly changes the structure of the stellar system.

The ONC-Trapezium consists of four very tight OB-star systems and its crossing time is about 13000 yr (Pflamm-Altenburg & Kroupa, 2006) and the corresponding formal relaxation time is about 4700 yr, roughly two orders of magnitude shorter than its estimated age. Thus, to investigate the dynamical evolution of a few-body system like the ONC-Trapezium, the direct N-body method has to be chosen.

CATENA - A FEW-BODY INTEGRATOR (APP. A)

On first sight the direct integration of the Newtonian equations of motion of a few-body system should not impose any problem. A four-body system like the ONC-Trapezium requires the integration of 4×3=12 coupled ordinary differential equations of second order, corresponding to 2×12=24 coupled ordinary differential equations of first order. But close encounters are a serious challenge for direct integration attempts:

If two stars approach each other then they are accelerated and the time scale of their close fly-by or close encounter is very much shorter than the time scale of the overall dynamics of the whole N-body system. Thus, during the encounter the close two-body sub-system can be considered as an un- or very-weakly-perturbed two-body system and

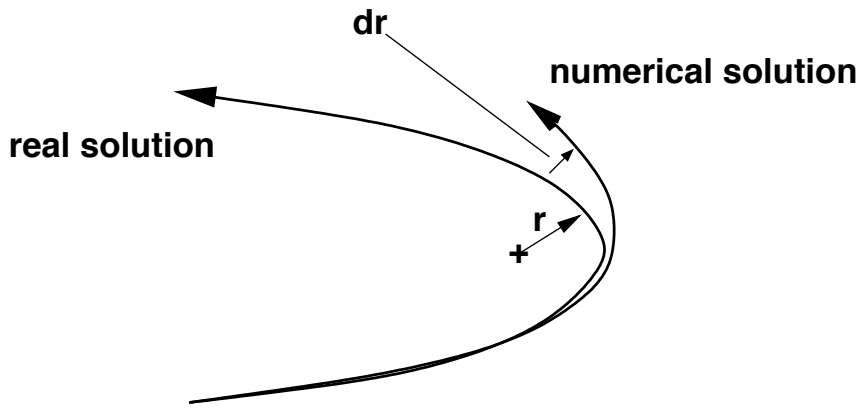

Figure 1.1: Divergence of the numerical solution from the true solution in case of an eccentric close encounter of two stars.

the total energy, E, of this two-body system is nearly conserved during the encounter. The total energy, E, of the close encounter is then given by

$$E = \frac{\mu}{2}\, v^2 - G\, \frac{m_1\, m_2}{r}\ , \tag{1.2}$$

where m_1 and m_2 are the masses of the interacting bodies, r and v are the distance and the relative velocity, and $\mu = m_1 m_2/(m_1 + m_2)$ is the reduced mass.

In the case of a highly eccentric encounter the curvature of the trajectory is large (Fig. 1.1). If the curvature of the true solution increases the Taylor-series coefficients of the true solution have to be matched up to higher orders by the numerical integration method in order to keep the displacement to the true solution small. This requires very small time steps, making normal integration methods for highly eccentric encounters inefficient. Parallely, the incompleteness of the numerical integration scheme leads to a displacement of dr from the true solution. Then the error in the energy is given by

$$dE = \mu\, v\, dv + G\, \frac{m_1\, m_2}{r^2}\, dr\ . \tag{1.3}$$

Although the total energy should be constant during the close encounter, the energy error becomes large in the case of a highly eccentric (large dr) and close (small r) encounter. The system then normally artificially gains energy. Commonly, close bound binaries can be artificially disrupted without any physical reasons.

The Kepler-potential ($\Phi \propto r^{-1}$) is not the only one which has closed orbits. The potential of the harmonic oscillator ($\Phi \propto r^2$) also allows closed orbits. The total energy of the harmonic oscillator is given by

$$E = \frac{\mu}{2}\, v^2 + \frac{k}{2}\, r^2\ . \tag{1.4}$$

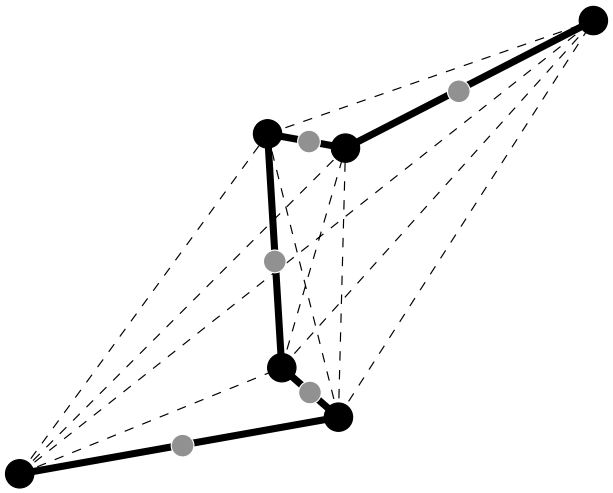

Figure 1.2: All stars (black filled circles) are arranged in a chain (thick solid lines), including the most dominant interactions. Each two-body *chain-interaction* is regularised by a KS-transformation representing a *virtual harmonic oscillator particle* (grey filled circles). The distances of all other gravitational interactions (dashed lines) are expressed as a vectorial sum of the chain-interactions.

A small displacement from the true solution thus leads to an energy error of

$$dE = \mu\ v\ dv + k\ r\ dr\ , \tag{1.5}$$

and the integration of a harmonic oscillator does not suffer from the same integration problems as the Kepler orbit.

As both potentials lead to closed orbits both solutions can be mapped onto each other using analytic space and time transformations. This has been shown by Kustaanheimo & Stiefel (1965), and these kinds of transformations are today called KS-transformations. The process which maps the Kepler-orbit onto the harmonic oscillator orbit is called *regularisation*.

The regularisation method of the two-body problem has been further developed to handle the few-body problem where the same numerical integration problems exist. One very sophisticated method is the so-called *chain-regularisation* (Mikkola & Aarseth, 1990, 1993). In this regularisation procedure all stars are arranged in a chain (Fig. 1.2) including the most dominant interactions. These interactions are then regularised by KS-transformations.

To use the chain-regularisation method for the theoretical exploration of the dynamical decay of the ONC-Trapezium the Catena code has been developed as part of this thesis (App.A), and is publicly available[1].

[1] `http://www.astro.uni-bonn.de/~webaiub/german/downloads.php`

THE ONC-TRAPEZIUM DECAY (CHAP. 2)

To dynamically evolve the ONC-Trapezium the CATENA code has been used to perform Monte-Carlo simulations. 1000 configurations consisting of four particles with the masses of the four Trapezium OB-stars have been set up. The initial positions are uniformly distributed over a sphere with 0.05 pc in diameter (in accord with observations). The velocities are drawn from a Gaussian distribution with a velocity dispersion corresponding to viral equilibrium. A trapezium system with four stars within a sphere of 0.05 pc diameter will survive for 0.5 Myr only with a probability of 1.0 % and for 1 Myr with a probability of only 0.4% (Pflamm-Altenburg & Kroupa, 2006), and the previously expected instability (Kroupa, 2004) of the ONC-Trapezium system has been numerically confirmed.

THE DISSOLUTION OF OB-STAR CORES (CHAP. 2, APP. B, D)

The straightforward question thus is, why does the ONC-Trapezium exist? There are two possibilities: i) The ONC-Trapezium is much younger than its assumed age of 1 Myr. The decay analysis by Pflamm-Altenburg & Kroupa (2006) constrains the age to be of the order 50000 yr (=a few crossing times). This seems to be unlikely as the gas in the central region of the ONC is already ionisied and the Trapezium system is optically accessible. ii) The ONC-Trapezium was part of an initially much larger OB-star configuration containing many more stars and is just the current snapshot of this larger OB-star core in its late stage of decay.

The observed total stellar mass in the ONC within a radius of 2 pc around its centre is about 1800 $M_\odot$ (Hillenbrand, 1997; Hillenbrand & Hartmann, 1998). In the total ONC 10 stars are observed with masses >5 $M_\odot$. Comparing this with the total stellar mass of $\approx$ 1800 $M_\odot$ a discrepancy arises. It can be shown that in the case of a canonical IMF and within the uncertainties of random drawing processes, 13–38 stars with masses >5 $M_\odot$ are expected to have formed initially in the ONC (Pflamm-Altenburg & Kroupa, 2006). For this purpose a practical mathematical description of the IMF has been formulated (App. B) and a C-code library developed (App. D).

To explore the full range of possible initial OB-star numbers Monte-Carlo simulations of decaying OB-star cores with i) 10 initial OB-stars and ii) 40 initial OB stars have been performed. It turns out that the decay of an OB-star core of initially 40 stars reproduces best the observed properties of the ONC and its Trapezium after 1 Myr, i.e. the existence of a four-body Trapezium at the ONC centre and a total number of 10 OB stars within 1 pc radius of the ONC centre.

FIELD O STARS - DO THEY FORM IN ISOLATION? (CHAP. 5, 8)

The remaining 30 OB stars have been totally ejected from the ONC in the CATENA computations and contribute to the OB-star field population. Indeed, a large fraction of O stars have been found in the Galactic field away from any star forming regions. Many of them have large observed radial velocities suggesting that they might have been ejected from young star clusters (Gies & Bolton, 1986). Identifying those O stars with the same origin among all O field stars seems to be an impossible task. However, one example exists where the common origin may have been discovered. Gualandris, Portegies Zwart, & Eggleton (2004) have shown that the two O stars, AE Aurigae and μ Columbae which have spatial velocities of >100 km s^{-1} and are moving in opposite directions, and the highly eccentric binary ι Orionis, might have been ejected from the ONC 2.5 Myr ago by calculating their orbits backwards in time through the Galactic potential.

If it is possible to demonstrate that four field O stars can have their origin in compact star clusters, it might be possible to show that all O stars have formed in compact star clusters.

However, inspecting the dynamical properties of a sample of field O stars, de Wit et al. (2004, 2005) have identified 4±2 % of all O-type stars to be candidates for massive star formation in isolation. The problem of whether massive stars can form in isolation, i.e. without a cluster, is currently being debated in the star formation community, as isolated O-star formation would have important implications for star-formation theory as well as for the physics of galaxy evolution. But interestingly, Gvaramadze & Bomans (2008) report the existence of a bow shock associated with the O-star HD165319, which is marked in de Wit et al. (2005) as a candidate for an O-star formed in isolation.

Furthermore, massive stars ejected from their parent star clusters have spatial peculiar velocities which allows them to explode in a supernova and release their energy and metals not only far away from their star cluster where they have formed but also at high Galactic latitude. The resulting Galactic vertical supernova distribution is thicker than the initial star formation layer which is restricted to the very thin disk of molecular gas (Pflamm-Altenburg & Kroupa – in prep.)

Understanding the process of ejection of massive stars from young star clusters is of fundamental importance to answer the question whether massive stars can form in isolation or whether their formation is entirely restricted to the regions of massive star clusters and how massive stars influence the chemical evolution of galaxies.

TWO STEP EJECTION OF MASSIVE STARS (CHAP. 5, 7)

The stellar densities in star clusters are much higher than in the Galactic field, e.g. the present-day central stellar number density of the ONC is approximately 2×10^4 pc^{-3} (Hillenbrand, 1997). Massive stars have been found to be more concentrated towards the cluster centre than low-mass stars (Brandl et al., 1996; Hillenbrand & Hartmann, 1998).

This may be due to primordial mass segregation, i.e. massive stars form predominantly in the central regions of star clusters or due to dynamical mass segregation. Time-scale arguments prefer the primordial origin for mass segregation (Bonnell & Davies, 1998). How fast a star cluster is mass segregated can be studied in the very massive young star cluster R136 in the LMC and gives constrains on the further evolution of star clusters (Pflamm-Altenburg & Kroupa – in prep.).

Independent of whether mass segregation is primordial or due to dynamical processes, close encounters of massive stars are common in the central region of young compact star clusters. Because the encounter time scale is much shorter than the dynamical time scale of the star cluster, encounters between two stars can be considered as being nearly undisturbed. Both stars move on fixed hyperbolic orbits and no kinetic energy can be transfered from one star to the other.

In order to redistribute kinetic energy among the stars involved in the close encounter, at least three stars are required. The two most common cases are the encounter between one single star and a binary (S+B) and the encounter between two binaries (B+B). During the encounter the binary shrinks and the gained potential energy is transfered to the centre-of-mass systems.

In the B+B case the other binary disintegrates and commonly two single stars are moving away with high velocities in nearly opposite directions, whereas a more compact binary with low velocity compensates the remaining linear momentum. In 10 per cent of all B+B encounters high velocity binaries are produced (Mikkola, 1983).

Thus, B+S encounters are expected to be the most likely sources for the ejection of binaries from star clusters. If both components of the ejected binary have different initial masses, then their life times are different, too. If one component explodes as supernova the other star is released with nearly its orbital velocity (e.g. Zwicky, 1957; Blaauw, 1961; Iben & Tutukov, 1997). As the orientation of the orbital plane of the ejected binary is randomly distributed the information of the previous binary orbit is lost. Thus the released star cannot be traced back to its parent star cluster where it has formed. This process which combines the dynamical ejection scenario from star clusters and the supernova ejection is called the *two-step-ejection* process (Pflamm-Altenburg & Kroupa, 2009c). The peculiar velocity of the released star is the vectorial sum of the binary velocity and the internal orbital velocity of the released star. Therefore, the released star can gain an additional kick or it may be decelerated. The resulting peculiar velocity can be very low such that it cannot originate from any nearby star cluster. Such a star can mistakenly be considered as a massive star which formed in isolation.

It can be shown (Pflamm-Altenburg & Kroupa, 2009c) that the process of two-step-ejection can account quantitatively for the number of massive stars which are thought to have formed in isolation (de Wit et al., 2005). The conclusion is therefore that massive stars do form exclusively in clusters.

IGIMF - THE GALAXY-WIDE IMF

If the IMF within star clusters, which describes the mass spectrum of newly formed stars, has the meaning of a simple probability distribution function, then small-N star clusters are expected to form which contain only one massive star or are dominated by massive stars. Thus, at first sight the few candidates of massive stars which have apparently formed in isolation seem to approve the simple probability distribution function interpretation of the IMF. However, the two-step-ejection mechanism of massive stars can account for these few candidates. Furthermore, the dynamical processes described above predict the existence of massive stars which appear to have formed in isolation. Thus, there is no room left for such massive stars formed in isolation as required by the simple probability distribution function interpretation of the IMF.

Additionally, both the form and the scatter of the observed relation between the most massive star in a young embedded star cluster and the total stellar mass of this star cluster are in disagreement with what is expected from pure random sampling of the IMF corresponding to the simple probability distribution function interpretation (Weidner & Kroupa, 2006; Weidner et al., 2009). Furthermore, a star formation scenario in which the IMF in a star cluster is populated in a sorted fashion, i.e. low-mass stars form first, is in much better agreement with the observed distribution of stellar masses in star clusters. This implies that the mass of the most massive star in a young embedded star cluster is not determined by a size-of-sample effect but depends on the local physical conditions for star formation such that the formation of massive stars is restricted to the regions of highest gas density and a large gas reservoir.

The fundamental consequence is that low-mass star clusters are void of massive stars. Adding all IMFs of all young star clusters leads to the integrated galactic initial stellar mass function (IGIMF), and is steeper than the canonical IMF in star clusters. As galaxies with a low star formation rate lack massive star clusters, the IGIMF steepens with decreasing star formation rate.

IGIMF - CONSEQUENCES

This concept of clustered star formation and its formulation in the IGIMF theory is of remarkable straightforwardness, but the implications for our understanding of galaxy evolution and the interpretation of cosmological observations and thus the derived cosmological picture itself are dramatic:

In the classical picture the relation between the total SFR in a galaxy and the total Hα luminosity of a galaxy is linear (Kennicutt et al., 1994; Kennicutt, 1998) and dwarf irregular galaxies have much lower star formation efficiencies than large disk galaxies (eg. Skillman et al., 2003; Karachentsev & Kaisin, 2007; Kaisin & Karachentsev, 2008). The IGIMF-theory provides a non-linear SFR-$L_{\mathrm{H}\alpha}$ relation (Pflamm-Altenburg, Weidner, & Kroupa, 2007) and reveals a linear relation between the global SFR and the total neutral

galaxy gas mass implying that dwarf irregular galaxies have the same star formation efficiency as large disk galaxies (Pflamm-Altenburg & Kroupa, 2009b). An unavoidable prediction of the IGIMF theory is that the FUV flux decreases more slowly than the total Hα luminosity with decreasing SFR (Pflamm-Altenburg, Weidner, & Kroupa, 2009). This prediction has been qualitatively (Meurer et al., 2009) and quantitatively (Lee et al., 2009) confirmed.

Furthermore, the IGIMF-theory naturally explains the observed mass-metallicity relation of galaxies (Köppen et al., 2007), the decreasing Fe/O-abundance ratio with decreasing galaxy velocity dispersion (Recchi et al., 2009) without any kind of tremendous parameter adjustments as required in the classical galaxy-wide constant IMF picture.

A local version of the IGIMF-theory naturally explains the observed radial Hα cutoff in disk galaxies and accounts for the differences in the observed radial Hα and FUV surface density luminosity profiles (Boissier et al., 2007).

This fundamental change in the understanding of star formation and galaxy evolution is entirely linked to the algorithm how the galaxy-wide IMF is calculated from all individual IMFs of all young star clusters. This algorithm depends on the meaning of the IMF in star clusters. To decide whether the IMF has the simple meaning of a general probability density distribution function or depends on the local physical conditions of star formation, i.e. whether the galaxy-wide IMF is identical to the IMF within star clusters or not, the theoretical and observational study of the dynamics and ejections of massive stars is of fundamental importance and interest. One can finally conclude that the sub-parsec star cluster research has substantial influence on the interpretation of cosmological observations.

A STAR CLUSTER: COMPOSED OF A SINGLE-AGED POPULATION? (CHAP. 3, 4, 6)

Star clusters are thought to have formed during a monolithic collapse of the dense part of large molecular clouds. Cooling and increasing gas density constitute a run-away process with on-going fragmentation of the dense gas material, out of which stars begin to form. Once the massive stars ignite their radiation and stellar wind feedback ionises the central region of the young star cluster and prevents the embedding gas cloud from further collapse. As this process is thought to occur on a free-fall time scale, i.e. on the order of one or a few Myr, the stars are believed to be coeval to within a Myr, which agrees in general with observations.

But in recent years observational hints and evidence has become available that the stellar population of star clusters may not be as simple as this picture of star cluster formation and evolution may suggest.

Palla et al. (2005) report the discovery of a few old low-mass stars in the ONC, on the basis of the analysis of isochrone and lithium-depletion ages. These stars have

derived ages ≥10 Myr, although the main bulk of stars in the ONC have ages of ≈1 Myr (Hillenbrand, 1997). The conclusion has therefore been drawn that the star formation time scale is much longer than a free-fall or central-star-cluster-crossing time and that the star formation process starts with the very moderate formation of low-mass stars, increases and peaks in the formation of massive stars. Additionally, the same situation as observed in the ONC has been found by Sacco et al. (2007) in the young star cluster σ Orionis.

The young star cluster R136 in the LMC is the most massive young star cluster in the Local Group with an age of at most a few Myr. Brandl et al. (1996) report the discovery of *faint red sources* in the R136 of unknown origin. They exclude the possibility that these faint red sources are red giants, because red giants of these luminosities require stellar ages >350 Myr. These stars would be too old to have formed in R136.

At the high mass end of the star cluster mass range the most massive old globular star clusters with mass $\geq 10^6$ $M_\odot$ show peculiarities in their stellar population, such as for example a split of the sub-giant branch, a gap in the RR Lyrae population or a spread in metallicity, which can be interpreted to mean that these massive star clusters may contain multiple stellar populations.

STAR CLUSTER CONTAMINATION BY FIELD STAR CAPTURE
(CHAP. 3, 6)

Summarising, there exist a growing amount of hints and evidences that the simple picture of star clusters being single-age simple stellar populations might not be universal.

In the case of the few older stars (10–18 Myr) in the ONC it has to be taken into account that the ONC is part of a much larger area with star formation in the recent past and on-going. Thus, 10–18 Myr old stars do exist in the vicinity of the ONC. In the absence of time-varying potentials the total energy, kinetic plus potential energy, of these older stars is conserved. But during the collapse of the pre-cluster cloud core out of which the new embedded star cluster forms the older stars moving in close-by orbits feel the increasing potential of the collapsing cloud. Their orbits are deflected and are focused towards the new cluster. The field star density is increased at the position of the new cluster. Furthermore, some of the stars get gravitationally bound. It has been shown that this process of field star capture can account for the few observed older stars in the ONC (Pflamm-Altenburg & Kroupa, 2007)

The concept of captured field stars can also be applied to massive star clusters. For example the 110 faint red sources in the central region of R136 reported by Brandl et al. (1996), which have been excluded to be old red giants on the basis of age arguments, can indeed be old red giants, if they have been captured from the surrounding stellar field during pre-cluster-cloud core collapse and the formation of R136 (Pflamm-Altenburg & Kroupa - in prep.).

This process in which older field stars are captured during pre-cluster cloud core collapse is of significant importance and has to be taken into account when interpreting the observed stellar population of star clusters. If not, wrong conclusions as for example concerning the time scale of star formation can be drawn.

GLUTTONOUS STAR CLUSTERS (CHAP. 4)

The process of the capture of field stars described above can only introduce stars into the newly formed star cluster which are older than the stars born during the formation of the star cluster. After its formation star clusters do not evolve in isolation but they are still embedded in a matter field composed of stars and gas. It is straightforward to ask how the whole system, the star cluster embedded in a field of stars and gas, will evolve.

The effect of field stars on already formed star clusters has been explored by Mieske & Baumgardt (2007). Field stars can move on their orbits and can pass through a star cluster. If the star cluster potential is considered to be fixed, then the field stars pass through the star cluster without energy exchange, i.e. their total energy before entering and after leaving the star cluster is equal. But the star cluster potential is build up by a set of moving stars. And due to two-body interactions between the cluster stars and the field stars energy will be redistributed among them and some field stars may loose energy or may even get bound to the cluster.

The second process, the interaction between an already formed star cluster and the surrounding inter-stellar medium (ISM) has not been considered in the literature before. To analyse the influence of the gravitational force of the star cluster on the ISM one can consider the limiting case of the hydrostatic solution of a gas in a gravitational potential exerted by a star cluster. This ansatz shows that the warm ISM ($\approx 10^4$ K) does not notice the existence of star clusters less massive than $\approx 10^6$ $M_\odot$. But star clusters with masses $\gtrsim 10^6$ $M_\odot$ have a rapidly rising gravitational influence on the surrounding ISM such that the ISM should become unstable and react with inflow towards the star cluster centre (Pflamm-Altenburg & Kroupa, 2009a). Thus, star clusters with a total mass of $\approx 10^6$ $M_\odot$ or more massive can cause an instability in the warm ISM. The accretion of new gas by the star cluster can lead to a new episode of star formation and, given that this process can recur, may account for the observed multiple stellar populations in star clusters with masses of $\gtrsim 10^6$ $M_\odot$.

The method used in the analysis of the evolution of a star cluster embedded in the warm ISM can be applied to other systems consisting of a spherical stellar ensemble embedded in a gaseous environment of a certain temperature.

Combining the observed half-mass-radius–total-mass relations (Dabringhausen et al., 2008) of pressure supported spherical stellar systems with the warm and the hot phase of the ISM two additional mass thresholds can be identified (Pflamm-Altenburg & Kroupa, 2009a) which corresponds to mass thresholds separating galaxies of different morphological types in the half-mass-radius–total-mass plane in Dabringhausen et al. (2008): i) a 10^8 $M_\odot$

threshold which separates dwarf spheroidals from dwarf ellipticals and ii) a threshold at $\approx 10^{11}$ $M_{\odot}$ which separates large ellipticals from dwarf ellipticals. To what degree a physical connection exists between these two types of mass thresholds is unclear at the moment and requires further research.

Part I

Finished work

Chapter 2

A highly abnormal massive-star mass function in the Orion Nebula Cluster and the dynamical decay of its Trapezium

Pflamm-Altenburg, J., Kroupa, P., 2006, **MNRAS**, 373, 295

The ONC appears to be unusual on two grounds: The observed constellation of the OB-stars of the entire Orion Nebula cluster and its Trapezium at its centre implies a time-scale problem given the age of the Trapezium, and an IMF problem for the whole OB-star population in the ONC. Given the estimated crossing time of the Trapezium, it ought to have totally dynamically decayed by now. Furthermore, by combining the lower limit of the ONC mass with a standard IMF it emerges that the ONC should have formed at least about 40 stars heavier than 5 $M_\odot$ while only ten are observed. Using N-body experiments we (i) confirm the expected instability of the trapezium and (ii) show that beginning with a compact OB-star configuration of about 40 stars the number of observed OB stars after 1 Myr within 1 pc radius and a compact trapezium configuration can both be reproduced. These two empirical constraints thus support our estimate of 40 initial OB stars in the cluster. Interestingly a more-evolved version of the ONC resembles the Upper Scorpius OB association. The N-body experiments are performed with the new C-code CATENA by integrating the equations of motion using the chain-multiple-regularization method. In addition we present a new numerical formulation of the initial mass function.

2.1 Introduction

Of all O-stars 46 per cent and of all B-stars 4 per cent are runaways exceeding 30 km/s (Stone, 1991). Furthermore the binary fraction among runaway O-stars is around 10 % (Gies & Bolton, 1986) while it is more than 50 % in young star clusters (Goodwin et al., 2006). This suggests that binaries are involved in close dynamical encounters leading to stellar ejections while the binary fraction among the ejected stars is decreased. Indeed, Clarke & Pringle (1992) deduced using an analytical approach that massive stars must form in compact small-N groups. The decay of non-hierarchical 3,4,5-body systems with equal masses as well as a mass spectrum has been investigated by Sterzik & Durisen (1998). They determined the spectrum of the remnant decay products but not the phase-space behaviour of compact few-body systems with time. Hoogerwerf, de Bruijne, & de Zeeuw (2000) and Hoogerwerf et al. (2001) were able to trace back the trajectories of some runaways to nearby associations. Ramspeck, Heber, & Edelmann (2001) determined the age and the calculated time-of-flight of early-type stars at high galactic latitudes and concluded that they can have their origin in the galactic disk. In the case of the runaways AE Aurigae and μ Columbae, which have spatial velocities greater than 100 km/s, in combination with the binary ι Orionis, Gualandris, Portegies Zwart, & Eggleton (2004) have shown that the encounter of two binaries with high eccentricities 2.5 Myr ago and in the co-moving vicinity of the current Orion Nebula Cluster (ONC) can reproduce the spatial configuration observed today. The spatial distribution of field OB-stars can thus be understood qualitatively using theoretical stellar-dynamical methods. But to obtain a more complete picture we need to study the details and frequency of occurrence of energetic ejections from the acceleration centres, namely the inner regions of young star clusters.

2.2 Motivating problems

In the case of the Orion Nebula cluster two main discrepancies concerning the properties of its OB-stars are found:

2.2.1 Existence of the Trapezium system

Given the total mass of all four Trapezium stars (Hillenbrand, 1997) of 88.4 $M_\odot$ and their occupying space of nearly 0.05 pc in diameter the corresponding crossing time can be estimated,

$$t_{\rm cr} = \sqrt{\frac{4\,R^3}{G\,M}}\,, \tag{2.1}$$

to be about 13 Kyr (Tab. 2.1), if the Trapezium is assumed to be a compact virialized subsystem of the ONC. Sterzik & Durisen (1998) noted that most systems in their decay

model	stars	$\frac{M_{\rm tot,OB}}{M_\odot}$	$\frac{\sigma_{\rm 3D}}{\rm km/s}$	$\frac{t_{\rm cr}}{\rm Kyr}$	runs
4-body	Θ^1 in Tab. 2.5	88.4	3.9	12.6	1000
10-body	all in Tab. 2.5	167.2	5.4	9.2	1000
40-body	4 × Tab. 2.5	668.8	10.7	4.7	1000

Table 2.1: Specification of the N-body systems. $M_{\rm tot}$ is the total mass in $M_\odot$. The velocity dispersion σ is calculated from the total mass placed within the initial radius of 0.025 pc corresponding to the ONC-TS size if virial equilibrium is assumed. t_{cr} is the crossing time, and runs are the total number of integrated configurations.

analysis decay within dozens of crossing times. So the ONC-TS is expected to have totally decayed by now, if its age is about 1 Myr (Kroupa, 2004).

2.2.2 The number of OB stars

The virial mass of the ONC is measured to be nearly 4500 $M_\odot$ but only about 1800 $M_\odot$ is visible in stellar mass (Hillenbrand & Hartmann, 1998) while cluster-formation models that match the ONC suggest that it may have formed with 10^4 stars plus brown dwarfs and that it is expanding now resembling a Pleiades type cluster embedded in an expanding association to a remarkable degree after 100 Myr (Kroupa et al., 2001). The observed mass of all stars heavier than 5 $M_\odot$ is 167 $M_\odot$. If the canonical IMF (App. C) is normalized such that 1633 $M_\odot$ are contained in the mass interval ranging from 0.01 up to 5 $M_\odot$ and for three different physically possible upper stellar mass limits, $m_{\rm max*}$, of 80, 150 $M_\odot$ or $+\infty$ (Weidner & Kroupa, 2004; Oey & Clarke, 2005; Figer, 2005; Koen, 2006), and different IMF-slopes above 1 $M_\odot$ the corresponding maximum stellar mass $m_{\rm max}$ and the expected number of OB-stars formed in the ONC can be calculated (Tab. 2.2). The calculations are based on the IMF by Kroupa (2001) but with a numerically more convenient description [1] (App. B).

Given the values in Tab. 2.2 the ONC should have formed about 38 OB-stars assuming the IMF to be canonical ($\alpha_3 = 2.35$). But in a thorough survey of the ONC Hillenbrand (1997) lists only 10 stars weighting more than 5 $M_\odot$ (Tab. 2.5). 9 of these 10 OB stars are located within a projected sphere of 1 pc around the Trapezium system. The remaining B star (5.7 $M_\odot$) is placed approximately 2.3 pc away from the Trapezium. 7 OB stars, including the three most massive stars, are located within 0.5 pc around the Trapezium in projection. If the IMF is steepened above 1 $M_\odot$ to $\alpha_3 = 2.7$ the number of expected OB-stars decreases down to 18. But the expected maximum stellar mass also decreases down to $m_{\rm max} = 28$ $M_\odot$, whereas two observed stars are heavier. The existence of these stars suggests that the IMF was indeed normal. Note that the time-scale problem would

[1] A utility-IMF package and CATENA including a full documentation can be downloaded from the AIfA-webpage: http://www.astro.uni-bonn.de/

persist even if we allow $\alpha_3 = 2.7$. Because the IMF seems to be universal (Kroupa, 2002) a significant deviation from the calculated number of 38 stars using the canonical IMF should not be expected.

As a check the number of stars heavier than 5 $M_\odot$ can also be estimated by normalising the canonical IMF to the number of stars in the mass range 1–2 $M_\odot$ in the cluster. Using the stellar sample of Hillenbrand (1997), the number of stars heavier than 5 $M_\odot$ can be derived from the number of stars between 1 and 2 $M_\odot$ (70) and noting that in this mass regime only the non-embedded sources are listed. These amount to approximately half of all stars (Hillenbrand, 1997). Thus, 26 OB-stars are expected to have formed in the ONC. The total mass derived from this mass regime is 1404 $M_\odot$, 22 % less than the total estimated mass used above. Given this uncertainty (13–38 stars heavier than 5 $M_\odot$), we perform computations with 10 and 40 stars. As will become apparent below, 40 OB stars are our preferred value.

Furthermore, if stars are drawn randomly from a universal IMF, the number of stars heavier than 5 $M_\odot$ may not be the expectation value of 38. The number can be smaller. To estimate the probability that less than k of n stars have masses less than 5 $M_\odot$, drawing stars from an IMF has to be interpreted as a Bernoulli experiment: For the mass of the ONC, $M_{\rm ONC}$, the total number of stars, $n_{\rm tot}$, and the number of stars, $n_{>5}$, heavier than 5 $M_\odot$ can be calculated. If one star is drawn from the IMF, the probability to get a star heavier than 5 $M_\odot$ is

$$p = n_{>5}/n_{\rm tot} \quad . \tag{2.2}$$

This experiment is repeated $n_{\rm tot}$ times. So the probability to have a star heavier than 5 $M_\odot$ k times is given by the Bernoulli-distribution,

$$p(k) = \binom{n_{\rm tot}}{k} p^k (1-p)^{n_{\rm tot}-k} \quad . \tag{2.3}$$

Because the event probability is small and the number of experiments large the Poissonian limit can be applied. The probability is approximately

$$p(k) = \frac{\mu^k}{\mu!} e^{-\mu} \quad , \tag{2.4}$$

where $\mu = p\, n_{\rm tot} = n_{>5}$. So the total probability to get k or fewer OB-stars is

$$P(\leq k) = \sum_{i=0}^{i=k} p(i) \quad . \tag{2.5}$$

The probability to get 20, 10 or fewer OB-stars for two different ONC-masses and two different physically possible upper stellar mass limits is given in Tab. 2.3. It is extremely unlikely that only ten stars have formed in the ONC if the IMF is universal.

We note that the same argument can be applied to a more-evolved population: In an exploration of the full stellar population of the Upper Scorpius OB association, Preibisch

α_3	$m_{\max *}/\mathrm{M}_\odot$:	$+\infty$	150	80	obs.
2.35	$m_{\max}/\mathrm{M}_\odot$	76.4	59.5	46.8	45.7
2.35	$N_{>5}$	38.7	38.3	37.8	10
2.35	$M_{\mathrm{tot}}/\mathrm{M}_\odot$	2103	2076	2048	1800
2.7	$m_{\max}/\mathrm{M}_\odot$	28.6	27.7	26.1	45.7
2.7	$N_{>5}$	18.4	18.4	18.3	10
2.7	$M_{\mathrm{tot}}/\mathrm{M}_\odot$	1799	1797	1794	1800

Table 2.2: Observed (Hillenbrand, 1997) and expected maximum stellar mass ($m_{\max}$), number of stars more massive than 5 $\mathrm{M}_\odot$ ($N_{>5}$), and total initial mass (M_{tot}) for the Orion Nebula Cluster in dependence of three different physically possible upper stellar mass limits, $m_{\max *}$, and two different IMF-slopes, α_3, for the mass range from 1 $M_\odot$ up to $m_{\max}$. The mass range less than 1 $\mathrm{M}_\odot$ is described by a Kroupa-IMF (Kroupa, 2001).

$M_{\mathrm{ONC}}/\mathrm{M}_\odot$	1800	1800	2200	2200
$m_{\max *}/\mathrm{M}_\odot$	80	150	80	150
n_{tot}	5209	5144	6337	6251
μ	33	33	41	41
$P(k \leq 10)$	$2.8 \cdot 10^{-6}$	$2.8 \cdot 10^{-6}$	$7.6 \cdot 10^{-9}$	$7.6 \cdot 10^{-9}$
$P(k \leq 20)$	$1.0 \cdot 10^{-2}$	$1.0 \cdot 10^{-2}$	$2.2 \cdot 10^{-4}$	$2.2 \cdot 10^{-4}$

Table 2.3: The probability to draw 20 ($P(k \leq 20)$), 10 ($P(k \leq 10)$) or fewer stars heavier than 5 $\mathrm{M}_\odot$ from a Kroupa-IMF, the expectation value μ of the number of stars heavier than 5 $\mathrm{M}_\odot$ and the total number of stars n_{tot} (equivalent to the number of repeated experiments) are calculated for two different total cluster masses and two different physically possible upper stellar mass limits.

et al. (2002) determined a total stellar mass of 2060 $\mathrm{M}_\odot$ covering a volume of 35 pc in diameter. For the supernova progenitor they deduced a mass of $\approx 40 - 60$ $\mathrm{M}_\odot$. An IMF steeper than 2.3 in the regime of massive stars would not have lead to the formation of such a massive star in the young star-cluster-stage of the Upper Scorpius OB association 5 Myr ago for this mass of 2060 $\mathrm{M}_\odot$ (Weidner & Kroupa, 2006). This further supports that the IMF may not be steeper than 2.3 for massive stars. Preibisch et al. (2002) listed 19 stars heavier than 5 $\mathrm{M}_\odot$. This is approximately half of the expected number of formed stars more massive than 5 $\mathrm{M}_\odot$ and constitutes the same problem as for the ONC due to similar initial cluster masses. Therefore, it can be argued that O and B stars may have been ejected from their star forming region very early after their formation.

So two questions arise assuming the IMF is invariant: Why does the Trapezium still exist and where are the missing OB-stars?

2.3 Integrator

To investigate the dynamics of the OB-stars in the ONC we perform direct N-body integrations. Because close encounters with high eccentricity are very frequent in compact few-body systems due to the grainy potential, a multiple regularization technique is required to reduce energy errors and speed-up the calculations. We combined in our own code (CATENA[1]) the very efficient CHAIN-regularization formalism developed by Mikkola & Aarseth (1990, 1993) with an embedded Runge-Kutta method of 8(9)-th order using a coefficient-set published by Prince & Dormand (1981), instead of the Aarseth-CHAIN-Burlisch-Stoer integrator, to integrate the regularized equations of motions.

Computer codes for studying the dynamics of few body systems and star clusters or planetary systems are available. A very valuable review of this kind of software industry is given in Aarseth (1999, 2003). But, interestingly, there is a lack of software for calculating the dynamical decay of systems with a few $\leq N \leq$ four dozen stars. Our endeavour is to fill this gap by a sophisticated software tool allowing us to efficiently study the decay of hierarchical and non-hierarchical configurations of some tens or hundreds stars down to the last remaining hard binaries or hierarchical higher-order multiple-stars, with the long-term-aim of embedding CATENA in a general-purpose N-body code.

An error analysis for the present application is provided in Sec. 2.7.

2.4 Initial conditions

To address the questions mentioned above we investigate three models which consist of the stars listed in Tab. 2.1.

In the first model we study the stability of the actually observed Trapezium system consisting of Θ^1 A, Θ^1 B, Θ^1 C and Θ^1 D precisely. In the second model, it is assumed that all currently observed OB stars in the ONC (Tab. 2.5) were initially in a compact configuration as a core at the centre of the ONC, due either to mass segregation or ab-initio. In the third model we start with an OB core coming close to the expected number of 38. To find a suitable set of stars, all presently observed OB stars are used four times giving 40 stars (4 times Tab. 2.5).

The compact settings of OB-stars are motivated by the outcome of the analytical investigation by Clarke & Pringle (1992) that massive stars form in compact groups. Bonnell & Davies (1998) concluded that the positions of massive stars in the Trapeziums cluster in Orion cannot be due to dynamical mass segregation, but must have formed in, or near, the centre of the cluster.

For each of these three models 1000 configurations are created where the stars from Tab. 2.1 are uniformly distributed over a sphere with the compact Trapezium radius of 0.025 pc (Hillenbrand, 1997). The velocities are drawn from a Gaussian distribution with

a velocity dispersion resulting from the virial theorem,

$$\sigma = \frac{G\ M_{\rm tot,OB}}{R} \tag{2.6}$$

(Tab. 2.1). After this the velocities are re-scaled slightly to ensure initial virialisation.

This simple model does not include the rest of the ONC. To estimate its effect on the core decay the ratio of the internal and external forces can be calculated. The OB-star core of radius r consists of n stars having the mean mass m. The gravitational force on one star is then

$$F_{\rm n} = G\frac{nm^2}{r^2} \quad . \tag{2.7}$$

The force exerted by the rest of the ONC on one star in the core can be estimated by the Plummer force

$$F_{\rm pl} = GmM_{\rm pl}(r^2+b^2)^{-\frac{3}{2}}r \quad , \tag{2.8}$$

assuming the cluster can be represented reasonably well by a Plummer model, which has been shown to be the case (Kroupa et al., 2001). The resulting force ratio is

$$\Phi = \frac{F_{\rm n}}{F_{\rm pl}} = \frac{nm}{M_{\rm pl}}\left(1+\frac{b^2}{r^2}\right)^{\frac{3}{2}} \quad . \tag{2.9}$$

The mass $M_{\rm pl}$ is the cluster mass minus the mass of the OB-stars. The resulting force ratios can be seen in Tab. 2.4. The core dynamics is dominated by its self-gravitation.

The escape velocities for the isolated core and the total Plummer sphere can also be compared. Both are obtained from the conservation-of-energy-theorem. The escape speed from the centre of the Plummer sphere, $v_{\rm e,pl}$, and the escape speed from the surface of an isolated OB-core are given by

$$v_{\rm e,pl} = \sqrt{\frac{2Gm_{\rm cl}}{b}} \quad , \quad v_{\rm e,OB} = \sqrt{\frac{2Gm_{\rm OB}}{r_0}} \quad , \tag{2.10}$$

respectively, where $r_0 = 0.025$ pc is the initial radius of the OB-core. For the 4- and 10-body model the escape speeds for the isolated model and the true embedded situation are comparable. In the 40-body model the escape speed from the core is dominated by the core itself.

A second issue associated with the cluster shell of low-mass stars is two-body relaxation between an OB-star and the low mass stars of the cluster. Energy may be transfered from the OB-star core and ejected or evaporated OB-stars to the rest of the cluster. The relaxation time of the ONC is about 18 Myr (Kroupa, 2005). The relaxation time for a heavy star is given by multiplying the relaxation time with the ratio of the mass of the most massive star and the mean stellar mass (Spitzer, 1987) and describes the time-scale of a massive star to sink towards the cluster centre,

$$t_{\rm relax,OB} \approx \frac{\bar{m}}{m_{\rm OB}} t_{\rm relax} \quad , \tag{2.11}$$

n	$M_{\rm OB}/{\rm M}_\odot$	$m/{\rm M}_\odot$	Φ	$v_{\rm e,OB}$	$M_{\rm cl}/{\rm M}_\odot$	$v_{\rm e,pl}$
4	88.4	22.1	94.5	5.6	1721.4	7.1
10	167.2	16.7	178.6	7.7	1800.2	7.3
40	668.8	16.7	714.2	15.4	2301.8	8.2

Table 2.4: n is the number of stars the model consists of, $M_{\rm OB}$ (cf. Tab. 2.1) is the total mass contained in the OB-stars, m is the mean mass of an OB-star, Φ is the resulting force ratio using a Plummer mass of 1633 $\rm M_\odot$. Given the observed core radius of the ONC of about 0.19 pc (Hillenbrand & Hartmann, 1998) the related Plummer parameter of the ONC is about 0.3 pc. $v_{\rm e,OB}$ is the escape speed in km/s from the surface of an OB-core with radius of 0.025 pc, $v_{\rm e,pl}$ is the escape speed in km/s from the centre of a Plummer sphere with mass $M_{\rm cl} = 1633\,{\rm M}_\odot + M_{\rm OB}$.

where the average mass $\bar{m}$ of a star is 0.35 $\rm M_\odot$ using a Kroupa-IMF. The resulting energy transfer time-scale ranges from 0.14 Myr (45.7 $\rm M_\odot$) up to 1.26 Myr (5 $\rm M_\odot$), thus being shorter or comparable to the time spanned by the simulations and therewith probably an important issue in our context, given the age of the ONC $\approx$ 1 Myr. In the case of no equipartition instability, energy transfer stops after reaching energy equipartition,

$$\bar{m} < v^2 >= m_{\rm OB} < v_{\rm OB}^2 > \quad , \tag{2.12}$$

where $< v^2 >$ ($< v_{\rm OB}^2 >$) is the mean square velocity of the mean-mass stars (OB-stars, respectively). Using a velocity dispersion of 2 km $\rm s^{-1}$ (Hillenbrand, 1997) for the mean-mass stars, the relation above and the energy theorem it can be calculated that the velocity of a 5 $\rm M_\odot$ (45 $\rm M_\odot$) is low enough such that the movement of the OB-stars is constrained to be within a radius of 0.026 pc (0.0084 pc). So the current observed OB core has an extension consistent with energy equipartition. Following Heggie & Hut (2003) the heavy stars are so concentrated that the lighter stars have been expelled from the core and they no longer have a significant role. This is also suggested by the observed deficit of low-mass stars in the core of the ONC (Hillenbrand & Hartmann, 1998).

We conclude that the effect of two-body relaxation between low-mass stars and the OB-stars may be of minor importance and that these simulations suffice to demonstrate the time-scale problem of the ONC, and that the OB-star core-decay-model may explain the OB-star number problem of the ONC. While full-scale N-body calculations capture the entire relevant physics, our approximations allow us to compute a very large number of renditions (here 5000 in total) which is necessary given the low frequency of massive stars. Future N-body calculations of individual set-ups will be used to check our results.

2.5 Finding Trapezium systems

We define a trapezium system to consist of a few stars having pairwise distances of the same order. Here the whole system is scanned to determine the maximum number of stars in a configuration in which the pairwise distances lie between two boundaries: When

Name	Parenago	SpT	$m/M_\odot$
Θ^1A	1865	O9V	18.9
Θ^1B	1863	B0V	7.2
Θ^1C	1891	O7V	45.7
Θ^1D	1889	B0Vp	16.6
Θ^2A	1993	O9V	31.2
Θ^2B	2031	B1V	12.0
LP Ori	1772	B2V	7.2
—	1956	B3	6.4
NU Ori	2074	B1V	16.3
HD37115	2271	B5V	5.7

Table 2.5: Stellar data for all OB-stars over 5 $M_\odot$ given by Hillenbrand (1997). Spectral type E after van Altena et al. (1988).

studying the stability of the ONC Trapezium these boundaries are 0.01 and 0.05 pc. When studying the total OB-star distribution these boundaries are 0 and 0.05 pc.

This procedure is illustrated in Fig. 2.1: Consider a configuration consisting of six bodies. A table containing the pairwise distances is created. All subsets of particles having a pairwise distance between two boundaries are determined. Of all these subsets the one having the most members is the extracted trapezium system. For the explicit example above, assume that a trapezium system of dimension a is searched. The pairwise distances may be allowed to deviate by 20 per cent from this dimension. Then the subsets found are: $\{2,3\}$, $\{2,4\}$, $\{2,5\}$, $\{3,4\}$, $\{3,5\}$, $\{4,5\}$, $\{2,3,4\}$, $\{2,3,5\}$, $\{2,4,5\}$, $\{3,4,5\}$, and $\{2,3,4,5\}$. So the trapezium system consists of four bodies.

If a trapezium system of the dimension b is searched all subsets extracted from the distance table are: $\{1,2,6\}$, $\{1,3,6\}$, $\{1,4,6\}$, and $\{1,5,6\}$. Four candidates for a trapezium system of dimension b are found. But they all have the same number of members.

Based on this algorithm a set of bodies can contain no trapezium system of a certain dimension, or a trapezium system can have two or more members. But it is not possible to find a trapezium system consisting only of one body.

If the number of stars within a certain sphere is of interest the lower boundary must only be set to zero.

The pairwise distances of the Trapezium stars in the ONC Θ1 lie approximately between 0.02 and 0.05 pc, whereby all of the OB stars can be found within nearly 1 pc radius around Θ1 (Hillenbrand, 1997).

2.6 Decay of OB-star cores

All 3000 configurations are integrated over 2 Myr. 95% of all runs have a relative energy error lower than 10^{-14} in the case of the 4-body model, 10^{-12} for the 10-body model and

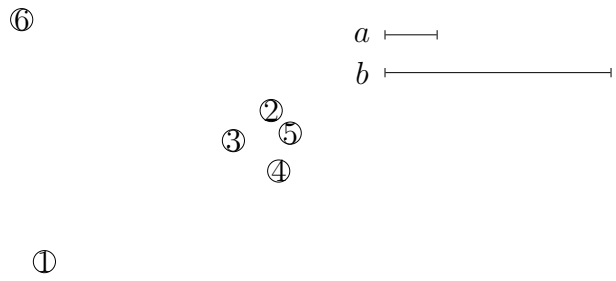

Figure 2.1: Illustration of the trapezium-finding routine (see Sec. 2.5 for explanation).

10^{-10} for the 40-body model.

2.6.1 Four-body model

In the top-diagram of Fig. 2.2 the decay curve of a four-body trapezium consisting of the four stars of Θ^1 Ori is plotted. After 1 Myr only 2.5 stars on average are found with a pairwise distance less than 0.05 pc, and 1 star on average is found with a pairwise distance between 0.05 and 0.01 pc, where in both cases the 3d curves lie slightly below the 2d-projection decay curve. This demonstrates the time-scale problem pointed out above for the observed Trapezium which is marked by the bold x. It can be argued that these are only mean values which are gained from a number distribution, and that a compact trapezium as is observed can survive for 1 Myr with some probability. That this is not the case can be seen in Fig. 2.3, where the distribution of the member numbers is plotted in a histogram. In 62.2 % of all runs no stellar configuration is found with a pairwise distance between 0.01 and 0.05 pc, while in only 0.4 % of all runs a trapezium of the observed size is found after 1 Myr.

On a first view this stands in contradiction to Allen & Poveda (1974), which is the only known work about stability of trapezia systems. Their result was that 63 % of all trapezia remain as a trapezia after 30 crossing times ($\approx$ 1 Myr). The reason is that they used a slightly different definition of a trapezium system: "let a multiple star system (of 3 or more stars)... if three or more such distances are of the same order of magnitude, then the multiple system is of trapezium type.... Two distances are of the same order of magnitude, in this context, if their ratio is greater than 1/3 but less than 3". A four-body system satisfying our definition of a trapezium system, i. e. all pairwise distances are of the same order of magnitude, can evolve into a system of two singe stars and one close binary. Then three distances are of the same order of magnitude, i. e. the distance between the two single stars, and the distances between each single star and one component of the binary. Their definition will detect a trapezium system. Our algorithm also detects a trapezium system but consisting only of three stars and having a different size than searched for. So

the criterion by Allen and Poveda does not take the number of members of the trapezium system into account nor the size of the trapezium. For a quantification of the stability of a four-body system, the crucial point is the number of stars the trapezium consists of. The Allen-and-Poveda trapezia consist initially of six stars, and only one of all 30 configurations (3.3 %) retains the initial size after 1 Myr, and consists finally only of four stars. Indeed in all their 30 runs binaries form consisting preferentially of the two most massive stars, therewith being quite consistent with our result.

2.6.2 10-body model

As in the four-body model the mean number of stars within 0.05 and 1 pc is plotted in Fig. 2.2. The decay of an initial ten-body OB star core can neither reproduce a four-body trapezium with a diameter of 0.05 pc nor the entire present-day ONC OB population (Fig. 2.3).

2.6.3 40-body model

If it is assumed that the ONC had an initial OB-star content of nearly forty as expected from the canonical IMF combined with the estimated stellar mass of the ONC of about 2200 $M_\odot$ then the remaining number of OB stars after 1 Myr within a sphere of 1 pc radius comes close to the observed value of ten (Fig. 2.2). The probability to observe a trapezium at an age of 0.5 Myr is 13.8 % but only 0.7 % at an age of 1 Myr (Fig. 2.3). But counted together with the systems containing more than four stars the probability to find a compact trapezium increases to $0.7 + 2.9 = 3.6\%$. Note that the estimated ONC mass is comprised of the observed mass (1800 $M_\odot$) plus the estimated mass in missing 30 OB stars (400 $M_\odot$). The true initial ONC mass may have been about 4000 $M_\odot$ (Kroupa et al., 2001).

In Fig. 2.4 the spatially cumulative and velocity distributions of the O and B stars after 1 and 2 Myr are plotted. After 1 Myr more than 75 % (30 of 40) of all stars have larger distances to their common centre of mass than 2 pc, and after 2 Myr 75 % of all stars are more than 4 pc away from their centre of mass. Therefore only ten of forty stars heavier than 5 $M_\odot$ remain at the cluster centre as observed in the ONC. It can be seen that more O stars than B stars are at very large distances as well as more O stars than B stars have very high velocities. This comes about because initially B stars tend to evaporate by energy redistribution rather than being ejected by close encounters. Because O stars are heavier they form tighter configurations than B stars and they are then involved in close binary interactions leading to high ejection velocities. This confirms the result of Clarke & Pringle (1992) qualitatively.

Given the spatial distribution of OB-stars after an evolution of 1 and 2 Myr, an extrapolation to an evolution age of 5 Myr predicts that nearly 50 % of all OB-stars cover

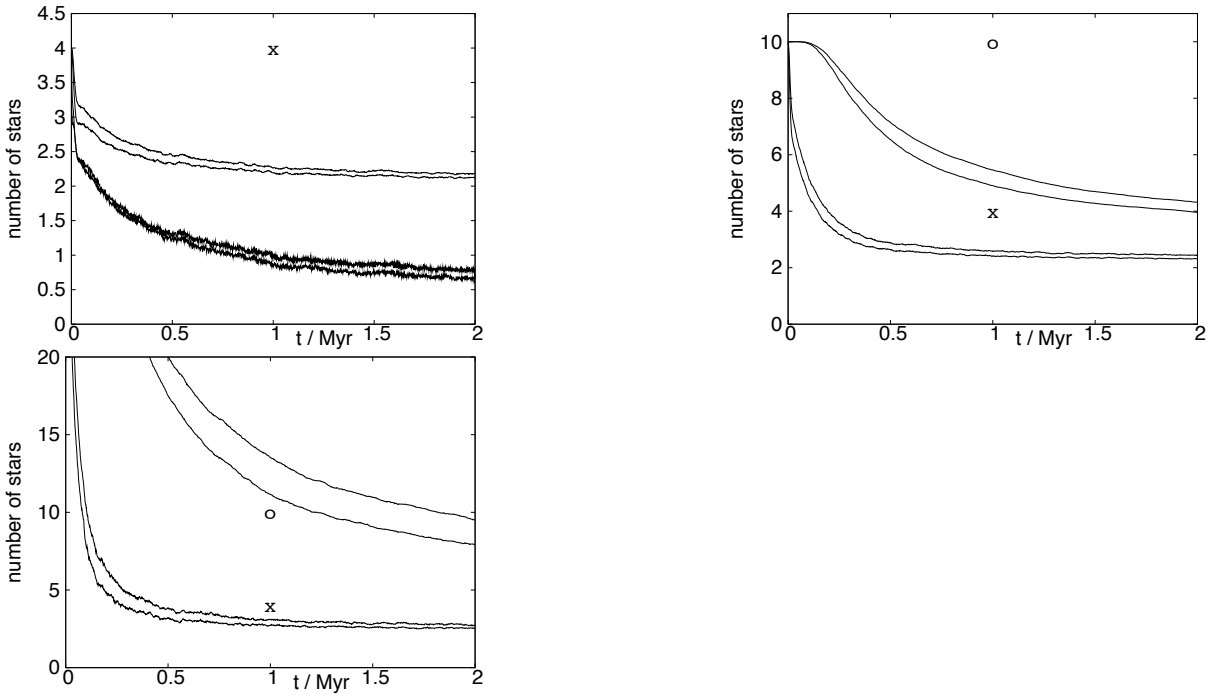

Figure 2.2: Decay curves for the N=4,10,40 models. Plotted is the mean number of stars for configurations with maximum member numbers having a certain pairwise distance as a function of time. The bold x marks the position of the present ONC-TS with an assumed age of 1 Myr, and the bold o marks the observed OB-stars in the ONC. *left*: Decay of the 4-body model where the pairwise distance lies (from bottom to top) between 0.01 and 0.05 pc (3d), between 0.01 and 0.05 pc (2d), below 0.05 pc (3d) and below 0.05 pc (2d). *middle*: Decay of the 10-body model where the pairwise distance lies (from bottom to top) below 0.05 pc (3d), below 0.05 pc (2d), below 1 pc (3d) and below 1 pc (2d). *rigth*: Decay of the forty-body model where the pairwise distance lies (from bottom to top) below 0.05 pc (3d), below 0.05 pc (2d), below 1 pc (3d) and below 1 pc (2d).

a volume of 25 pc in diameter which comes close to the observed properties of the Upper Scorpius OB association as pointed out in Sec. 2.2.2.

2.7 Error Analysis

An important question concerning N-body simulations is whether we can trust them. This question arises from the fact that the basic process for the decay of N-body systems are close and highly eccentric encounters of stars with a consequent redistribution of energy. These kind of encounters are the most important sources for orbit-errors. Due to the exponential instability the numerical and true solution deviate increasingly with time. (Goodman et al., 1993; Heggie & Hut, 2003)

As there exists no general analytic solution for systems with more than 2 bodies the integrals of motion have to be checked for conservation to control the integration. The

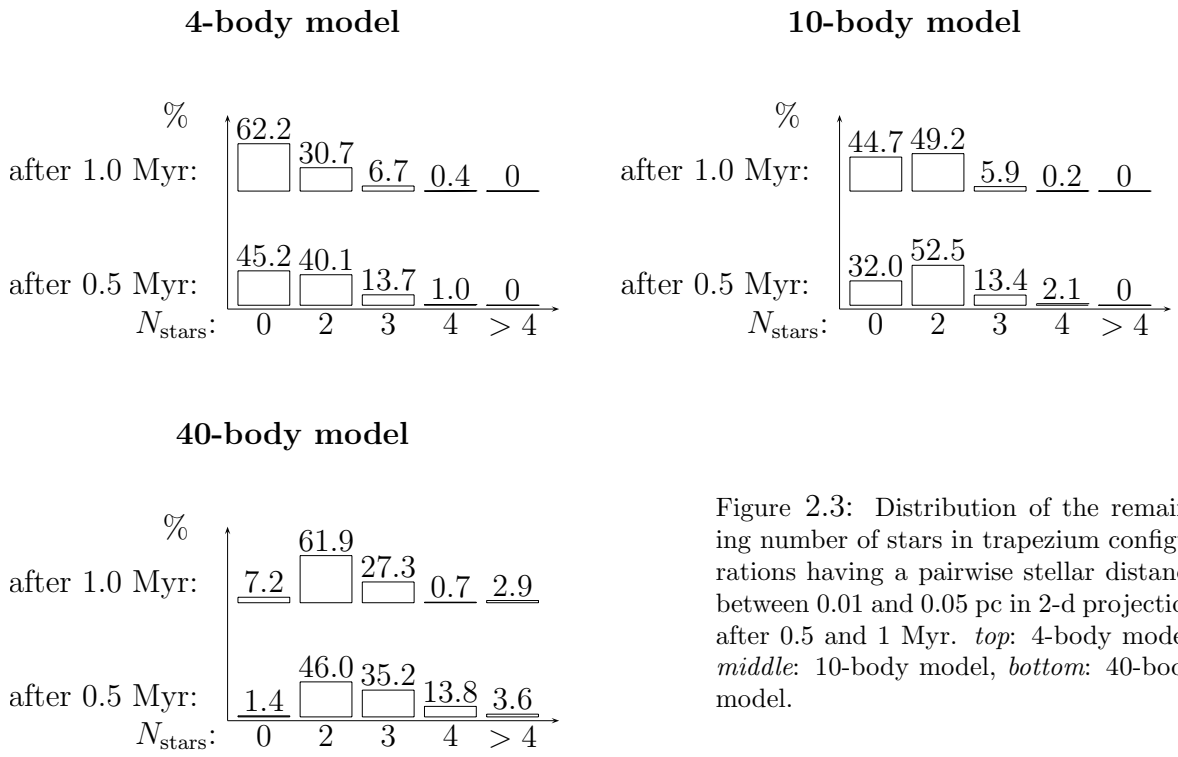

Figure 2.3: Distribution of the remaining number of stars in trapezium configurations having a pairwise stellar distance between 0.01 and 0.05 pc in 2-d projection after 0.5 and 1 Myr. *top*: 4-body model, *middle*: 10-body model, *bottom*: 40-body model.

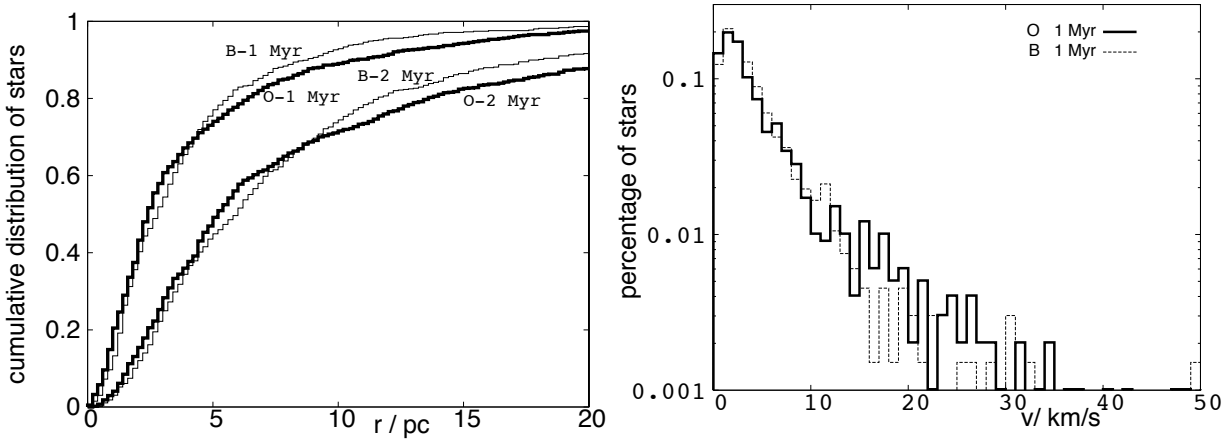

Figure 2.4: *left*: Cumulative spatial distribution of O and B stars for the 40-body model after 1 and 2 Myr measured relative to the total centre of mass. *right*: logarithmic Distribution of the velocities of O and B-stars for the 40-body model after 1 Myr. Double stars are considered using their centre of mass velocity.

most sensitive quantity is the total energy. Smaller step sizes reduce the amount of the error but prolong the duration of the integration, while step-sizes that are too small lead to the accumulation of roundoff errors. So a balance between efficiency and accuracy needs to be found.

Dejonghe & Hut (1986) determined the accuracy of the integration of 14 small-N configurations using the time-reversal-test compared with energy conservation, leading to the conclusion (Aarseth, 2003) that using the energy error only is questionable for establishing exact integrations.

When using the statistical approach, high accuracy is not essential to obtain meaningful results, provided the sample is sufficiently large (Aarseth, 2003). Valtonen (1974) determined that the distributions of eccentricity, terminal escape velocity and life-time in 200 3D experiments did not show any clear accuracy dependence for a relative energy error range from $5 \cdot 10^{-4}$ to $3 \cdot 10^{-2}$.

Therefore, despite the fact that the orbits are completely wrong after many crossing times, the statistical outcome from many equivalent N-body experiments is reliable.

To test what value of energy error is acceptable we run all 1000 four-body configurations three times with different step-size parameters. The resulting mean energy errors are $5.65 \cdot 10^{-12}$, $2.73 \cdot 10^{-6}$ and $6.19 \cdot 10^{-2}$ with increasing step-size parameter (Fig. 2.5).

To compare the statistical error with the numerical error we interpret this analysis as a series of Bernoulli-experiments. One experiment is the determination of a trapezium consisting of $N_{\rm stars}$ stars after a certain time T. The outcome can be *yes* with probability p and *no* with the probability $1-p$. This experiment is repeated $n = 1000$ times. Therefore the probability to get k times the event *yes* is given by

$$P(k) = \binom{n}{k} \; p^k \; (1-p)^{n-k} \, . \tag{2.13}$$

The event probability is approximated by the mean probability

$$p = \bar{p} = (k_1 + k_2 + k_3/3)/n = \bar{k}/n, \tag{2.14}$$

where $k_{\rm i}$ is the number of events in each of the three experiment series. The variance of the Bernoulli-distribution is given by

$$\Delta k^2 = n \; p - p^2. \tag{2.15}$$

The corresponding probability p, number of experiments n, mean number of events $\bar{k}$, variance $\sqrt{\Delta k^2}$ and one sigma errors $\Delta\%$ for the histograms in Fig. 2.5 are given in Tab. 2.6. As an example we consider trapezia consisting of 2 bodies after 1 Myr. The mean number of runs having a trapezium of 2 bodies after 1 Myr is 802 out of 1000 (80.2 %). The one sigma variance is 2.8 %. So all three experiments (81.9 %, 79.9 % and 78.9 %) lie within 1 sigma around the mean value (80.2 % $\pm$ 2.8 % = 77.4 % – 80.2 %). So if a

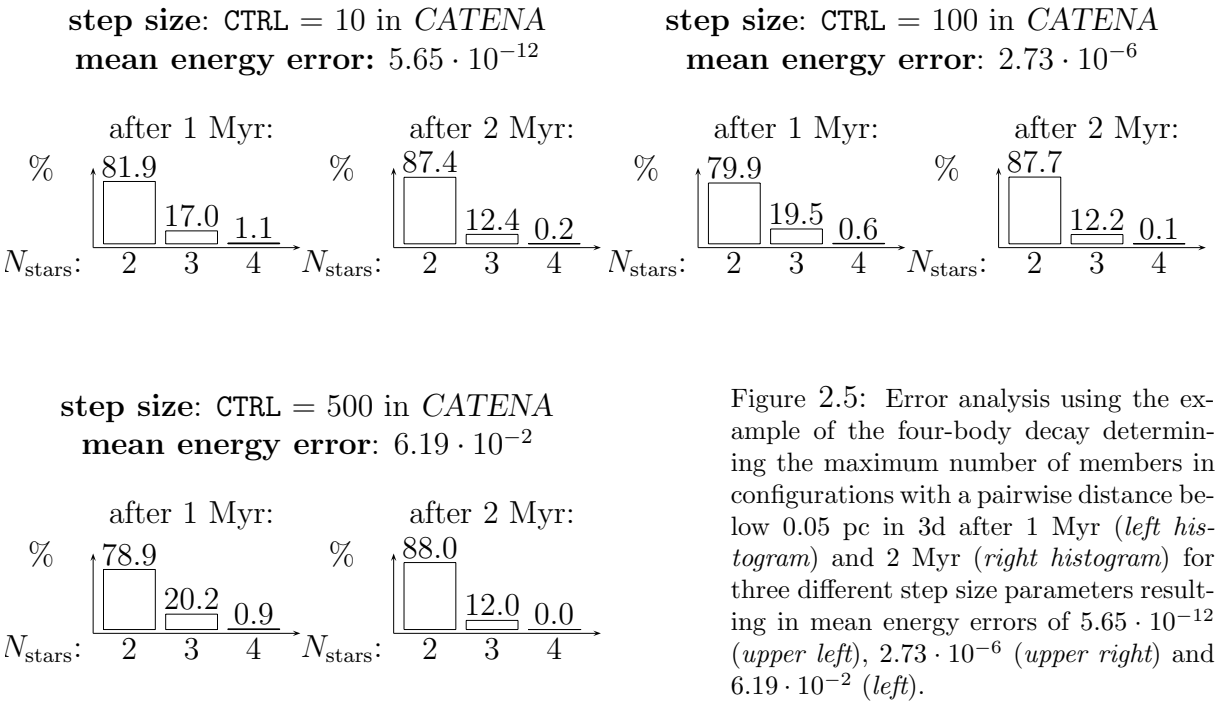

Figure 2.5: Error analysis using the example of the four-body decay determining the maximum number of members in configurations with a pairwise distance below 0.05 pc in 3d after 1 Myr (*left histogram*) and 2 Myr (*right histogram*) for three different step size parameters resulting in mean energy errors of $5.65 \cdot 10^{-12}$ (*upper left*), $2.73 \cdot 10^{-6}$ (*upper right*) and $6.19 \cdot 10^{-2}$ (*left*).

numerical error arises from the different choice of the step-size parameter it is not larger than the statistical error. We conclude that we can trust these N-body simulations.

From the virial theorem

$$E = V/2, \tag{2.16}$$

where E is the total energy and V is the potential energy, the relative energy error is

$$\Delta E/E \approx \Delta V/V, \tag{2.17}$$

and with

$$V = -G\,\frac{M^2}{R}, \tag{2.18}$$

$$\Delta E/E \approx \Delta R/R, \tag{2.19}$$

follows. This means that uncertainty in the pairwise distances is of the order of the mean energy error. As the energy errors are smaller than $6 \cdot 10^{-2}$ the distance errors have only a very slight effect on the number statistics.

2.8 Conclusions

We have pointed out that in the case of the Orion Nebula cluster two main problems exist: Its short decay-time implying the question as to why it exists, and the significant number

T/Myr	1	1	1	2	2	2
$N_{\rm stars}$	2	3	4	2	3	4
n	1000	1000	1000	1000	1000	1000
$\bar{k}$	802.3	18.9	8.7	877.0	122.0	1.0
p	0.802	0.189	0.087	0.877	0.122	0.010
$\sqrt{\Delta k^2}$	28.3	13.7	9.3	29.6	11.0	3.2
$\Delta\%$	2.8	1.4	0.9	3.0	1.1	0.3

Table 2.6: Resulting variances for the error histograms in Fig. 2.5 if the search for a trapezium consisting of $N_{\rm stars}$ is interpreted as a Bernoulli-experiment.

of missing OB stars implying either that they have been lost if the IMF is invariant, or that the IMF had a highly non-standard $\alpha_3 > 2.7$ which is unlikely because no other stellar population in a cluster with such an IMF is known to exist and the observed most-massive star in the ONC is significantly larger than that expected for this non-standard IMF. It is extremely unlikely (3 out of 1000 cases) that a compact Trapezium system consisting of four stars can survive for more than 1 Myr. The assumption that the initial number of OB stars was about 40 increases the probability to observe a Trapezium system after 1 Myr (36 out of 1000 cases). We infer that the ONC Trapezium system could be an OB-star core in its final stage of decay.

This scenario is supported by the fact that the spatial distribution of these forty OB-stars obtained from the numerical simulations after 5 Myr comes close to the observed spatial distribution of the OB-stars in the Upper Scorpius OB association which is assumed, using the total mass, to have had the same young star-cluster progenitor as the ONC.

Given its total mass the ONC indeed ought to have four times as many OB stars than are observed, namely 40. This suggests that about 30 OB stars may have been expelled from the ONC if the IMF is invariant. Starting with an initial number of OB stars of about 40, stars are ejected due to three-body encounters, so that this model matches the observed number of OB stars in the ONC and the ONC Trapezium.

As it has been shown that the probability that only 10 OB-stars have formed in the ONC is very small, the missing stars must be somewhere. After 1 (2) Myr 90 (70) % of all OB-stars should be found within a 10 pc radius around the ONC centre. It is straightforward to search for these missing OB-stars in OB catalogues. If they cannot be found then the IMF may be steeper at the high mass end. Or OB stars form with an initially high binary fraction so that ejections occur faster and the resulting velocities are higher, placing them even further away from the ONC centre after 1 (2) Myr.

Due to the absence of primordial binaries ours is a conservative result because binaries enhance the ejection rates. Therefore the influence of primordial binaries must be investigated in further experiments, which will also need to consider gas expulsion from the embedded cluster (Kroupa et al., 2001; Vine & Bonnell, 2003). Vine & Bonnell (2003)

investigated the evolution of cores of young star clusters and their massive stars but used a smoothed potential to avoid the difficulties coming up with the occurrence of close encounters. But these close encounters are the energy sources for massive star ejections and the reasons why young stars can be found far away from the cluster centre within a short period of time.

The influence of the cluster potential and especially of two-body relaxation with low-mass stars in the cluster shell may also be investigated in further simulations. Of what kind this influence is is still somewhat unclear. Stronger constraining forces by the cluster potential and energy-loss by two-body relaxation may return some of the OB-stars evaporated with low velocities from the core. This may stabilize the core on the one hand, but may also lead to a faster decay by shifting the velocity spectrum of the ejected stars to higher velocities because the stellar density at the centre would be higher. This would increase the probability of close encounters and high velocity ejections. If relaxation indeed stabilises the core then more OB-stars are expected to remain in the ONC worsening the OB-stars discrepancy. Ours is therefore a conservative result.

As a final note, Kroupa et al. (2001) have presented star-cluster-formation calculations that reproduce the ONC at an age of 1 Myr *and* the Pleiades at an age of 100 Myr. These models, however, are about 1.8-times as massive as the ONC mass used here ($2200\,M_\odot$) implying that if the IMF was canonical then the ONC may have had $1.8 \times 40 = 72$ stars more massive than $5\,M_\odot$. This would pose an increased challenge, because as is evident from Fig. 2.2, 40 OB stars already lead to an acceptable match with the data, so 72 would increase the probability of finding a trapezium-configuration at an age of 1 Myr, but would lead to too many OB stars within the cluster (as can be deduced from the lower-panel in Fig. 2.2).

Clearly, such models with a high initial multiplicity fraction need to be constructed for further studies of the intricate interrelation of the IMF with stellar dynamics in young clusters.

Chapter 3

Captured older stars as the reason for apparently prolonged star formation in young star clusters

Pflamm-Altenburg, J., Kroupa, P., 2007, **MNRAS**, 375, 885

The existence of older stars within a young star cluster can be interpreted to imply that star formation occurs on time scales longer than a free-fall time of a pre-cluster cloud core. Here the idea is explored that these older stars are not related to the star formation process forming the young star cluster but rather that the orbits of older field stars are focused by the collapsing pre-cluster cloud core. Two effects appear: The focussing of stellar orbits leads to an enhancement of the density of field stars in the vicinity of the centre of the young star cluster. And due to the time-dependent potential of the forming cluster some of these stars can get bound gravitationally to the cluster. These stars exhibit similar kinematical properties as the newly formed stars and can not be distinguished from them on the basis of radial-velocity or proper-motion surveys. Such contaminations may lead to a wrong apparent star-formation history of a young cluster. In the case of the ONC the theoretical number of gravitationally bound older low-mass field stars agrees with the number of observed older low-mass stars.

3.1 Introduction

Palla et al. (2005) determined the ages of 84 low-mass ($m \approx 0.4 - 1.0$ M$_\odot$) stars in the Orion Nebula cluster (ONC) from isochrones and lithium depletion. Four of these stars have ages between 10 and 18 Myr, whereas the bulk of all stars have ages below 3 Myr.

They conclude that stars in the ONC formed moderatly over a long time period exceeding 10 Myr ending in a sharp peak of star formation. This age spread of stars in the ONC has already been recognised by Isobe & Sesaki (1982), who determined ages from 10^4 yr up to 30 Myr and that low-mass stars in the Orion Nebula region have the same ages as the oldest stars in the Orion association Ia.

This contradicts recent results that the process of star formation is rapid. In the case of the Taurus star forming region Hartmann (2003) has shown that after correcting the sample of stars for possible foreground contamination, the age spread narrows. Also, observations suggest that star formation occurs in only one or two crossing times (Elmegreen, 2000) which results in age spreads much smaller than 10 Myr.

Contrary to this, Tan, Krumholz, & McKee (2006) present observational and theoretical arguments that rich star clusters requires at least several dynamical time-scales to form and they are quasi-equilibrium structures during their assembly. For the ONC they concluded that it has formed over $\gtrsim$ 3–4 dynamical times.

Indeed, the measurements by Palla et al. (2005) are excellent, comparing ages of stars in the ONC derived with different methods. But the existence of older stars in the ONC must not stringently imply that star formation is an extended process. Given the velocity dispersion of the low-mass stars in the ONC is approximately 2.5 km s^{-1} (Hillenbrand & Hartmann, 1998) a star not originating from the ONC can come from a place up to 25 pc away if it is 10 Myr older than the cluster member stars.

In the case of ω Cen ($2.5 \cdot 10^6$ $M_\odot$) Fellhauer, Kroupa, & Evans (2006) have shown that a massive stellar super-cluster may trap older galactic field stars during its formation process that are later detectable in the cluster as an apparent population of stars with a very different age and metallicity. Up to about 40% of its initial mass can be additionally gained from trapped disc stars, while certain conditions may even lead to such a massive cluster capturing a multiple of its own mass.

Here we show that a collapsing pre-ONC cloud core leads to an enhancement of fore- and background stars and to the capture of some older field stars so that they are gravitationally bound by the new star cluster. Given realistic initial conditions the order of magnitude of the number of captured stars agrees with the number of older low-mass stars in the ONC. These captured older stars have similar radial velocities and proper motions as the newly formed stars in the ONC and can therefore not be distinguished kinematically from the new stars, which will lead to a much wider derived age spread.

3.2 Model

The entire model consists of a collapsing pre-cluster cloud core embedded in a uniform field population of older stars, which — in the case of the ONC — can be a slowly expanding association.

The collapsing pre-cluster cloud core is described by a time-dependent Plummer po-

tential

$$\Phi_{\rm cl}(t) = -M_{\rm cl}\ G\ \left(r^2 + b_{\rm cl}^2(t)\right)^{-\frac{1}{2}}, \tag{3.1}$$

where $M_{\rm cl}$ is the constant total mass of the collapsing cloud. The Plummer parameter, $b_{\rm cl}(t)$, is a function of time to describe the growing potential starting with an infinite value and ending with a finite final value within a finite time to account for the ongoing concentration of the pre-cluster cloud core forming a new star cluster.

The background stars are set up in a sphere centred on the origin of the Plummer potential. The positions of the stars are uniformly distributed and their initially isotropic velocities have a Gaussian distribution. Choosing a field-sphere is uncritical as long as its radius is large enough.

In this model the stars do not interact gravitationally. They move as test particles in an external potential. The stellar masses can be eliminated in the equation of motion and the result does not depend on the masses of the stars.

The orbit of the field stars are integrated using a standard Hermite scheme (Makino, 1991; Hut et al., 1995; Aarseth, 2003). The total energy is used to control the integration. Due to the time-dependent cloud potential the total energy is not conserved. Therefore the path integral,

$$W = \int \mathbf{F}_{\rm cl}{\cdot}{\rm d}\mathbf{r} \quad , \tag{3.2}$$

of the stars in the force field of the cloud is computed. Given the energies,

$$E_0 = U_0 + T_0 \quad \text{and} \quad E_t = U_t + T_t \quad , \tag{3.3}$$

where E_0, U_0 and T_0 are the total, potential and kinetic energies at the initial time t_0 and E_t, U_t and T_t are the total, potential and kinetic energies at an arbitrary time point t, we control the calculations by the total energy error

$$\epsilon = \frac{E_0 - (E_t - W)}{E_0}. \tag{3.4}$$

In all simulations the total relative energy error is less than 10^{-11} per particle.

3.3 Initial Conditions

To simulate the capture of stars by the above model, initial conditions for the underlying stellar field population and the collapsing cloud must be specified. In the case of the ONC the stellar background population is given by a postulated surrounding association.

3.3.1 Collapsing cloud

According to Hillenbrand & Hartmann (1998) the virialized total mass of the ONC is determined to be about 4500 $M_\odot$ while only one half is visible in stellar material. If

virialisation of the very young ONC is assumed before gas expulsion has started then the cloud mass, $M_{\rm cl}$, can be set to 4500 $M_\odot$.

The cloud collapse begins at time t_b and ends at t_e after the collapse time, $\tau_{\rm cl}$, has elapsed. For a constant cloud mass the increasing compactness of the collapsing cloud is described by a Plummer parameter of $+\infty$ before the collapse starts and has the constant value b_0 when the collapse finishes. Between these points the Plummer parameter is interpolated simply by

$$b_{\rm cl}(t) = \begin{cases} +\infty & ; \quad t < t_b \quad , \\ b_0 \, \frac{(t_e - t_b)}{t - t_b} & ; \quad t_b \leq t \leq t_e \quad , \\ b_0 & ; \quad t > t_e \quad , \end{cases} \tag{3.5}$$

where $t_e - t_b$ is the collapse time $\tau_{\rm c}$. Hillenbrand & Hartmann (1998) specify the core radius (projected half-density radius) of the current ONC to lie between 0.16 and 0.21 pc. The actual core radius $r_{\rm c}$ and the Plummer radius b_0 are related by

$$r_{\rm c} = \left(\sqrt{2} - 1\right)^{\frac{1}{2}} \, b_0 \approx 0.64 \, b_0 \quad , \tag{3.6}$$

which implies a current Plummer radius for the ONC between 0.25 and 0.33 pc. Here we choose $b_0 = 0.30$ pc for the ONC as a mean value.

The collapse time, $\tau_{\rm c}$, of the pre-cluster cloud core is estimated by the free-fall time scale (Elmegreen, 2000)

$$t_{\rm ff} \approx \sqrt{\frac{R}{G \, M_{\rm cl}}} \quad . \tag{3.7}$$

If the extension of the cloud at the onset of collapse was 1 pc, the corresponding free-fall time is computed to be about 0.22 Myr, in the case of 5 pc as the initial radius the free-fall time-scale is 2.50 Myr and 7.07 Myr for a 10 pc radius. By measuring the offset between HII- and CO-arms in spiral galaxies Egusa et al. (2004) determined the time for star clusters to "hatch" from their natal cluster to be about 5 Myr. Also Weidner, Kroupa, & Larsen (2004) conclude from a comparison of star formation rates and maximum cluster masses in a large ensemble of galaxies that pre-cluster cloud cores have radii of about 5 pc if they form in a free fall period. Because the possible collapse time-scale can vary over 2 decades the collapse time $\tau_{\rm c}$ is taken here to vary between 0.1 up and 10.0 Myr.

3.3.2 Underlying field population

The task to make a specific setup for the underlying field population at the onset of the collapse is far more difficult than for the collapsing cloud. The conditions of the stellar density before collapse have to be estimated. For example, the stellar local mass density of the solar neighbourhood is about 0.1 $M_\odot$ pc^{-3} (Bahcall, Flynn, & Gould, 1992; Bienayme, Robin, & Creze, 1987; Kuijken & Gilmore, 1989; Kroupa, Tout, & Gilmore, 1993). In

the compiled radial morphology around Θ^1C (Hillenbrand & Hartmann 1998; Herbig & Terndrup 1986) the outermost population (the Orion Ic association) has an extent of more than 25 pc. The embedding cloud Orion A also contains a large number of small groups and a significant distributed population (Megeath et al., 2005; Strom & Strom, 1993). The ONC is thus part of a region with low- and high mass star formation in the recent past and at present. So it can be assumed that the stellar density must have been higher at the onset of the pre-cluster cloud collapse than in the solar vicinity. We choose the background as a sphere with a radius of 12.5 pc, corresponding to the extent of the embedding association. 2410 stars distributed in this sphere would give a mean number density of 0.3 stars pc^{-3} or a mass density of 0.1 M$_\odot$ pc^{-3} equal to the mean stellar mass density of the solar vicinity. Here, the number of background particles is rather taken to be 20000 on two grounds: the resulting density, 2.44 stars pc^{-3} or 0.83 M$_\odot$ pc^{-3}, is slightly higher than the density in the solar vicinity and this high number of particles guaranties useful statistical results. These 20000 stars could have been formed e.g. in two ONC-type star clusters.

In fact, the total number of stars within the setup sphere and its radius are not the primary parameters affecting the results, but rather the resulting number density and the initial velocity dispersion. As these stars act as test particles the results can be scaled linearly with the initial uniform density.

For the brightest members of the ONC van Altena et al. (1988) found a one-dimensional velocity dispersion of 1.49 km s^{-1}, while Jones & Walker (1988) specify the velocity dispersion to be slightly larger with 2.34 km s^{-1}. In Hillenbrand & Hartmann (1998) a value of 2.81 for stellar masses between $0.1 < m/\mathrm{M}_\odot < 0.3$ and 2.24 km s^{-1} between $1 < m/\mathrm{M}_\odot < 3$ is reported. If the underlying stellar background population had a similar progenitor the velocity dispersion can be assumed to be of the same order, i.e. 1$\sim$3 km s^{-1}. Thus we vary the one dimensional initial velocity dispersion of the background sphere from 0.5 (0.87) up to 3 (5.20) km s^{-1} (three dimensional dispersion in parentheses).

Summarising, the choice of the initial background population is a follows: 20000 particles are uniformly distributed over a sphere with a radius of 12.5 pc, giving a stellar density of 2.4 stars pc^{-3}. The particles have a Maxwellian velocity distribution and a random direction. The velocity dispersion, σ, of the different models varies from 0.5 km s^{-1} to 3.0 km s^{-1}. The background sphere and the collapsing cloud have the same velocity centroid.

3.4 Stellar capture

3.4.1 Number of expected captured stars and the IMF

Palla et al. (2005) selected a sample of 84 stars in the range $\approx$0.4–1.0 M$_\odot$ and with isochronal ages greater than $\sim$ 1 Myr out of the ONC-survey made by Hillenbrand (1997).

This ONC-survey covers 3500 stars within 2.5 pc of the central Trapezium. The low-mass stars of the sample have a membership probability greater than 90 per cent. 6 stars (7.1 per cent) of the sample of 84 stars have isochronal ages $\gtrsim$ 10 Myr, whereas four of them show a significant lithium depletion. The ages derived from the amount of lithium depletion confirm the ages derived from isochronal lines.

To estimate the expected total number of older stars in the ONC this sample must be extrapolated to the entire ONC. The actual total mass of the ONC is given by Hillenbrand & Hartmann (1998) to be about 1800 $M_\odot$. Using the universal or standard/canonical IMF (Kroupa, 2001; Weidner & Kroupa, 2006; Pflamm-Altenburg & Kroupa, 2006) and the "WK-normalisation" method the ONC should have formed 694 low-mass stars in the mass regime 0.4–1.0 $M_\odot$. Note that the "WK-normalisation" refers to the maximum mass of the star being determined by the cluster mass (Weidner & Kroupa, 2004, 2006). This determines the normalisation constant of the IMF. Given 6 older stars out of a sample of 84 stars, then 78 stars of this sample should have formed in the ONC. Thus, $6/78 \times 694 \approx 53$ older stars are expected among 694 newly formed stars after linear extrapolation.

3.4.2 Calculated number of captured stars

After the collapse time τ_c, when the collapse has stopped, then a star is identified to be captured by the collapsed cloud if the star is gravitationally bound and lies within a 2.5 pc radius of the centre of the potential, according to the extend of the ONC-survey by Hillenbrand (1997): after the collapse stops the distance of the star to the origin of the Plummer sphere is less than 2.5 pc and the total energy of the stars is less than required to get farther away than 2.5 pc from the centre of the potential. This means that a captured star is gravitationally bound to the new cluster. As the virial mass of the current ONC is about 4500 $M_\odot$ but only one half is visible in stellar material (Hillenbrand & Hartmann, 1998), the ONC is super-virial (kinematically too hot). This can be solved if the ONC is expanding after gas expulsion (Kroupa, Petr, & McCaughrean, 1999; Kroupa, Aarseth, & Hurley, 2001). The whole cluster is expected to have been virialized between the stop of the pre-cluster cloud core collapse and the start of gas expulsion. After gas expulsion the older captured stars follow the dynamical evolution of the young star cluster. So it is justified to identify a captured star by the criterion that it be gravitationally bound to the collapsed cloud when the collapse of the pre-cluster cloud core stops.

The number of captured stars in dependence of the collapse time-scale, τ_c, can be seen in Fig. 3.1. The initial stellar density is 2.44 stars/pc^3 implying a total number of stars placed initially within a 2.5 pc radius around the centre of the potential of 160 (Section 3.3.2). A decreasing collapse time means that the time-dependent period becomes shorter and the potential behaves increasingly as an instantaneously switched on potential. Therefore only those stars being initially within the 2.5 pc sphere can be captured for short τ_c. Out of these candidates only that fraction of stars is captured

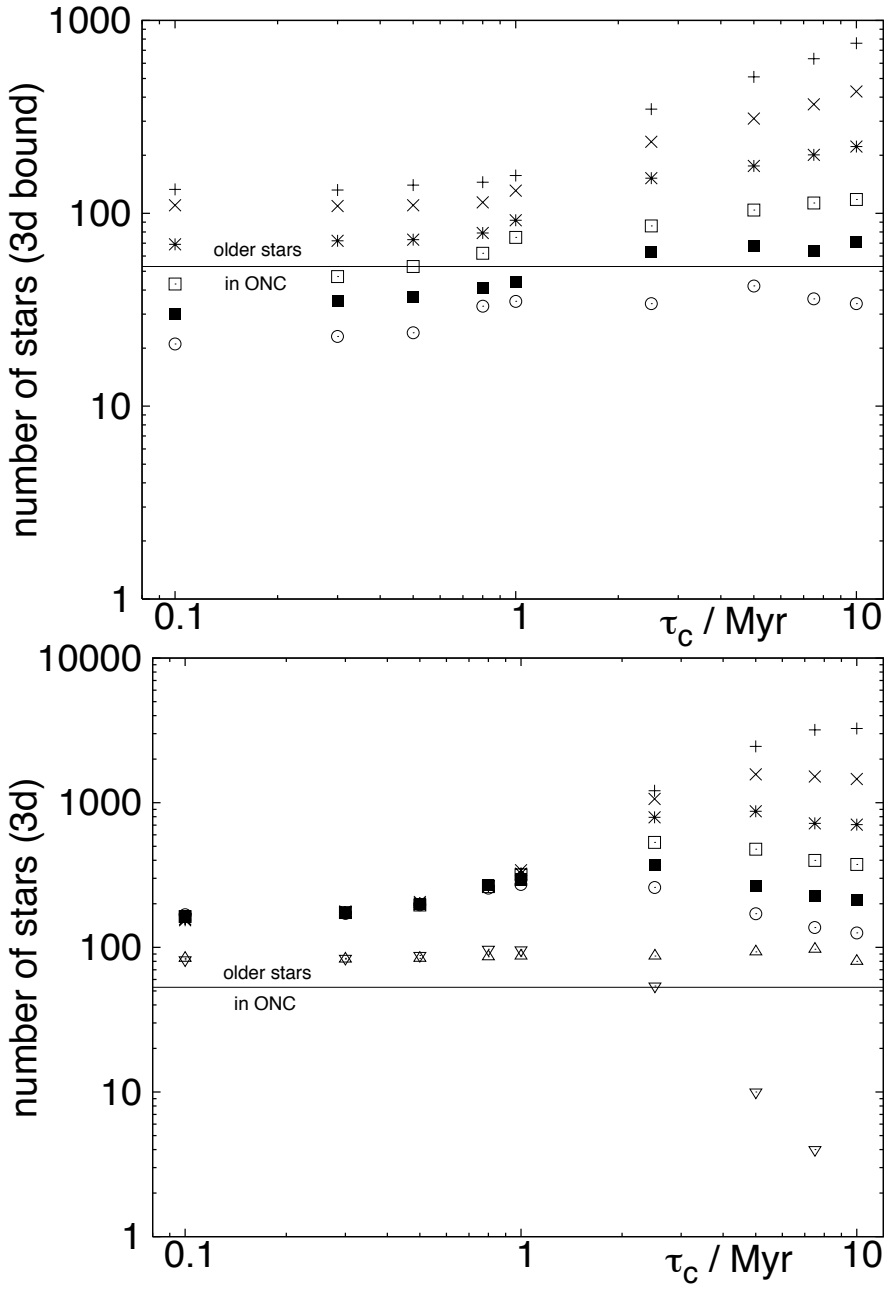

Figure 3.1: Number of stars within 2.5 pc of the centre after the collapse time-scale, τ_c, has elapsed and the collapse stops. *Top*: Number of stars within 2.5 pc of the centre of the potential *and* gravitationally bound. *Bottom*: Number of stars within 2.5 pc of the centre of the potential. *Symbols*: Models with a one-dimensional velocity dispersion, σ, of the background field in presence of the collapsing cloud: σ = 0.5 km s^{-1} (+), 1.0 km s^{-1} ($\times$), 1.5 km s^{-1} ($*$), 2.0 km s^{-1} ($\boxdot$), 2.5 km s^{-1} ($\blacksquare$), 3.0 km s^{-1} ($\odot$). The open triangles denote the number of stars within 2.5 pc radius of the centre of the background sphere with time if *no* cloud potential is present for two different field-star velocity dispersions: σ = 0.5 km s^{-1} ($\triangle$) and 3.0 km s^{-1} ($\triangledown$). The horizontal line marks the region of the 53 expected older low-mass stars in the ONC. For details see text.

having a velocity less than a certain limit. Thus the models with the shortest collapse time of 0.1 Myr converge against the initial star number of 157 with decreasing field-star velocity dispersion (Fig. 3.1, top). With increasing collapse-time more stars are able to move inwards loosing energy in the time-dependent potential and the number of captured stars increases. In the case of the highest field-star velocity dispersion the number of captured stars turns over at large collapse times because the potential is very low initially for a longer period. The diffusion of the background sphere then dominates over orbit focussing by the increasing potential.

To compare the number of captured stars calculated in these simulations with the number expected it has to be taken into account that the test particles forming the background sphere represent a realistic stellar population having a mass spectrum. Given a canonical IMF 13.5 per cent of all stars lie in the mass regime 0.4–1.0 $M_\odot$. For the preferential value of the collapse time of 5 Myr the number of captured stars is 42 (510) if the velocity dispersion of the background sphere is 3.0 (0.5) km s^{-1}, resulting in 6 (69) captured low-mass stars.

Given its age of about 1 Myr the ONC is already dynamically evolved and has expelled its gas almost completely. Its virial mass of about 4500 $M_\odot$ is more than twice larger than the stellar mass. Being nearly virialized at its formation the ONC has already started to expand implying that its concentration must have been larger initially and its describing Plummer parameter b_0 must have been smaller than 0.3 pc, when cloud collapse has stopped. This has been confirmed by numerical simulations (Kroupa et al., 2001). Thus the potential would have been deeper than assumed in the present calculation, and the number of captured stars would be higher than determined here.

Therefore, the existence of older stars in the ONC does not necessarily imply that star formation is prolonged – dynamical capture can explain the presence of older stars in the ONC and in young star clusters in general.

From the dynamical point of view these gravitationally bound stars are true cluster members. It is not a question of measurement accuracy that these stars are identified to be cluster members. So even GAIA can not distinguish between the older stars captured by cloud collapse and the stars formed in the young star cluster, although on average the captured stars would have a flatter density profile than the stars formed in the cluster (Fellhauer et al., 2006).

As the membership probability of the sample of low-mass stars in the ONC, selected by Palla et al. (2005), is greater than 90 per cent but not 100 per cent, based on proper motion and radial velocity studies, it is possible that these older stars (or some of them) are part of the fore- and background contamination. But independently of the true origin of these older stars, stellar capture during pre-cluster cloud collapse must be a true physical process and older stars among newly formed stars in a young star cluster should exist.

3.5 Enhancement of stellar density

In the previous section only those stars were considered which are gravitationally bound. These constitute a fraction of all those field-stars which are deflected from their initial orbit and are focussed towards the centre of the cluster. In general, the density of the field-stars will deviate from their constant initial density in two ways.

3.5.1 Slowed-down dilution of an OB association

In absence of a collapsing pre-cloud cluster core the OB association will disperse due to its internal velocity dispersion. In presence of such a collapsing cloud the stars are increasingly attracted towards the centre of the newly formed cluster. Therefore the field-star density near the cluster centre will be kept higher during the cluster formation than in absence of the cluster potential. In the case of a collapse-time of 5 Myr and a field-star velocity dispersion of 3 km s^{-1} the number of stars within 2.5 pc of the centre of the background sphere is 108 (with cloud collapse) and 10 (without cloud collapse) when the collapse stops. This means that the field-star density will be kept higher by a factor of 10 due to the attracting potential by the collapsing cloud (Fig. 3.1, bottom).

3.5.2 Underestimation of background subtraction

When the pre-cluster cloud becomes increasingly compact then the radial dependence of its potential increases. The density of the field-stars is expected to show a similar dependence, getting higher towards to the cluster centre. The corresponding ratios of the field-star densities in the newly formed cluster and the cluster vicinity are plotted in Fig. 3.2. After the collapse has stopped the cluster density, $\rho_{\rm c}$, is calculated by the number of field stars within 2.5 pc radius of the cluster centre. The density of the field-stars, $\rho_{\rm sh}$, in the cluster vicinity is calculated by the number of stars within the shell limited by the radii of 10.0 and 7.5 pc. For a collapse time of 5 Myr and a field-star velocity dispersion of 3 km s^{-1} the density of the field-star in the new cluster is almost 10 times higher than in the vicinity of the cluster. This has to be taken into account when surveys of star clusters are corrected by the fore- and background contamination.

In general three tendencies can be seen. i)The density contrast increases with an increasing collapse-time. ii) For a constant collapse time the density contrast increases with an increasing initial velocity dispersion of the background population. iii) With increasing collapse-time the final density ratios for different initial velocity dispersions are less different.

The behaviour of the data in Fig. 3.2 can be understood by noting the following: If the full potential would be switched on instantaneously then the density contrast would be unity. With an increasing collapse-time more stars can move towards the cluster centre

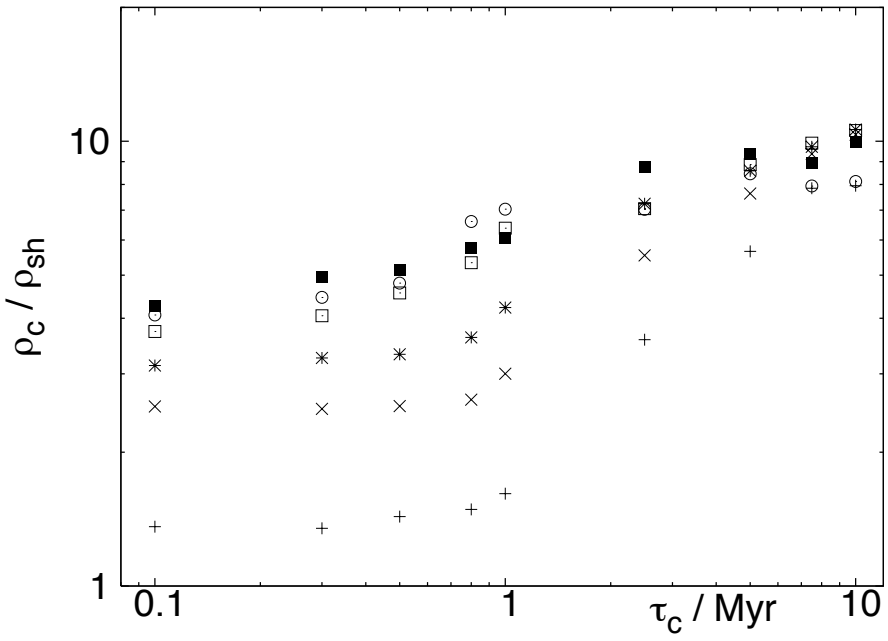

Figure 3.2: Ratio of the field-star density in the cluster, $\rho_{\rm c}$, and in the vicinity of the cluster, $\rho_{\rm sh}$, after the collapse has stopped. *Density in the cluster*: Number of stars within 2.5 pc radius of the cluster centre divided by the volume of the sphere. *Density in the vicinity*: Number of stars in the shell between 10 and 7.5 pc divided by the volume of the shell. *Symbols*: Models with a one-dimensional velocity dispersion, σ, of the background field in presence of the collapsing cloud: $\sigma = 0.5$ km s^{-1} (+), 1.0 km s^{-1} ($\times$), 1.5 km s^{-1} ($\ast$), 2.0 km s^{-1} ($\square$), 2.5 km s^{-1} ($\blacksquare$), 3.0 km s^{-1} ($\odot$).

and the density contrast increases. Within a constant collapse-time more stars can move towards the cluster centre if the initial velocity dispersion is higher.

3.6 Discussion

As the region, where the ONC lies in, is a location of high star formation, the initial conditions prior to pre-cluster cloud collapse, i.e. the stellar density and distribution, are difficult to estimate. If the older ONC stars have not formed in the ONC as a result of prolonged star formation then where could they have formed?

Given the age of the association Orion OB1c surrounding the ONC of about 4.6 Myr (Brown et al., 1994) the observed older stars in the ONC, having an age greater than 10 Myr, can not have formed in the parent cluster of this association.

The association Orion OB1a has an age of approximately 11 Myr. The projected distance from its centre to the ONC is of about 5 degrees, i.e. 35 pc given a mean distance of 400 pc of both associations. The line-of-sight distance between Orion OB1a and the

ONC is approximately 117 pc (Brown et al., 1999). Then the probably captured low-mass stars, if formed in the association Orion OB1a, must have had a spatial velocity of 12 km s^{-1} relative to the centre of the ONC for them to have drifted to the current distance of the ONC. If the time-scale of the pre-cloud core collapse is taken into account the velocity must be even higher. Stars from such a population would not have been captured. Additionally, Brown et al. (1999) listed 61 OB stars for the Orion OB1a association. Given a canonical IMF the parent cluster should have contained about 3150 $M_\odot$ in stars and therefore 1100 stars between 0.4 and 1.0 $M_\odot$. If all these low-mass stars are completely radially dispersed during the expansion of the OB-association the stellar flux at the ONC would have been 6×10^{-3} stars/pc^2. Given a radius of 2.5 pc of the ONC then 0.5 stars with masses between 0.4 and 1.0 $M_\odot$ have passed through the ONC, too few compared to the estimated number of older low-mass stars of 53. It seems to be unlikely that these older stars have formed in Orion OB1a, although its age would be consistent with this.

The nearer association Orion OB 1b has an age of 1.7 Myr (Brown et al., 1994). This is contrary to the ages determined by Blaauw (1991) (7 Myr) and by Warren & Hesser (1978) (5.1 Myr). Nevertheless, it can be concluded that Orion OB 1b might be too young to be the origin of the older stars in the ONC.

The compact ONC has 3500 stars within a radius of 2.5 pc around Θ^1 C (Hillenbrand, 1997), giving a number density of 528 stars pc^{-3}. As the current ONC has an age of approximately 1 Myr it is already dynamically evolved. Using full N-body simulations including gas expulsion Kroupa, Aarseth, & Hurley (2001) have shown that initially the ONC may have contained approximately 10^4 stars and brown dwarfs to match its current state. This means that the ONC has already lost 65 per cent of stars. To get 20000 stars within a sphere of 25 pc in diameter 2 ONC-type cluster are required. This huge amount of past star formation should still be observable in terms of an association. At least the $2 \times 39 = 78$ O-stars, given a canonical IMF, should still be visible. Given the live time of a 20 $M_\odot$ star of approximately 9.9 Myr (Schaerer et al., 1993), then $2 \times 10 = 20$ supernovae should have occurred, where 10 $m \geq 20$ $M_\odot$ stars occur in a population of 39 $m \geq$ $M_\odot$ stars. Reducing the radius of the background sphere to 9.9 pc then only 10000 stars or one ONC-type star cluster would be required to keep the initial stellar density of 2.4 stars/pc^3. Using a canonical IMF the mass of a star cluster must be less than 160 $M_\odot$ to contain less than 1 O star. Nearly 20 such low-mass clusters are required to produce 2×10^4 stars in total. If the background sphere had only a radius of 9.9 pc then only 10 such low-mass clusters are needed to form the initial background density. If these low-mass clusters formed more than 10 Myr ago, then they are not expected to be still visible, as such small star clusters disperse rapidly. Also, many of these older stars should be mixed up with the ONC.

However, our results do not exclude the possibility that the ONC formed over about 3 Myr, i.e. a few free-fall times (Tan et al., 2006). The important time scale for the effects described here is the time scale of potential formation and not the time scale of star formation.

Possibly, the most likely source of the older low-mass star population might be a large number of small groups producing low-mass stars as are also observed today but only 10 Myr earlier (Megeath et al., 2005). For example, Kroupa & Bouvier (2003) have shown that small Taurus-Auriga-type groups disperse on a time scale of a few Myr.

In our initial conditions it is assumed that the ONC and the background sphere have the same velocity centroid. If the relative velocity between the background sphere and the collapsing pre-cluster cloud core increases then fewer stars are expected to be captured. But the pre-cluster cloud core of the ONC as well as the earlier star clusters or groups, which formed the background stars, may have formed within the same molecular cloud. So a relative velocity between the different velocity centroids may have been small.

The increasing potential of the collapsing pre-cluster cloud core should not only act on already formed stars but also on protostars. Applying the results of the enhancement of the background density on the stellar population in the molecular cloud Orion A the mean motion of the young stars and the protostars should be directed towards the centre of the ONC, being more pronounced in the region of the cloud nearest to the ONC.

3.7 Conclusions

We have shown that the existence of older stars in the ONC must not necessarily imply that star formation was prolonged in the ONC. The time-dependent potential of a collapsing cloud can capture older stars of the underlying OB association. These stars exhibit similar kinematical properties leading to their identification as cluster members. The number of captured stars is in agreement with the number of observed older low-mass stars for reasonable assumptions about the pre-existing field-star population. Nevertheless, some open issues concerning the origin of the field-star population remain.

Additionally, the increasing potential of the collapsing cloud leads to an enhancement of the local stellar background density causing larger fore- and background contamination.

The number of captured stars and the amount of fore- and background enhancement significantly depend on the deepness of the final potential when the cloud collapse stops. Therefore these effects should be more distinctive for more compact and more massive star clusters (Fellhauer et al., 2006).

Moreover, the number of capture stars and the number of focussed but not captured stars depend on the surrounding density of the field stars. Therefore the number of older stars found in young star clusters that are part of a greater star-formation region and/ or are embedded in an OB association should be higher than in young star clusters formed in isolation.

We conclude that the apparent long formation time of young star clusters may be brought into agreement with the recent notion that the formation of clusters is a highly dynamic and violent process by taken into account that the short formation process leads to stellar capture from an underlying older field population. This process depends on the

time-scale of cluster potential formation, the velocity dispersion and density of the field population.

Chapter 4

Recurrent gas accretion by massive star clusters, multiple stellar populations and mass thresholds for spherical stellar systems

Pflamm-Altenburg, J., Kroupa, P., 2008, **MNRAS**, 397, 488

We explore the gravitational influence of pressure supported stellar systems on the internal density distribution of a gaseous environment. We conclude that compact massive star clusters with masses $\gtrsim 10^6\ M_\odot$ act as cloud condensation nuclei and are able to accrete gas recurrently from a warm interstellar medium which may cause further star formation events and account for multiple stellar populations in the most massive globular and nuclear star clusters. The same analytical arguments can be used to decide whether an arbitrary spherical stellar system is able to keep warm or hot interstellar material or not. These mass thresholds coincide with transition masses between pressure supported galaxies of different morphological types.

4.1 Introduction

Stars are believed to form during one single event in compact star clusters with a total mass ranging from a few solar masses to a few million solar masses. But in recent years observations have revealed that stellar populations of compact star clusters are more complex than a single aged stellar ensemble.

Very young star clusters such as the ONC (Palla et al., 2005) and σ Orionis (Sacco et al., 2007) may probably harbour a few low mass stars which are more than 10 Myr older than the main bulk of their stars. This may be the result of extended star formation

(Palla et al., 2005) or the capture of stars, which are born in surrounding former star formation events, through the deepening potential during cloud collapse (Pflamm-Altenburg & Kroupa, 2007).

On the other hand some of the old massive globular clusters of both the Milky Way and Andromeda exhibit a spread in metallicity and/or have subpopulations with a helium overabundance suggesting the occurrence of multiple star formation events in these compact star clusters in the past (see Section 4.2 for a compilation of observational evidences).

All star clusters with evidences for multiple stellar populations have in common that their total mass is around $10^6\ M_\odot$ or higher. Furthermore, star clusters with a mass larger than $\sim 10^6\ M_\odot$ show a correlation between the cluster mass and the cluster size, whereas star clusters less massive than $\sim 10^6\ M_\odot$ have a constant radius (Walcher et al., 2005; Haşegan et al., 2005; Dabringhausen et al., 2008).

Mass thresholds of globular clusters have been considered by several authors (Morgan & Lake, 1989; Shustov & Wiebe, 2000; Recchi & Danziger, 2005) addressing the question how massive a star cluster must be in order to keep ejected material by AGB stars or supernovae. However, these thresholds can not explain the suggested growth of nuclear star clusters by repeated accretion (Walcher et al., 2005) and large internal spreads in metallicity.

Lin & Murray (2007) discussed the collective accretion of gas by globular clusters onto their member stars embedded in a 10^6 K hot back ground gas corresponding to todays circumstances. But globular clusters are assumed to have formed in denser environments, as for example nuclear star clusters are forming today. Additionally, the treatment by Lin & Murray (2007) does not reveal the existence of a mass threshold at $10^6\ M_\odot$.

In this paper we show that compact massive star clusters with masses $\gtrsim 10^6\ M_\odot$ are able to accrete gas from an embedding warm inter stellar medium. We first summarise the observational evidences for multiple stellar populations in massive star clusters in Section 4.2. The theoretical criterion for possible gas accretion by massive star clusters is derived in Section 4.3 and the $10^6\ M_\odot$ accretion mass threshold is obtained in Section 4.4. Additional mass thresholds are found and identified with transitions in the radius-mass plane of spherical and pressure supported stellar systems (Section 4.8).

4.2 Evidence for multiple populations

The most massive globular cluster, ω Cen, with a mass of $\sim 2.5{\cdot}10^6\ M_\odot$ (McLaughlin & van der Marel, 2005) shows a wide spread in metallicity (Freeman & Rodgers, 1975). Hilker & Richtler (2000) determined by Strömgren photometry three different stellar populations being ∼1–3 Gyr and ∼6 Gyr younger than the oldest one. Bedin et al. (2004) confirmed the existence of multiple evolutionary sequences in ω Cen.

The properties of RR Lyrae stars observed in the globular clusters NGC 6388 and NGC 6441 with masses of $\sim 1.1{\times}10^6\ M_\odot$ and $\sim 1.6{\times}10^6\ M_\odot$, respectively (McLaughlin &

van der Marel, 2005), can be reproduced by the composition of two distinct populations (Ree et al., 2002; Yoon et al., 2008).

Recently, Milone et al. (2007) showed that the split of the sub-giant branch of the Galactic globular cluster NGC 1851 with a mass of $\sim 3.1 \times 10^5\ M_\odot$ (McLaughlin & van der Marel, 2005) corresponds to the existence of two different stellar populations with an age spread of about 1 Gyr. Furthermore, Milone et al. (2007) concluded that the observed RR Lyrea gap in NGC 1851 requires an age difference of ∼2–3 Gyr.

Lehnert et al. (1991) reported a possible metallicity spread in M22 with a mass of $4.4 \cdot 10^5\ M_\odot$ (McLaughlin & van der Marel, 2005), whereas Richter et al. (1999) found no evidence for a metallicity spread using Strömgren photometry.

Metallicity spreads are also reported for G1 (Meylan et al., 2001), the most massive globular cluster in M31 with a mass of $\sim 8 \cdot 10^6\ M_\odot$ (Baumgardt et al., 2003) and M54 (Sarajedini & Layden, 1995) with a mass of $\sim 2.0 \cdot 10^6\ M_\odot$ (McLaughlin & van der Marel, 2005).

Evidence for metallicity spreads in the three massive globular clusters G78, G213 and G280 of M31 are reported by Fuentes-Carrera et al. (2008). These clusters have internal velocity dispersions as high as G1 (Djorgovski et al., 1997) and therefore must have masses larger than $10^6\ M_\odot$.

Various explanations for the origin of multiple stellar populations in globular clusters and abundance anomalies such as ejecta from AGB stars (eg. Ventura & D'Antona, 2008) or rotating massive stars (eg. Decressin et al., 2007) exist (see Renzini 2008 for a summary). Self-enrichment by rotating massive stars works for the first few Myr (Fig. 4.1) after star formation and might be attributed to observed anti-correlations of elements such as the Na-O anti-correlation for star clusters with masses $\gtrsim 10^4\ M_\odot$.

Gas and metal return by supernovae occurs up to a few dozen Myr. As the ejecta by supernovae are much more energetic than winds by massive stars, star cluster masses must be high in order to keep a significant fraction of the material supplied by supernovae. Using energy arguments, Baumgardt, Kroupa, & Parmentier (2008) derived a lower mass threshold of $\approx 10^7\ M_\odot$ for star clusters to retain their residual gas despite multiple supernova events. Wünsch, Tenorio-Tagle, Palouš, & Silich (2008) show using 2D-hydrodynamical simulations that also lower mass star clusters may be able to retain matter ejected by supernovae as a substantial fraction of such material can thermalise its high kinetic energy before escape from the star cluster.

After all supernovae have exploded the massive AGB stars begin to evolve and are able to continuously replenish the gas reservoir in the star cluster and in its vicinity (e.g. D'Antona & Caloi, 2004).

After the epoch of massive energy feedback by the radiation and winds of massive ionising stars and supernovae, which prevents gas of the surrounding ISM from being accreted, the gas of the ISM is able to react to the gravitational potential of the new star cluster. It is expected that the more massive the star cluster is the stronger is the gravitational influence on the ISM by the new star cluster. In this paper we investigate

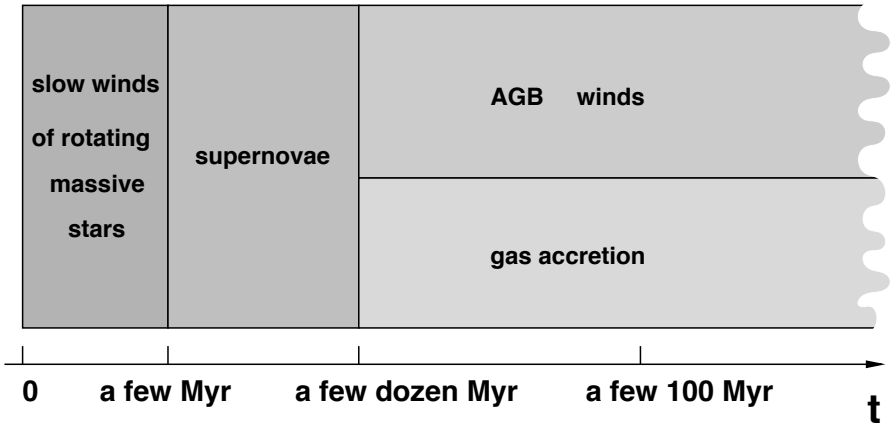

Figure 4.1: Sketch of different element and gas enrichment processes in massive star clusters.

this new possible scenario of gas accretion from the surrounding ISM by massive star clusters.

Additionally, Fellhauer et al. (2006) showed that if ω Cen formed in a dwarf galaxy then it could have captured field stars during its formation from the underlying stellar field population contributing up to 40% to the total final star cluster mass and showing the complex stellar population composition of the host galaxy.

All existing explanations have in common that the material of further stellar generations has already assembled during cluster formation and thus their total mass does not increase with time.

In contrast, Walcher et al. (2005) determined the masses of nuclear star clusters near the photometric centre of bulge-less spiral galaxies to lie between $0.8 \times 10^6\ M_\odot$ and $6 \times 10^7\ M_\odot$. As these nuclear clusters have luminosities by up to 2 orders of magnitude larger than the most luminous Milky Way globular clusters, Walcher et al. (2005) suggested that these nuclear clusters grow by repeated accretion of gas and show subsequent star formation.

Böker et al. (2004) found that nuclear star clusters have dimensions ($r_{\rm hl} \approx 3.5$ pc) comparable to massive globular clusters, and some of these with masses $\gtrsim 10^6\ M_\odot$ show evidence for multiple structural components and estimated periods between star formation episodes of about 0.5 Gyr (Seth et al., 2006).

4.3 Model

From the hydrodynamical point of view the ISM as a self-gravitating gas is described by the three conservation equations for mass, momentum, and energy, the Poisson equation

and the equation of state (Martel, Evans, & Shapiro, 2006, e.g.),

$$\frac{\partial \rho}{\partial t} + \nabla \bullet (\rho \mathbf{v}) = 0 \ , \tag{4.1}$$

$$\frac{\partial \mathbf{v}}{\partial t} + (\mathbf{v} \bullet \nabla)\, \mathbf{v} = -\frac{\nabla P}{\rho} - \nabla \Phi \ , \tag{4.2}$$

$$\frac{\partial \epsilon}{\partial t} + \mathbf{v} \bullet \nabla \epsilon = -P \nabla \bullet \mathbf{v} + \frac{\Gamma}{\rho} - \frac{\Lambda}{\rho} \ , \tag{4.3}$$

$$\nabla^2 \Phi = 4\pi G(\rho - \bar{\rho}) \ , \tag{4.4}$$

$$P = f(\rho, \epsilon) \ , \tag{4.5}$$

where ρ is the mass density, P is the pressure, ϵ is the specific energy, $\mathbf{v}$ is the velocity, Φ is the gravitational potential, Γ is the radiative heading rate and Λ is the cooling rate. $\bar{\rho}$ is the mean density. Following Martel et al. (2006) this term has to be included to prevent the overall collapse of the ISM and the term $-\bar{\rho}$ accounts for whichever process makes the ISM globally stable. If a compact massive star cluster is present within a homogeneous part of the ISM, then the potential in eq. 2 has to be split into a self-gravitating part and the external potential of the compact star cluster acting on the ISM. If the density fluctuations $\rho - \bar{\rho}$ are initially small then the total potential in the vicinity of the star cluster is mainly given by the star cluster itself. To further simplify the problem we assume that the star cluster has no relative velocity with respect to the embedding ISM, i.e. $\mathbf{v} = 0$. With increasing relative velocity between the star cluster and the embedding ISM the effect of gas accretion is expected to become less dominant. Therefore, the stationary case gives a lower limit of a resulting mass threshold.

As a final simplification only the static case can be considered, i.e. all time derivatives vanish. This can be interpreted such that the out-of-equilibrium ISM, for which the density distribution does not follow the static solution, attempts to reach this state. Thus, the static solution can be used to explore the gravitational influence of a compact massive star cluster on the surrounding ISM and the full set of equations which are only numerically solvable reduces to the hydrostatic equation,

$$\frac{1}{\rho} \nabla P = -\nabla \Phi_{\rm cl} \ , \tag{4.6}$$

$$P = f(\rho, \epsilon) \ , \tag{4.7}$$

where $\Phi_{\rm cl}$ is the potential of the massive star cluster.

The potential of the star cluster is assumed to be spherical. Then for a simple isothermal ideal gas,

$$P = \rho \frac{k_{\rm B}}{\mu m_{\rm u}} T \ , \tag{4.8}$$

with a temperature T and a molecular mass $\mu m_{\rm u}$ of the isothermal ISM, the static solution is given by

$$\rho(r) = \rho_0 \; e^{-\frac{\mu m_{\rm u}}{k_{\rm B} T} \left(\Phi_{\rm cl}(r) - \Phi_{\rm cl,0}\right)} \; , \tag{4.9}$$

where ρ_0 and $\Phi_{\rm cl,0}$ are the mass density and the star-cluster potential at a given reference radius, r_0, introduced by the integration. The integration constants in eq. 4.9 are chosen such that the potential vanishes at infinity, i.e. for a large distance from the cluster centre, and the particle density is the particle density of the undisturbed ISM ,

$$\rho(\infty) = \mu m_{\rm u} n_{\rm ISM} \;\; , \;\; \Phi_{\rm cl,0} = \Phi(\infty) = 0 \; , \tag{4.10}$$

where $n_{\rm ISM}$ is the particle density of the ISM.

The potential created by the compact star cluster is described analytically by a Plummer potential (Plummer, 1911),

$$\Phi_{\rm cl}(r) = -G \; M_{\rm cl} \; \left(r^2 + b_{\rm cl}^2\right)^{-\frac{1}{2}} \; , \tag{4.11}$$

where $M_{\rm cl}$ is the mass of the star cluster and $b_{\rm cl}$ is the Plummer parameter describing the compactness of the cluster potential and is equal to the projected half-mass radius (Heggie & Hut, 2003).

The final expression of the static solution is

$$n(r) = n_{\rm ISM} \; e^{\frac{G m_{\rm u}}{k_{\rm B}} \frac{\mu M_{\rm cl}}{T} \left(r^2 + b_{\rm cl}^2\right)^{-\frac{1}{2}}} \; . \tag{4.12}$$

The composition of the ISM is assumed to be primordial with $X = 0.75$ relative mass fraction of hydrogen and $Y = 0.25$ for helium. This corresponds to a mean molecular mass of $\mu = 4/(4X + Y) = 1.23$. In the following the solutions for ISM-star-cluster systems are plotted as a function of the star cluster mass and are parametrised by the ISM temperature and/or the Plummer parameter. If the ISM is enriched to for example $Y = 0.3$ then the mean molecular mass is $\mu = 1.29$, and the solutions correspond to the solution with the primordial composition but a star cluster mass reduced by 4.8 per cent. In the n-$M_{\rm cl}$ plot the curves then have to be shifted by 0.02 dex to the left. Thus the choice of a primordial ISM composition is appropriate for this analysis.

4.4 The 10^6 $M_\odot$-mass threshold

The Plummer parameter of a star cluster is equal to the projected half-mass radius (Heggie & Hut, 2003). Assuming that the mass-to-light ratio of a massive star cluster is independent of the radius then the projected half-mass radius is equal to the half-light radius. For Galactic globular clusters the median half-light radius is about 3.2 pc and ranges from 2 pc to 4 pc (Haşegan et al., 2005; Dabringhausen et al., 2008). The interstellar

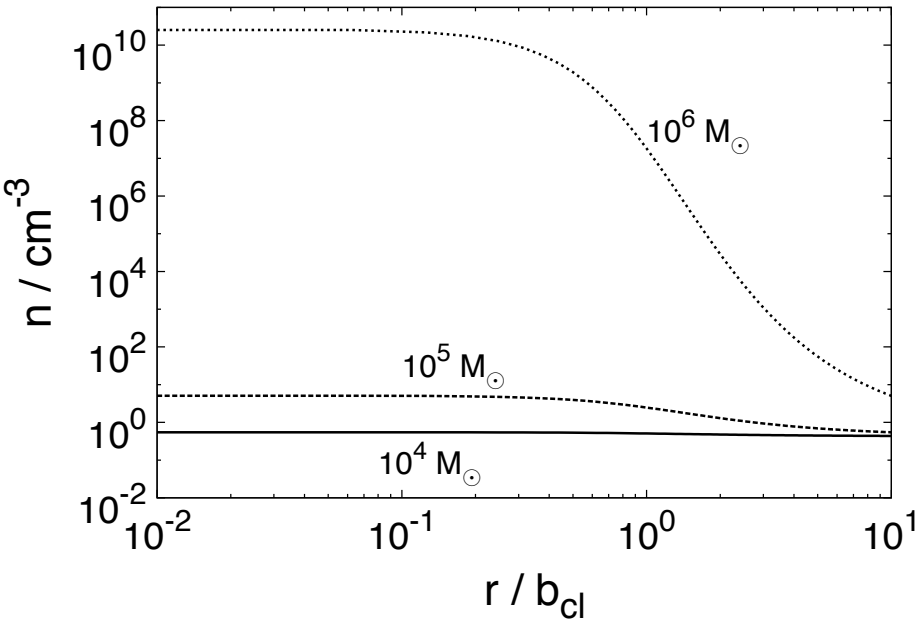

Figure 4.2: Radial density profile of the static solution (eq. 4.12) for three different star cluster masses (10^4, 10^5, 10^6 $M_\odot$) and a Plummer parameter $b_{\rm cl}$ = 3.2 pc. The embedding ISM has a temperature of 8000 K and a particle density of 0.5 cm^{-3}.

medium of the Galaxy consists of three main components (McKee, 1995; Ferrière, 2001; Cox, 2005): a molecular and atomic cold component below 100 K but occupying only 1–2 per cent of the interstellar volume, a warm atomic and ionised component between 6×10^3 K and 10^4 K with a particle density of $\sim$0.1–1.0 cm^{-3} corresponding to the ionisation of hydrogen, and a hot component with temperatures with $\gtrsim 10^6$ K and a particle density less than 10^{-2} cm^{-3} fed by supernovae. The warm and the hot components have roughly the same volume filling factor of about 50 per cent. So it is most likely that star clusters are embedded in the warm or hot component of the ISM.

The radial gas density profiles of three different star clusters ($M_{\rm cl} = 10^4$, 10^5, 10^6 $M_\odot$) with a Plummer parameter $b_{\rm cl}$=3.2 pc embedded in a warm ISM with a temperature of 8000 K and a particle density of 0.5 cm^{-3} are plotted in Fig. 4.2. It can be seen that the hydrostatic gas density within the Plummer radius does not vary much. We therefore use the central gas density, $n_{\rm c} = n(r = 0)$, to characterise the static gas density in the inner part of a star cluster.

In order to explore the influence of the cluster potential on the embedding warm ISM we calculate the central density of the static solution (eq. 4.12) in dependence of the star cluster mass with a Plummer radius of 3.2 pc shown in Fig 4.3. To cover the full range of the observed warm interstellar medium four different models are calculated with

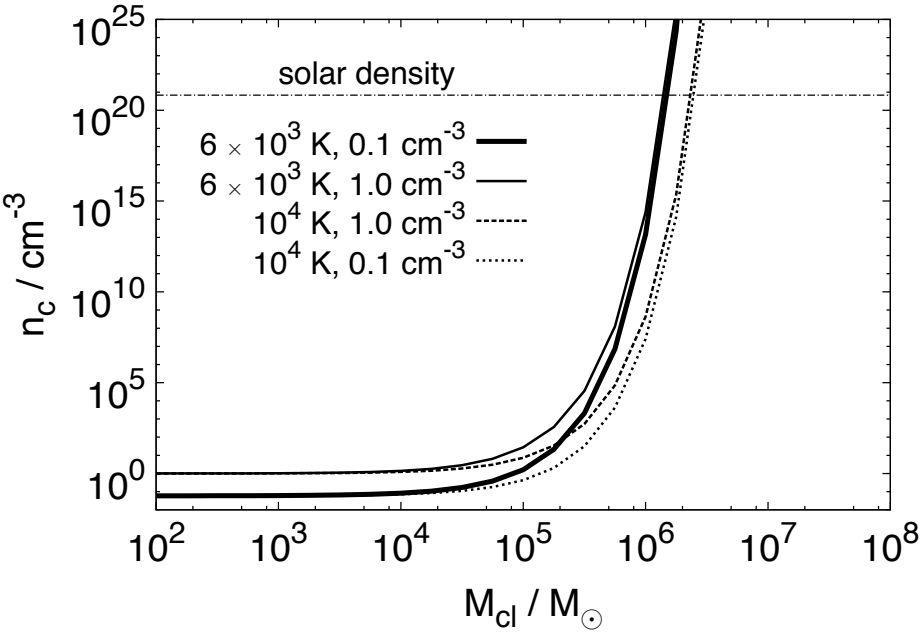

Figure 4.3: Central density in dependence of the star cluster mass with a Plummer radius of 3.2 pc for four different embedding interstellar media with a temperature of 6000 and 10^4 K and a density of 0.1 and 1 cm^{-3}. The horizontal line denotes the average density of matter in the solar interior.

temperatures of 6000 K and 10^4 K and densities of 0.1 cm^{-3} and 1 cm^{-3} corresponding to the boundary values of the observed warm ISM. For cluster masses smaller than 10^5 $M_\odot$ the central particle density does not differ from the density of the undisturbed ISM. Between 10^5 and 10^6 $M_\odot$ the central density starts to rise and becomes dramatically large above 10^6 $M_\odot$.

The potential of massive star clusters with a mass larger than 10^6 $M_\odot$ thus produces an instability in the warm ISM such that the ISM is expected to react with starting inflow towards the cluster centre. In other words: A self-gravitating ISM does not notice the existence of star clusters with a total mass lower than 10^6 $M_\odot$, but star clusters more massive than 10^6 $M_\odot$ become immediately attracting holes in the warm ISM. Note, how rapidly the instability rises with increasing cluster mass only depends on the temperature but not on the density of the ISM. Keeping the properties of the ISM constant (T = 8000 K and $n = 0.5$ cm^{-3}) the instability region also appears at cluster masses of about 10^6 $M_\odot$ when varying the Plummer parameter between 2 and 4 pc (Fig. 4.4).

Present-day Milky Way globular clusters do not belong to the disk and are not embedded in a comoving warm ISM. But in early times when they formed they may have been embedded in a warm ISM, e.g. in a dwarf proto-galactic building block. ω Cen for example is believed to have been hosted in a dwarf galaxy disk before being accreted by

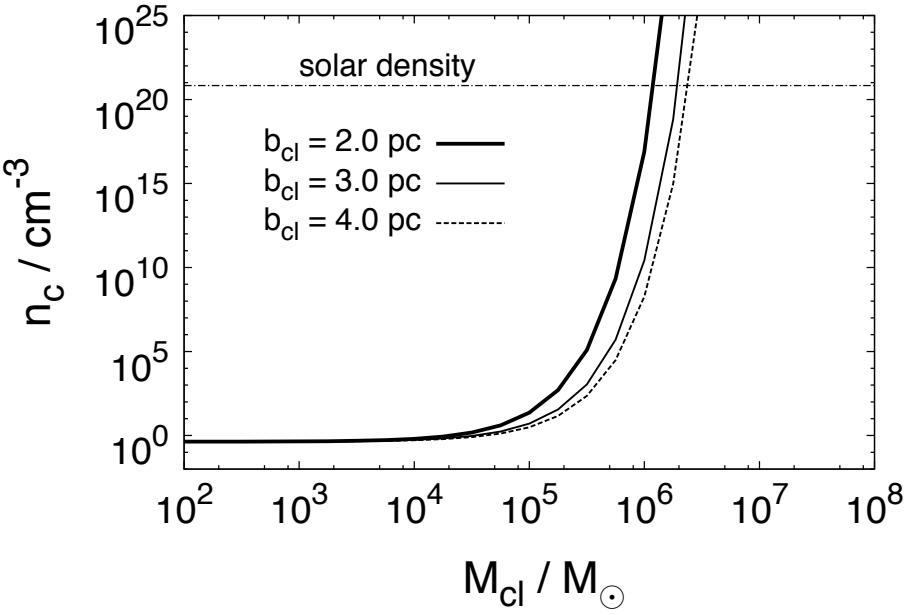

Figure 4.4: Central density in dependence of the star cluster mass for three different Plummer radii of 2, 3.2 and 4 pc embedded in an ISM with $T = 8000$ K and $n = 0.5$ cm^{-3}.

the Milky Way. Because it was massive enough it could have accreted additional gas when the conditions were appropriate. Star formation events within the young ω Cen or in its vicinity are expected to have caused varying ISM properties. Thus it could have been placed alternatingly in the warm or hot ISM and the accretion history could have been fluctuating. Ionising OB stars in the young ω Cen would have prevented it from further accretion from the embedding ISM and star formation rested in ω Cen. Meanwhile star formation would have been ongoing in the ISM of the dwarf galaxy disk being continuously enriched with metals. After all ionising sources in ω Cen disappeared accretion would have restarted if the coomoving conditions were appropriate. When enough gas accumulated in ω Cen star formation would have restarted and the newly formed stars would have been more metal rich than the younger stellar populations. Thus, distinct populations with different metallicties are expected in such a scenario in ω Cen as observed.

To underline the strength of this instability threshold for star cluster masses $\gtrsim 10^6 M_\odot$ the cooling time scale, $\tau_{\rm cool}$, corresponding to the central gas density is calculated. We use the cooling function provided in Köppen, Theis, & Hensler (1995) in the temperature regime from 100 to 10^4 K giving an estimate of the cooling time-scale of

$$\tau_{\rm cool}/{\rm yr} = 16400\,(T/{\rm K})^{0.5}\left(n/{\rm cm}^{-3}\right)^{-1}\ . \tag{4.13}$$

The resulting central cooling time-scale for the static solution of an ISM with a temperature of 8000 K and a density of 0.5 cm^{-3} is plotted in dependence of the star cluster

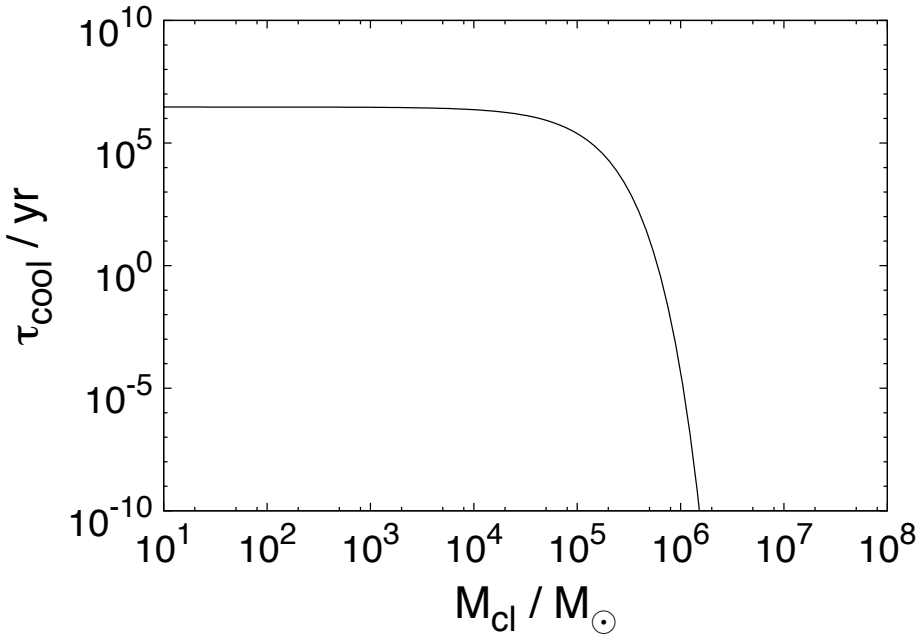

Figure 4.5: Cooling time-scale of the central static gas density in dependence on the star cluster mass for a Plummer parameter $b_{\rm cl} = 3.2$ pc. The embedding ISM has a temperature of 8000 K and a particle density of 0.5 cm^{-3}.

mass with a Plummer parameter of 3.2 pc (Fig. 4.5). If the gas of the ISM starts to flow into the massive star cluster due to the instability caused by the cluster potential the increasing central gas density has a decreasing cooling time-scale supporting the gas accretion. For comparison, a thermal instability leading to an expected cooling flow of hot gas is known for galaxy clusters (Fabian, 2003) and massive elliptical galaxies (Kroupa & Gilmore, 1994). New star formation is inhibited by the ISM in massive elliptical galaxies being kept at a temperature of $\approx 10^6$ K due to the random stellar motions with velocities of a few hundred km s^{-1} (Mathews & Brighenti, 2003; Parriott & Bregman, 2008). The massive-star-cluster instability, however, leads to a cooling instability and the onset of star formation until the new OB stars reheat the cluster ISM.

The argument can also be turned around. If warm material is released inside the cluster then the gas attempts to reach the hydrostatic solution. The warm gas of a star cluster less massive than 10^6 $M_\odot$ will be distributed nearly uniformly in space, i.e. it escapes from the cluster, whereas a star cluster more massive than 10^6 $M_\odot$ is able to keep its warm gas.

It may be rashly argued that the reason for accretion or keeping of warm material is that the sound speed of the gas is smaller than the escape velocity from the star cluster.

The sound velocity of an ideal gas is given by

$$c_\mathrm{s} = \sqrt{\frac{\gamma k_\mathrm{B} T}{\mu m_\mathrm{u}}} = 91.2 \frac{\mathrm{m}}{\mathrm{s}} \sqrt{\frac{\gamma}{\mu}} \sqrt{\frac{T}{\mathrm{K}}} \,. \tag{4.14}$$

For a monatomic gas, $\gamma = 5/3$, the sound speed is about 10.6 km/s ($T = 10^4$ K) or 8.2 km/s ($T = 6000$ K). The escape velocity at a distance of $r = l b_\mathrm{cl}$ from the centre of a Plummer potential with mass M_cl and Plummer parameter b_cl is

$$v_\mathrm{esc} = \sqrt{\frac{2G}{\sqrt{1+l}} \frac{M_\mathrm{cl}}{b_\mathrm{cl}}} = 92.7 \frac{\mathrm{km}}{\mathrm{s}} \, (1+l)^{-\frac{1}{4}} \sqrt{\frac{M_\mathrm{cl}}{M_\odot} \frac{\mathrm{pc}}{b_\mathrm{cl}}} \,. \tag{4.15}$$

The lowest threshold mass of $2.5 \times 10^4 M_\odot$ is calculated in the case of the lowest temperature of the warm ISM (6000 K) and the central escape velocity ($l = 0$). The largest threshold mass of $6.4 \times 10^4 M_\odot$ is calculated in the case of the highest temperature of the warm ISM (10^4 K) and an escape velocity from the outer region of the cluster, e.g. the half mass radius ($l = 1.305$). Nevertheless, by comparing these two characteristic velocities describing the potential of the star cluster and the internal energy content of the gas threshold masses are obtained which are more than one order of magnitude smaller than the lower limit of masses of star clusters which multiple stellar population are observed in. In any case, the sound speed of a gas describes the velocity with which a pressure change propagates through space. No large scale motion of matter is involved in the propagation of sound, whereas the accretion of material is such a process.

In any real situation of interest the gas will not be static and the interstellar medium will be turbulent and clumpy. Thus, it might be questionable how much is learned by computing static gas densities. Indeed, the calculated static solutions are not reached by the gas. The static solution describes a stage of an equilibrium. In the case of the presence of a star cluster less massive than $10^6 M_\odot$ this equilibrium is described by a nearly uniform density distribution. I.e. the warm ISM does not notice the existence of the star cluster. In the case of a star cluster more massive than $10^6 M_\odot$ the static solution is charactarised by a required central gas density many orders of magnitude larger than the surrounding gas density. At the position of the massive star cluster a uniformly distributed ISM is far from equilibrium. Thus, the gas tries to asymptotically reach this equilibrium by increasing its density at the position of the massive star cluster, i.e. the star cluster accretes. It will never reach the exact static gas density distribution as the increase of the central gas density will result in a more efficient cooling and restarted star formation will stop further accretion by heating the infalling gas.

Turbulences and inhomogeneities of the warm interstellar medium lead to condensation of material and the formation of cold molecular clouds at random locations in the galaxies. In this context massive compact star clusters with masses $\gtrsim 10^6 M_\odot$ stimulate this process at certain locations, i.e. the star clusters act as cloud condensation nuclei.

4.5 The amount of accreted mass by a massive star cluster

The threshold criterion derived here can be used to decide whether a star cluster is able to accrete gas from a warm medium or not. If a massive star cluster is able to accrete the question arises how much material can be accreted and if the amount of accreted material can account for the observed multiple stellar populations. Finding an accurate answer to this question requires extensive numerical simulation. However, a reasonable estimation can be done using the accretion rate expression for a star from its surrounding medium (Bondi, 1952). The star has a potential of a point mass, whereas the potential of the star cluster is extended. But due to the spherical symmetry of the star cluster, the potential at a certain radius from the centre of the potential is given by the enclosed mass within this radius placed at the origin of the potential (Newtons's second theorem). Therefore, outside the cluster radius the cluster potential is the same as if the cluster is assumed to be a point mass and the application of the Bondi-accretion is justified. The accretion rate, A, is given by

$$A = 2\pi \left(G M_{\rm cl}\right)^2 c_{\rm s} \rho_\infty \ , \tag{4.16}$$

where $c_{\rm s}$ is the sound speed and ρ_∞ is the mass density of the gas far from the cluster, i.e. the density of the surrounding ISM. With

$$\frac{A}{M_\odot/{\rm Myr}} = 2.9 \times 10^{-6} \mu \left(\frac{M_{\rm cl}}{M_\odot}\right)^2 \left(\frac{c_{\rm s}}{\rm km/s}\right)^{-3} \frac{n_{\rm ISM}}{\rm cm^{-3}} \tag{4.17}$$

and for a metallicity of $\mu = 1.23$, a sound speed of $c_{\rm s} = 10.2$ km/s and a particle density of $n_{\rm ISM} = 1$ cm^{-3} the accretion rate is about 3400 $M_\odot$/Myr. Thus on a time scale of a few 100 Myr corresponding to derived age gaps between the multiple stellar populations the possible amount of accreted material is of the order of 3.4×10^5 $M_\odot$ for a 10^6 $M_\odot$ star cluster. The accreted material can account for the observed multiple stellar populations.

We note in passing that the accretion may also be modulated by the cluster orbit about its host galaxy. For example it may experience more significant accretion events when it passes through the ends of a galactic bar or through major spiral arms where the likelihood of it encountering cold gas is enhanced.

4.6 On the cold-gas threshold for star clusters and the star-cluster birth instability

The criterion above which star cluster mass a density instability of the ISM can arise depends only on the ratio, $n_{\rm c}/n_{\rm ISM}$, of the central and surrounding gas density in eq. 4.12. The threshold expression is proportional to $e^{M_{\rm cl}/T b_{\rm cl}}$. Thus, it should be easier to accrete

cold cloud material than warm material. But the volume filling factor of cold cloud material in galaxies is about 1–2 per cent and much smaller than the volume filling factor of the warm material ($\approx$ 50 per cent). The possibility that a massive star cluster is long-term embedded in a cold molecular cloud is much smaller than the possibility that the star cluster is embedded in the warm ISM. If a star cluster is surrounded by cold dense material it is expected that accretion occurs for even less massive star clusters. As shown above the threshold is surpassed for typical values of $M_{\rm cl} = 10^6 M_\odot$, $b_{\rm cl} = 3$ pc , and $T = 10^4$ K. Star clusters should be able to accrete cold material with a temperature of about 100 K if the their mass-size ratio is larger than $M_{\rm cl}/b_{\rm cl} = 10^4\ M_\odot/3$ pc. For young embedded star clusters with $b_{\rm cl} = 0.3$ pc (as the ONC for example) a total cluster mass of about $1000 M_\odot$ is sufficient to accrete cold gas.

It may be possible that this characterises the transition from distributed star formation within giant molecular clouds in the form of loose groups hosting a few low-mass stars to star formation in well defined compact embedded star clusters: star formation in giant molecular clouds starts with distributed loose groups of a few low-mass stars. If regions in the low-mass-star forming giant molecular cloud surpasse the threshold expression, run-away accretion starts and a well defined star cluster appears. The ONC for example is a well defined young embedded star cluster within a molecular cloud showing many loose groups of few low-mass stars distributed over the molecular cloud.

4.7 Nuclear star clusters

Nuclear star clusters, which are embedded long-term in a warm comoving ISM and have masses less than $10^6\ M_\odot$, may not accrete additional material after their formation. But nuclear star clusters which are born or end up through mergers of smaller clusters more massive than $10^6\ M_\odot$ should be able to accrete additional gas after their formation and show further star formation events. Therefore they are expected to grow as suggested by Walcher et al. (2005). The star cluster mass region at $10^6\ M_\odot$ should be underpopulated predominantly for star clusters located in gas rich environments, i.e. the central regions of galaxies.

Indeed, the ensemble of nuclear clusters observed by Georgiev et al. (2009b) in gas rich dwarf irregulars have absolute V-band luminosities of -9.4 mag and less corresponding to stellar masses of $\approx 10^6 M_\odot$ and more. Compared with the population of blue and red globular clusters hosted in dIrrs, dEs and dSphs, which populate the distribution of V-band luminosities uniformly down to ≈ -8.7, these nuclear star clusters seem to form a distinct population as they are separated from the rest of the less massive GCs by a small gap in the luminosity sample (Georgiev et al., 2009b, fig. 1). These nucear star clusters are candidates for repeated accretion events and so should contain complex stellar populations, as opposed to the clusters below the threshold which should not contain significant complex populations.

It may be argued that nuclear star clusters are just fed with additional gas because they are located at the origin of the potential of the galaxy. But the location of nuclear star clusters and the dynamical centers of disk galaxies do not always coincide (Matthews & Gallagher, 2002; Walcher et al., 2005). Recently, Georgiev et al. (2009a) found that seven of ten nuclear star clusters in dwarf irregular galaxies are off-centre by up to 480 pc. The overall process can be as follows.

The central regions of galaxies are fed with gas due to the deep gravitational potential of the galaxy. For a nuclear star cluster to be able to accrete gas from this continuously refilled central gas reservoir then depends only on the mass of the massive star cluster. Due to differential rotation the accreted material is expected to form a more rotationally than pressure supported new stellar system in the star cluster. Furthermore, younger stellar populations in these compact massive star clusters should be more elliptical and aligned with the galactic gas disk, whereas the initial population should be more spheroidal if the formation of the star clusters occurred in a monolithic collapse. Indeed it has been found that older stellar populations in nuclear star clusters have a more spheroidal morphology and nuclear star clusters appear flattened along the plane of the galaxy disk (Seth et al., 2008).

Milosavljević (2004) calculated the time-scale required for nuclear star clusters to have migrated from distant eccentric orbits in the disk towards the central regions of their host galaxies. Such migration time-scales are too long and nuclear star clusters must have formed in situ in the centres. However, if massive star clusters accrete gas from the long-term embedding ISM their masses grew. If the angular momentum of the star cluster is conserved their orbit must shrink and the inspiral may be accelerated. Places of the formation of such massive star cluster could have been for example the massive clumps observed in chain galaxies at higher red shift (Elmegreen & Scalo, 2006).

4.8 Other mass thresholds

In the previous sections the influence of a few pc sized star cluster on the warm interstellar medium has been explored. But such globular/nuclear star cluster type objects constitute only a subset of pressure supported stellar systems, which do not have arbitrary dynamical properties but show distinct size-mass relations (Haşegan et al., 2005; Dabringhausen et al., 2008; Forbes et al., 2008).

Figure 4.6 is a sketch of figure 2 of Dabringhausen et al. (2008) showing the half-light-radius–dynamical-mass relations of pressure supported stellar systems. Here, the dynamical mass, M, is the total mass within the optical extend of the object as obtained by solving the Jeans equations. Globular clusters do not show a mass-dependence of their half-light radius, whereas above about 10^6 $M_\odot$ the half-light radius becomes mass dependent. The ultra compact dwarfs (UCDs), bulges of spiral galaxies and high-luminous ellipticals constitute a steep branch in the half-light–dynamical-mass plane. The radius-

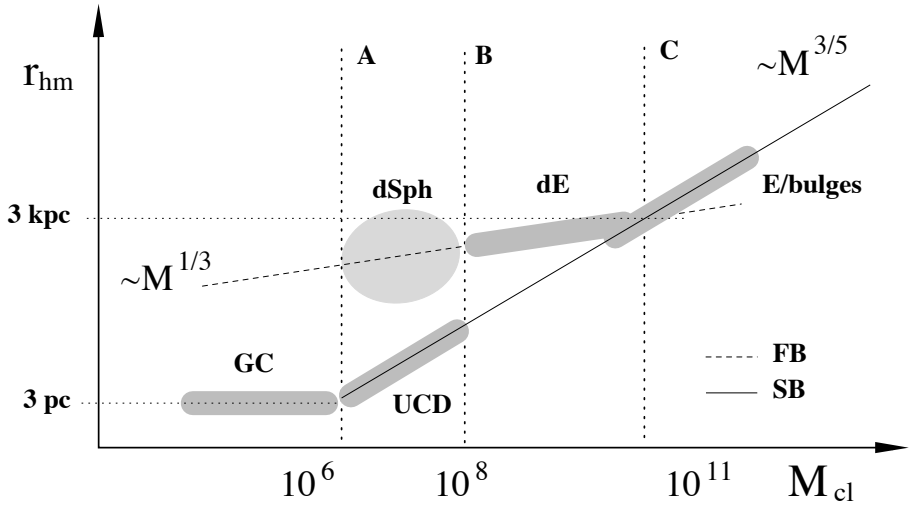

Figure 4.6: Illustration of the half-light radius dynamical mass relation of pressure supported stellar systems from Dabringhausen et al. (2008). See text for details.

mass relation of these objects lying on the steep branch (SB) presented in Dabringhausen et al. (2008) can be converted into a $b_{\rm cl} - M$ relation,

$$\frac{b_{\rm cl}}{\rm pc} = 2.95 \left(\frac{M}{10^6\ M_\odot} \right)^{0.60} \quad . \tag{4.18}$$

The flat branch (FB) is build by dwarf spheroidals and low-luminous ellipticals. The $b_{\rm cl} - M$ of the flat branch is

$$\frac{b_{\rm cl}}{\rm pc} = 92.8 \left(\frac{M}{10^6\ M_\odot} \right)^{0.33} \quad , \tag{4.19}$$

corresponding to a constant mass density.

These two branches can be combined with the warm and the hot interstellar medium. The ratio of the central density and the density of the gas at infinity of the static solution (eq. 4.12) is plotted in Fig. 4.7 as a function of the total mass of the system. Systems with $M \geq 10^6\ M_\odot$ on the steep branch are able to keep their warm gas, whereas systems on the flat branch are able only to do so if their mass is $10^8\ M_\odot$ or larger. This mass threshold coincides with the mass separating the dwarf spheroidals and low-luminous ellipticals from each other. The hot interstellar medium can only be kept by systems more massive than about $10^{11}\ M_\odot$. This threshold mass corresponds to the transition region from low-luminous ellipticals on the flat branch to high-luminous spirals and bulges of disk galaxies on the steep branch.

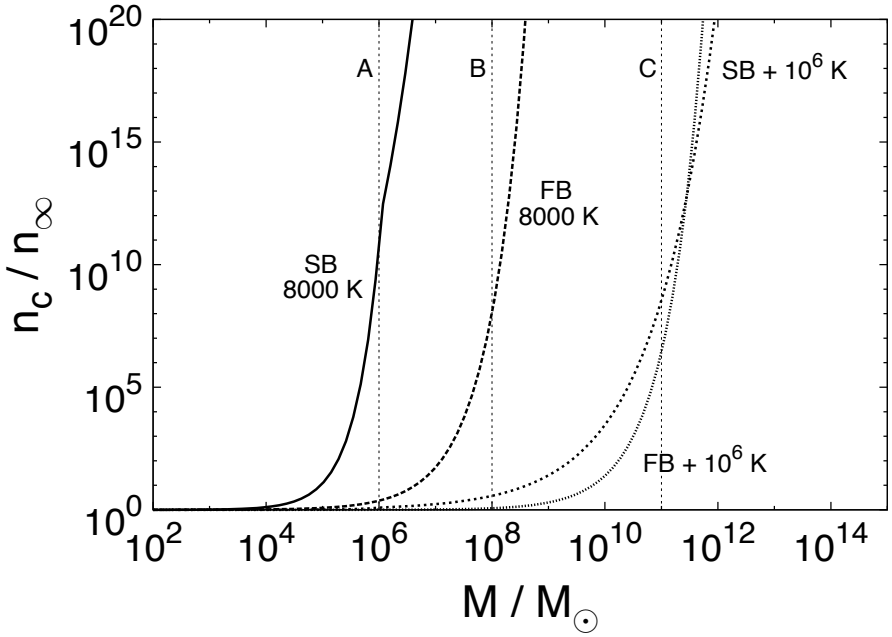

Figure 4.7: Density ratio of the static gas as a function of the total system mass of stellar systems lying on the flat (FB) and steep (SB) branch (Fig. 4.6) for the cases of the warm and hot interstellar medium.

One may speculate if these coincidences of the mass thresholds obtained from the instability argument and the mass transitions observed in the mass-radius plane of pressure supported stellar systems has a direct physical origin.

4.9 Conclusions

We have shown that an ISM instability occurs for massive compact star clusters with masses of $M_{\rm cl} \gtrsim 10^6 M_\odot$. This instability may relate to episodic gas accretion from the embedding ISM and subsequent star formation. Such an extended star formation history leads naturally to a spread in metallicity as observed in globular star clusters more massive than $\approx 10^6\ M_\odot$.

This type of gas accretion can also account for the ongoing star formation in massive nuclear star clusters which are still embedded in a comoving dense interstellar medium.

The 'massive-star-cluster' instability adds to the well-known instabilities of the ISM, e.g. the Parker, Kelvin-Helmholz or Rayleigh-Taylor instability.

Furthermore, for the combination of observed size-mass relations of pressure supported systems and different phases of the ISM the same analysis reveals other mass thresholds which coincide with transitions in the size-mass diagram of pressure supported stellar systems composed of globular clusters, ultra compact dwarf galaxies, bulges of disk galaxies,

dwarf spheroidals and dwarf and large ellipticals.

Chapter 5

Two step ejection of massive stars and the issue of their formation in isolation

Pflamm-Altenburg, J., Kroupa, P., 2009, **MNRAS** – submitted

In this paper we investigate the combined effect of massive binary ejection from star clusters and subsequent binary disintegration due to a supernova explosion. We call this scenario the *two-step-ejection* scenario. The main results are: i) Massive field stars produced via the two-step-ejection process can not in the vast majority of cases be traced back to their parent star clusters. These stars can be mistakenly considered as massive stars formed in isolation. ii) The expected O star fraction produced via the two-step-ejection process is of the order of 1–4 per cent, in quantitative agreement with the observed fraction of candidates for isolated-O-star formation. iii) Stars ejected via the two-step-ejection process can get a higher final velocity (up to 1.5–2 times higher) than the pre-supernova velocity of the massive-star binary.

5.1 Introduction

Considering pure number counts massive stars are by far only a tiny minority in the stellar population of galaxies. But they mainly drive galactic evolution due to their dominating chemical and energetic feedback. Although the importance of massive stars for galactic astrophysics has been accepted, the physical circumstances of their formation are still not resolved, i.e. where, why, and how they form.

It is currently strongly debated whether the formation of massive stars is entirely restricted to the interior of massive star clusters or if they can form in isolation in the galactic field.

Indeed, on the basis of a the statistical analysis of a sample of galactic O stars de Wit et al. (2005) conclude that 4±2 per cent of all O-type stars can be considered as formed outside a cluster environment. They further show that this fraction of isolated O stars is expected if the slope of the cluster mass function (CMF) is $\beta = 1.7$. This assumed CMF slope in the low mass star cluster regime is in disagreement with the slope of $\beta = 2$ observed in the solar neighborhood (Lada & Lada, 2003).

The definiton of an isolated O star in the IMF-Monte-Carlo simulations of de Wit et al. (2005) is restricted to stellar ensembles which contain only one O star. Parker & Goodwin (2007) strenghened the definition of an isolated O star being an O star without B-star companions but allowed the O star to be surrounded by a cluster with a mass of <100 $M_\odot$. Using this definition Parker & Goodwin (2007) conclude that an observed CMF slope of $\beta = 2$ can quantitatively explain the statistical analysis by de Wit et al. (2005)

The analysis by de Wit et al. (2004, 2005) identifies a small number of O-stars which are deemed to be truly isolated in the sense of not being traceable to an origin in a cluster or OB association. However, Gvaramadze & Bomans (2008) reported the existence of a bow shock associated with the O-star HD165319, which is marked in de Wit et al. (2005) as a very likely candidate for an O-star formed in isolation.

In general, two main processes exist for the production of high-velocity O- and B-stars: i) close encounters between binaries and single stars or binaries and binaries can result in the ejection of massive stars (e.g. Poveda et al., 1967; Hoffer, 1983; Mikkola, 1983, 1984; Leonard, 1991). The ejection velocity is of the order of the orbital velocity of the binary (Heggie, 1980). Thus tighter binaries can produce larger ejection velocities. ii) The disintegration of a binary during a supernova event of one component and the release of the other (e.g. Zwicky, 1957; Blaauw, 1961; Iben & Tutukov, 1997). The supernova ejection scenario only requires the existence of massive binaries, whereas ejection rates in the dynamical ejection scenario depend on the close encounter frequency. This frequency will be increased if massive stars form in compact few-body groups (Clarke & Pringle, 1992; Pflamm-Altenburg & Kroupa, 2006).

Various studies on the individual ejection processes exist. But these two processes have not yet been combined. In this contribution we investigate for the first time the combination of the dynamical and supernova ejection process which we refer to as the *two-step-ejection process* of massive stars.

We start our investigation in Section 5.2 with the calculation of the velocity spectrum of stars which are released with the same velocity during a supernova from binaries with identical ejection velocities We then derive the probability that stars released by a supernova from ejected binaries can be traceed back to their parent star cluster (Section 5.3), and discuss the maximum possible velocity which stars can get in the two-step-ejection process in Section 5.5.

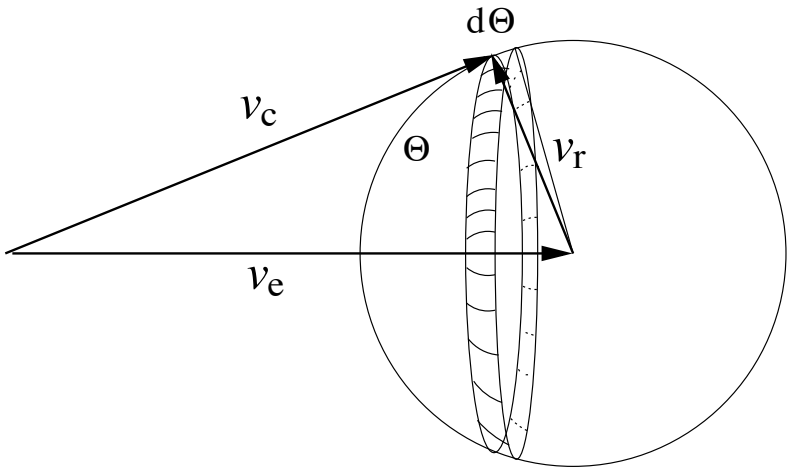

Figure 5.1: Illustration of the compound velocity. A binary is ejected with the velocity v_e. One component is then released with the velocity v_r resulting in the compound velocity, v_c, given by the vectorial sum.

5.2 Compound velocity spectrum

Due to dynamical interactions during close encounters of stars, binaries can be ejected from star clusters with the ejection velocity, v_e. If one component of the ejected binary explodes as a supernova, the surviving companion normally gets unbound and is released with a velocity, the release velocity v_r, comparable to its previous orbital velocity. The vectorial sum of both velocities, the ejection and release velocity, is the new velocity of the released star. We call this velocity the compound velocity, v_c. For fixed ejection velocity, v_e, and release velocity, v_r, the compound velocity, v_c, is distributed, because the direction of the release of the star from the disintegrating binary during the supernova is randomly distributed in space. The corresponding spectrum of the compound velocity, $f_c(v_c)$, defines the number of stars, $dN(v_c)$, which have a compound velocity, v_c, after they have been released from ejected binaries.

5.2.1 Calculating $f_c(v_c)$

We start the calculation of the resulting compound velocity spectrum with the definition of the compound velocity through vectorial addition,

$$\mathbf{v}_c = \mathbf{v}_e + \mathbf{v}_r \ . \tag{5.1}$$

The relation between the absolute values of the velocities follows from the cosine theorem (Fig. 5.1),

$$v_c^2 = v_e^2 + v_r^2 - 2v_e v_r \cos\theta \ . \tag{5.2}$$

Differentiation leads to the relation

$$\frac{dv_{\rm c}}{d\theta} = \frac{v_{\rm e}v_{\rm r}}{v_{\rm c}}\sin\theta \tag{5.3}$$

between the compound velocity and the release angle θ.

The orientations of the binaries are randomly distributed in space. Thus, the released stars are 4π distributed with respect the centre-of-mass system of the binary. If a set of binaries release N stars isotropically the number of stars $dN(\theta)$ released in a small angle $d\theta$ is given by the ratio of the area of the small circular stripe, $dA(\theta)$, with the angle θ and the unit sphere, 4π (Fig. 5.1) ,

$$\frac{dN(\theta)}{N} = \frac{dA(\theta)}{4\pi} \ , \tag{5.4}$$

where the area of the small circular stripe is

$$dA(\theta) = 2\pi\sin(\theta)d\theta. \tag{5.5}$$

By combining these equations the number fraction of stars having the compound velocity $v_{\rm c}$ is

$$\frac{dN(v_{\rm c})}{dv_{\rm c}} = \frac{N}{2v_{\rm e}v_{\rm r}}v_{\rm c} \ . \tag{5.6}$$

As the angle θ varies from 0 to 2π, the allowed range of the compound velocity can be obtained from the cosine theorem above and is

$$|v_{\rm e} - v_{\rm r}| \leq v_{\rm c} \leq v_{\rm e} + v_{\rm r} \ . \tag{5.7}$$

The distribution function, $f_{\rm c}(v_{\rm c})$, of the compound velocity is normalised by

$$1 = \int f_{\rm c}(v_{\rm c})\ dv_{\rm c} \ , \tag{5.8}$$

and is for a constant ejection velocity, $v_{\rm e}$, and constant release velocity, $v_{\rm r}$,

$$f_{\rm c}(v_{\rm c}) = \frac{1}{2v_{\rm e}v_{\rm r}}v_{\rm c}\Theta(v_{\rm c} - |v_{\rm e} - v_{\rm r}|)\Theta(v_{\rm e} + v_{\rm r} - v_{\rm c}) \ , \tag{5.9}$$

where the Θ-mapping is defined by

$$\Theta(x) = \left\{ \begin{array}{ll} 1 & ; x \geq 0 \\ 0 & ; x < 0 \end{array} \right. \ . \tag{5.10}$$

The form of the compound spectrum can be seen in Fig. 5.2. Compound velocities at the high speed end are preferred. But the distribution function, $f_{\rm c}(v_{\rm c})$, flattens with increasing

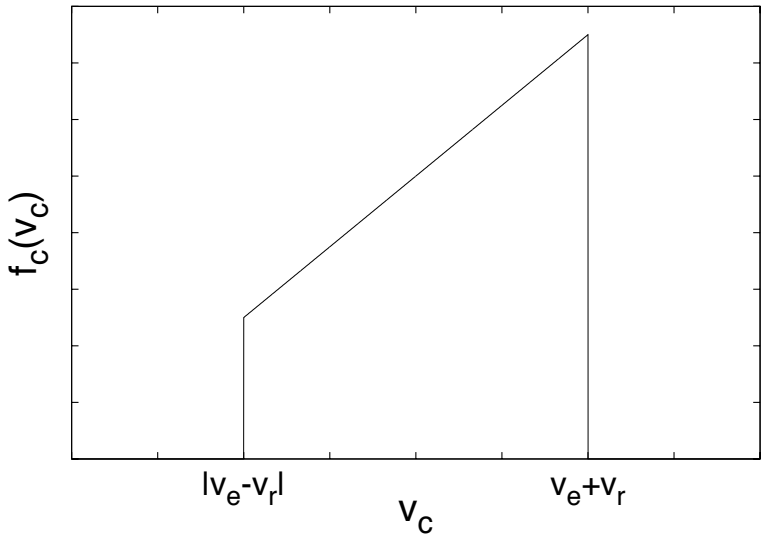

Figure 5.2: The form of the compound velocity spectrum $f_{\rm c}$ (eq. 5.9).

ejection or release velocity. The distribution is symmetric in $v_{\rm r}$ and $v_{\rm e}$. Note that in eq. 5.8 an additional factor $4\pi\ v_{\rm c}^2$, as for example in the Maxwellian distribution calculated a from three-dimensional Gaussian distribution function, is not required, because $f_{\rm c}(v_{\rm c})$ refers already to an absolute velocity value and is not calculated from spatial integration over a three-dimensional distribution function.

If the velocities of the ejected binaries and of the released stars are distributed according to uncorrelated distribution functions, $f_{\rm e}(v_{\rm e})$ and $f_{\rm r}(v_{\rm r})$, then the resulting distribution of compound velocities is calculated by integration over both distributions,

$$\begin{aligned} f_{\rm c}(v_{\rm c}) &= \frac{v_{\rm c}}{2} \int\int \frac{f_{\rm e}(v_{\rm e}) f_{\rm r}(v_{\rm r})}{v_{\rm e} v_{\rm r}} \\ &\quad \Theta(v_{\rm c} - |v_{\rm e} - v_{\rm r}|)\ \Theta(v_{\rm e} + v_{\rm r} - v_{\rm c})\ dv_{\rm e}\ dv_{\rm r}\ . \end{aligned} \tag{5.11}$$

5.2.2 Properties of $f_{\rm c}(v_{\rm c})$

In the following we derive some properties of the compound velocity spectrum.

i) The simplest case we can consider is that if one of the velocities, $v_{\rm e}$ or $v_{\rm r}$, is zero. If for example $v_{\rm r}$ converges against zero then the velocity spectrum converges against the delta-distribution

$$f_{\rm c}(v_{\rm c}) = \lim_{v_{\rm r} \to 0} f_{v_{\rm r}}(v_{\rm c}) = \delta(v_{\rm c} - v_{\rm e})\ . \tag{5.12}$$

Because $f_{\rm c}(v_{\rm c})$ is symmetric in $v_{\rm r}$ and $v_{\rm e}$, the same result follows for $v_{\rm e} \to 0$. The compound velocity is identical to the ejection or release velocity.

ii) The released stars are not necessarily faster than the previous binaries. They can also be deccelerated. The fraction of stars ($\mu_{>v_\mathrm{e}}$) which are accelerated, i.e. having a compound velocity greater than the ejection velocity is given by the integral

$$\mu_{>v_\mathrm{e}} = \int_{v_\mathrm{e}}^{v_\mathrm{e}+v_\mathrm{r}} f_\mathrm{c}(v_\mathrm{c})\,\mathrm{d}v_\mathrm{c}\ . \tag{5.13}$$

The evaluation of the integral leads to

$$\begin{aligned}\mu_{>v_\mathrm{e}} &= \frac{1}{4v_\mathrm{e}v_\mathrm{r}}\left(v_\mathrm{r}^2 + 2v_\mathrm{e}v_\mathrm{r} - \right.\\ &\left.\Theta(|v_\mathrm{e}-v_\mathrm{r}|-v_\mathrm{e})\left(v_\mathrm{r}^2-2v_\mathrm{e}v_\mathrm{r}\right)\right)\ .\end{aligned} \tag{5.14}$$

The fraction of accelerated stars in dependence of the ejection and release velocity can be seen in Fig. 5.3. Two cases can be distinguished:

$$|v_\mathrm{e}-v_\mathrm{r}| \geq v_\mathrm{e}\ :\ \mu_{>v_\mathrm{e}} = 1\ , \tag{5.15}$$

and

$$|v_\mathrm{e}-v_\mathrm{r}| < v_\mathrm{e}\ :\ \mu_{>v_\mathrm{e}} = \frac{v_\mathrm{r}}{4\ v_\mathrm{e}} + \frac{1}{2}\ . \tag{5.16}$$

The number fraction of accelerated stars is always larger than 50 per cent and all stars are accelerated for $v_\mathrm{r} > 2\ v_\mathrm{e}$.

For the case that $v_\mathrm{e} = v_\mathrm{r}$, which will be important for Section 5.5, i.e. the ejection velocity is comparable to the orbital velocity of the ejected binary, the fraction of accelerated stars is 75 per cent.

iii) We now calculate the resulting mean compound velocity, $\bar{v}_\mathrm{c}$, by the integral

$$\bar{v}_\mathrm{c} = \int_{|v_\mathrm{e}-v_\mathrm{r}|}^{v_\mathrm{e}+v_\mathrm{r}} v_\mathrm{c} f(v_\mathrm{c})\mathrm{d}v_\mathrm{c} = \frac{1}{6v_\mathrm{e}v_\mathrm{r}}\ v_\mathrm{c}^3\Big|_{|v_\mathrm{e}-v_\mathrm{r}|}^{v_\mathrm{e}+v_\mathrm{r}} \tag{5.17}$$

We define

$$v_\mathrm{min} = \min\{v_\mathrm{e}, v_\mathrm{r}\} \quad , \quad v_\mathrm{max} = \max\{v_\mathrm{e}, v_\mathrm{r}\} \tag{5.18}$$

and write

$$v_\mathrm{e} + v_\mathrm{r} = v_\mathrm{min} + v_\mathrm{max} \tag{5.19}$$

and

$$|v_\mathrm{e}-v_\mathrm{r}| = v_\mathrm{max} - v_\mathrm{min}\ . \tag{5.20}$$

and finally the mean compound velocity can be written as

$$\bar{v}_\mathrm{c} = \frac{1}{3}\ \frac{v_\mathrm{min}^2 + 3v_\mathrm{max}^2}{v_\mathrm{max}}\ . \tag{5.21}$$

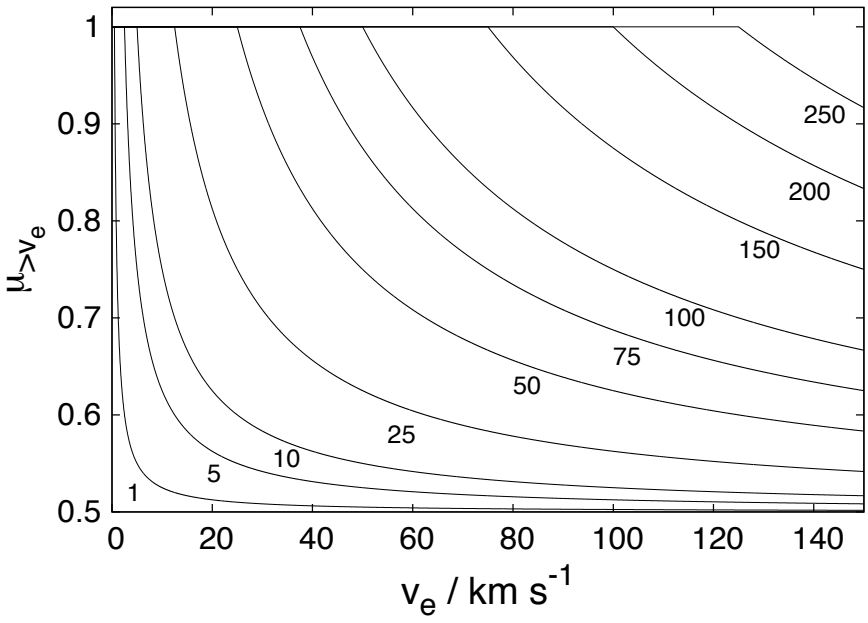

Figure 5.3: The fraction of accelerated stars in dependence of the ejection and release velocity for different release velocities in km s^{-1}.

It follows that the mean compound velocity is always greater than or equal to the ejection and release velocity:

$$\bar{v}_{\rm c} \geq \frac{1}{3}\,\frac{3\,v_{\rm max}^2}{v_{\rm max}} = v_{\rm max}\ . \tag{5.22}$$

For the case that $v_{\rm e} = v_{\rm r}$, which will be important for section 5.5, i.e. the ejection velocity is comaparable to the orbital velocity of the ejected binary, the mean compound velocity is

$$\bar{v}_{\rm c} = \frac{4}{3}\,v_{\rm e} \tag{5.23}$$

5.3 Back-tracing probability

If single stars or binaries are ejected from star clusters it is theoretically possible to calculate their orbits backward, if the force field, through which the objects have moved in time, is given. In such a case the star cluster, where the stars have their origin, can be identified.

If the binary disintegrates due to a supernova, the released component suffers a strong deflection of its previous binary orbit, and the cluster, from where it is expelled, can only

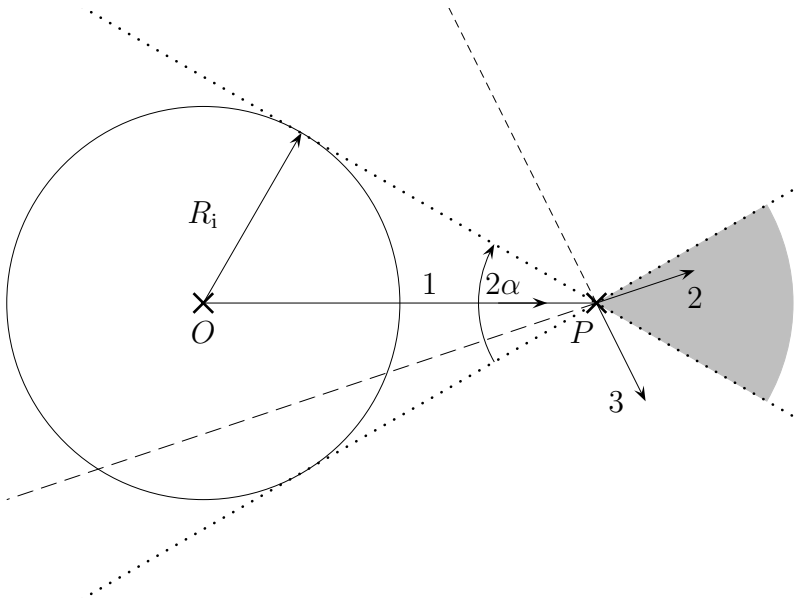

Figure 5.4: Illustration of the back-tracing-probability. See text for details.

be identified if the angle between the deflected and previous orbit is not too large (Fig. 5.4).

A binary is ejected from a star cluster and moves along path 1. After the binary has moved the distance ξ from the centre of the cluster, O, it disintegrates at the position P and one component of the binary is released. The star cluster, from which the star has been ejected, is identified, if the extrapolated path of the released star intersects a sphere with the identification radius, R_i, round the star cluster. If the released star moves along path 2, the star cluster is identified (extrapolated long dashed line). If the star moves along path 3, the parent star cluster can not been identified (extrapolated short dashed line). Only stars which have new orbits within the gray shaded region between the dotted lines can be traced back to their parent star cluster.

At the location of binary disintegration (point P) the identification sphere appears under the angle 2α, i.e. a solid angle of $2\pi(1-\cos\alpha)$. Because the directions of the released stars are randomly distributed over the full solid angle of 4π, the probability that the star cluster can be identified is given by the ratio of the solid angle of the identification sphere and the full solid angle,

$$P = \frac{1-\cos\alpha}{2} \quad . \tag{5.24}$$

The cosine can be expressed by the identification radius, R_i, and the disintegration dis-

Table 5.1: Back-trace probability

$R_{\rm i}/\xi$	1	1/2	1/5	1/10	1/15	1/50
P [‰]	500	67	10	2.5	1	0.1

$R_{\rm i}$ is the radius of the identification sphere around the star cluster from which the binary has been ejected. ξ is the distance between the location of the disintegration of the binary and the centre of the identification sphere which coincides with the centre of the star cluster. P is the back-tracing probability in ‰.

tance, ξ,

$$\cos\alpha = \sqrt{1-\sin^2\alpha} = \sqrt{1-\frac{R_{\rm i}^2}{\xi^2}} \quad . \tag{5.25}$$

Then the identification probability is

$$P = \frac{1}{2}\left(1-\sqrt{1-R_{\rm i}^2/\xi^2}\right) \quad . \tag{5.26}$$

The resulting probabilities for different ratios of the identification radius and disintegration distance are listed in Table 5.3.

5.4 Observed statistics of runaways and apparently isolated O stars

Massive stars and massive binaries can only be ejected dynamically from star clusters during the early stage of their life. If they form within compact few-body configurations or trapezia systems (Clarke & Pringle, 1992), then the decay time scale of these few-body systems (<1 Myr, Pflamm-Altenburg & Kroupa, 2006) implies only early ejections of massive stars. If massive stars and binaries are formed distributed over the star cluster, then ejections can only occur as long as the stellar densities are high. Due to gas expulsion young embedded star clusters become super-virial and start to expand and the stellar density decreases rapidly (Kroupa, Aarseth, & Hurley, 2001). The time scale of decrease of the stellar density is comparable to the gas expulsion time scale, of the order of ≈1 Myr. Thus the time of flight of ejected binaries is comparable to their maximum-lifetime.

Taking a lower velocity cut-off for O-star runaways of 30 km s^{-1} as considered in Gies & Bolton (1986) and a mean life-time of 5 Myr of O-stars implies a disintegration distance ξ =150 pc. For a large identification radius of $R_{\rm i}$ =10 pc of the star cluster, the back-tracing probability is 1 ‰(Table 5.3). Lowering the cut-off velocity of the runaway-star definition to 10 km s^{-1} results in a back-tracing probability of 1 per cent. Thus, ejected massive binaries which are listed in runaway O-star surveys will produce O stars which can not be traced back to their parent star cluster. But one might expect that in this case

the massive star can be traced back to a supernova shell. However, as single supernova shells disappear on a time scale of 0.5–1 Myr (Chevalier, 1974) it might be possible to identify the parent supernova of the released star only in very rare cases.

The observationally derived runaway fraction among O stars varies widely in the literature, (see for example Table 13 in Gies & Bolton, 1986 or Table 5 in Stone, 1991). Gies & Bolton (1986) identified 15 stars out of a sample of 36 runaway candidates with confirmed peculiar radial velocities $\geq$30 km s^{-1}. Comparing with their stated total number of about 90 O stars within their sample space, a runaway fraction of 15/90= 16 per cent results. They further conclude that the true runaway fraction of O stars depends on the adopted velocity cut-off and may lie in the range of 10–25 per cent. Gies & Bolton (1986) also found the binary fraction among runaway O stars in their sample to be about 10 per cent. As explained above, O stars released in a supernova in an ejected massive binary result in field O stars which can not be traced back to their parent star clusters. Thus, on the basis of the O-star runaway fraction and binary fraction of O-runaway data published by Gies & Bolton (1986) 1–2.5 per cent of O stars can not be traced back to the star cluster where they have form. These O stars will appear to have formed in isolation, although they were born in an ordinary star cluster.

The different O-star runaway fractions in the literature have been unified by Stone (1991) by considering true space frequencies: The radial velocity spectrum of O stars is decomposed into two different Gaussian velocity distributions, which correspond to two different Maxwellian space velocity distributions. The high velocity component has a number fraction of $f_{\rm H}$=46 per cent and a velocity distribution of $\sigma_{\rm H}$=28.2 km s^{-1}. By transforming individual O star runaway studies, which are based on individual runaway definitions, to true space frequencies based on bimodality in the velocity distribution of O stars, Stone (1991) achieves good agreement between the different individual studies.

From the runaway fraction of 46 per cent derived by Stone (1991) it follows that a fraction of 4.6 per cent of O stars will apparently form in isolation, if the runaway binary fraction of 10 per cent by Gies & Bolton (1986) is used.

Thus, the two-step-ejection process predicts a fraction of O stars which have formed apparenty in isolation in the range of 1–4.6 per cent. de Wit et al. (2004, 2005) conclude, based on the actually observed positions and velocities of O stars, that 4$\pm$2 per cent of O stars can be considered as candidates of massive stars formed in isolation, because such stars can not be traced back to a young star cluster. Consequently, the process of two-step ejection can quantitatively account for the proposed fraction of massive candidates formed in isolation.

5.5 Maximum possible velocity

The maximum possible velocity in the two-step-ejection process is $v_{\rm max} = v_{\rm r} + v_{\rm e}$, i.e. if the star is released in the moving direction of the previous binary. Binaries can be

ejected from star clusters due to dynamical interactions. Two common situations are the scattering of two binaries (B+B) and the scattering of one binary and one single star (B+S). B+B-events lead commonly to two single runaway stars and one tight binary. But also high velocity binaries can be produced in roughly 10 per cent of all cases (Mikkola, 1983).

In the B+S event high velocity binaries must be produced due to local conservation of linear momentum. The ejection velocity of the single star is typically of the order of the orbital velocity of the binary (Heggie, 1980), $v_{\rm o}$. In the case of equal masses the ejection velocity of the binary, $v_{\rm e}$, is half of the ejection velocity of the single star, $v_{\rm e} = \frac{1}{2}\ v_{\rm o}$. When the ejected binary disintegrates due to a supernova explosion then the maximum possible velocity of the released star is $v_{\rm max} = \frac{3}{2}\ v_{\rm o}$.

If on the other hand, the companion of the massive star is a low-mass star then the ejection velocity of the binary is equal to the ejection velocity of the single star, thus we have $v_{\rm e} = v_{\rm o}$. The maximum possible velocity of the released (less-massive companion) star after binary disintegration is of the order $v_{\rm max} = 2\ v_{\rm o}$. It might be expected that in the case of binaries consisting of a high-mass and a low-mass star encountered by a high-mass star the low-mass star will be ejected and an equal-mass binary will form. To what amount binaries with a large mass ratio will not suffer an exchange has to be quantified numerically in further studies.

5.6 Conclusions

Various theoretical and numerical studies exist on individual ejection processes of masive stars, namely the dynamical ejection scenario and the supernova ejection scenario, but the combined effect of both scenarios has not been considered yet. In this paper we investigate for the first time the combination of the dynamical and the supernova ejection scenario. We call this combined effect the *two-step-ejection* process of massive stars. The main results are as follows:

i) The compound velocity, $v_{\rm c}$, which is the vectorial sum of the ejection velocity, $v_{\rm e}$, of the binary from the star cluster and the release velocity, $v_{\rm r}$, with which a star is released during a supernova, can be larger or smaller than the previous ejection velocity. Stars can be both, accelerated and decelerated.

ii) The mean compound velocity is always greater than each of the initial velocities, $v_{\rm e}$ and $v_{\rm r}$ (eq. 5.22).

iii) It is very unlikely that the parent star cluster of a massive field star produced by the two-step-ejection scenario can be identified. The expected number fraction of such massive field stars which are formed apparently in isolation can account quantitatively for the number of candidates for isolated massive star formation derived in de Wit et al. (2005).

iv) Massive stars which are ejected via the two-step scenario can get higher maximum

space velocities (up to 1.5 times higher for equal-mass binary components or 2 times higher for significantly unequal-mass companion masses) than can be obtained by each process (dynamical or supernova ejection) individually.

Part II

Outlook

Chapter 6

Multiple stellar populations in R136?

The process of capturing field stars by a collapsing pre-cluster cloud core as described in Chapter 3 is not restricted to the ONC, but should occur in any collapsing cloud embedded in an ensemble of field stars. Both the enhanced number of field stars within the cluster and the number of captured field stars mainly depend on the number density and the velocity dispersion of the field stars, and the total mass and the compactness of the newly formed star cluster. Thus, it is expected that massive star clusters should be able to capture more field stars than the ONC.

Brandl et al. (1996) observed 110 faint red sources, the physical nature of which is still unclear, within a field of about 3×3 pc^2 of the centre of R136 in the LMC, and argued that old red giants of that luminosity must be older than 350 Myr and therefore cannot be the explanation of these red sources due to the very young age of R136 of about 1–2 Myr. But such old stars could have been captured by the forming R136.

To determine the number of field stars which can be captured during the formation of a massive star cluster like R136, calculations using the method described in Chapter 3 but using parameters suitable for the formation of a R136-type star cluster need to be done.

Brandl et al. (1996) determined different core radii, $r_{\rm c}$, for different lower stellar mass thresholds, $m_{\rm th}$, ranging from $r_{\rm c}$=0.048 pc for $m_{\rm th}$=40 M$_\odot$ to $r_{\rm c}$=0.29 pc for $m_{\rm th}$=2 M$_\odot$ (see Figure 7.1 in Chapter 7). This range of observed core radii corresponds to Plummer parameters, $b_{\rm cl}$, ranging from $b_{\rm cl}$=0.075 pc to $b_{\rm cl}$=0.45 pc. The total stellar mass above 0.1 M$_\odot$ interior to 20 pc has been estimated to be about 2.7×10^5 M$_\odot$ (Selman et al., 1999). Assuming a common star formation efficiency of 30 % (Lada & Lada, 2003), the total mass of the collapsing cloud would have been $M_{\rm cl}$=9.7×10^5 M$_\odot$. The ensemble of field stars has been set-up by 4×10^6 particles which are uniformly distributed in a sphere of 100 pc giving an initial field density of 0.95 stars/pc^3.

The centre of R136 and the centre of the CCD-image taken by Brandl et al. (1996) do not coincide (Figure 6.1). Thus, the total number of faint red sources must be estimated by extrapolation of the 110 faint red sources observed in a 3.1×3.1 pc^2 field in R136. 68

out of 110 faint red sources lie within a quadrant with a radius of 2.75 pc. Extrapolated to a full disk of radius 2.75 pc around the centre of R136 272 faint red sources are expected to exist in R136.

A grid of simulations, which are carried out as described in Chapter 3, are computed with different final Plummer parameters of the cloud potential and different initial velocity dispersions of the field stars. After 10 Myr the collapse of the pre-cluster cloud core stops. Then the number of all stars within a radius of 2.75 pc (Figure 6.2) and the number of gravitationally bound stars within a radius of 2.75 pc are calculated (Figure 6.3).

In order to compare the results of the simulations with the number of faint red sources in the LMC the two most uncertain parameters, the initial field star density and the velocity dispersion of field stars in the LMC, have to be constrained. Graff et al. (2000) measured the velocity dispersion of 551 carbon stars in the LMC and identified two main groups: a young disk population with a velocity dispersion of 8 km s^{-1} and an old disk component with 22 km s^{-1}. The field star density is much more uncertain. For comparison, in the solar neighbourhood the number density is roughly 0.3 stars pc^{-3} (Chapter 3), three times smaller than the number density in the simulations. If old red giants contribute with ≈25% (Brandl et al., 1996) to the field population then the number of stars obtained in the simulations must be lowered by a factor of ≈10 (dotted lines in Figure 6.2 and 6.3). Therefore, the observed faint red sources can be captured old red giants.

Although the initial question has been answered, a few interesting topics remain and will be explored in the future: i) For the same total collapse time, how do different time evolutions of the increasing cluster potential during cloud collapse affect the number of captured stars? ii) How do different total collapse times affect the number of captured stars? iii) What is the age spectrum of captured stars if the initial field population is composed of stars with distributions of ages and velocity dispersions that are correlated?

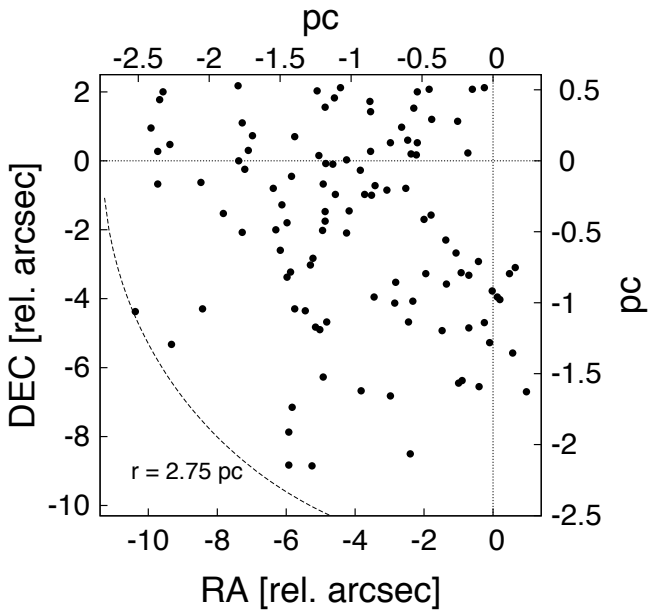

Figure 6.1: Positions of the 110 faint red sources observed by Brandl et al. (1996) in relative arcsec with respect to the centre of R136 (0,0). The relative spatial distance in pc is calculated for an adopted distance of the LMC of 50.1 kpc (Freedman et al., 2001). The outer-most faint red source has a distance of 2.75 pc from the centre of R136. 68 faint red sources lie within the quadrant confined by the dotted lines and the dashed circle. Extrapolated to a full disk with a radius of 2.75 pc 272 faint red sources are expected to exist in this region of R136.

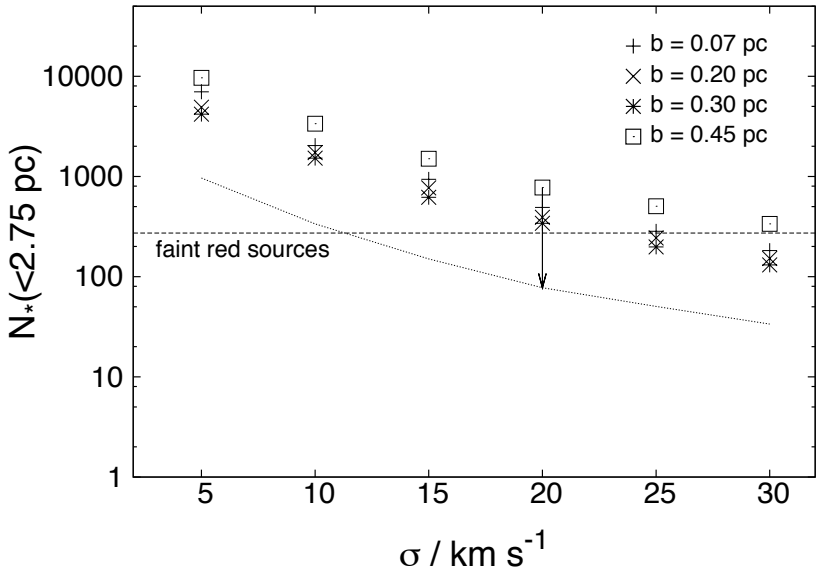

Figure 6.2: Number of all field stars with an initial density of 0.95 stars pc^{-3} after a 10 Myr collapse time within a sphere with a radius of 2.75 pc. The lower dotted curve shows the reduction by a factor of ten (arrow) of the modelled red sources if the true initial density of 0.3 stars pc^{-3} of which 25 % are red giants. The horizontal dashed line shows the number of 272 faint red sources expected to be in R136 after extrapolation to the whole cluster of the 110 observed faint red sources in the imaged region of R136.

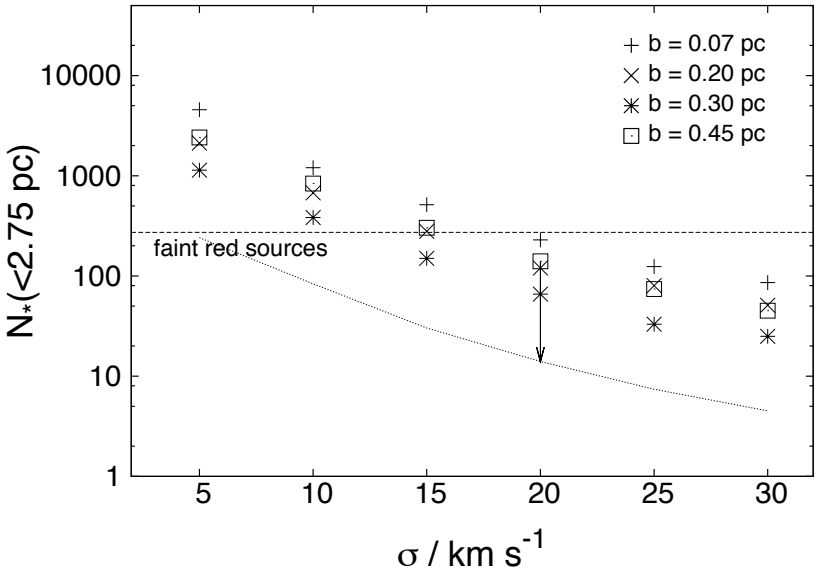

Figure 6.3: Number of gravitationally bound field stars with an initial density of 0.95 stars pc^{-3} after a 10 Myr collapse time within a sphere with a radius of 2.75 pc. The lower dotted curve shows the reduction by a factor of ten (arrow) of the modelled red sources if the true initial density of 0.3 stars pc^{-3} of which 25 % are red giants. The horizontal dashed line shows the number of 272 faint red sources expected to be in R136 after extrapolation to the whole cluster of the 110 observed faint red sources in the imaged region of R136.

Chapter 7

Producing effectively top-heavy IMFs

During star cluster formation not all gas of the collapsing pre-cluster cloud core transforms into stars. The star-formation efficiency is about 30 % (Lada & Lada, 2003). In virial equilibrium the velocity dispersion of the stellar component compensates the gravitational forces of both stars and gas. After the massive stars have ignited their stellar feedback pushes the remaining gas out of the cluster. Then the velocity dispersion of the "naked" stellar ensemble is too large to ensure virial equilibrium and the star cluster starts to expand (Kroupa et al., 2001; Baumgardt & Kroupa, 2007). Through expansion and loss of stars the star cluster can reach a new equilibrium, if it does not dissolve completely.

If the stellar masses are randomly distributed over the pre-gas-expulsion star cluster the IMF of the remaining re-virialised star cluster should be the same as the IMF of the pre-gas expulsion star cluster. In star cluster simulations with gas expulsion it is found that stars which are lost during gas expulsion mostly originate from the outer parts of the pre-gas expulsion star cluster (Marks et al., 2008). Thus, if a significant mass segregation is present before gas expulsion the remaining star cluster is enriched with massive stars compared to the pre-gas-expulsion star cluster. In Marks et al. (2008) this model has been successfully applied to the stellar mass range <1 $M_\odot$ in order to explain the relation between the low-mass IMF slope and the concentration parameter of old Galactic globular clusters observed by De Marchi et al. (2007). But the combined effect of gas expulsion and pre-gas-expulsion mass segregation has not been applied to the high-mass range of the IMF yet.

In order to construct a handy analytical description of the process explained above we first define the spatial or three-dimensional IMF,

$$\xi_3(m, \mathbf{r}) = \frac{dN}{dm\ dx\ dy\ dz} \tag{7.1}$$

which gives the number of stars, dN, with mass m in the interval $[m, m+dm]$ per volume,

$dx\ dy\ dz$, at the position $\mathbf{r} = (x, y, z)$. The integration over the whole star cluster must be equal to the canonical IMF, $\xi(m)$, of the whole star cluster,

$$\xi(m) = 4\pi \int_0^\infty \xi_3(m, r)\ r^2\ dr. \tag{7.2}$$

Here and throughout the whole paper we restrict to spherical symmetry. The cluster-wide IMF is normalised by the total cluster mass,

$$M_{\rm ecl} = \int_{m_{\rm low}}^{m_{\rm max}} \xi(m)\ m\ dm. \tag{7.3}$$

After rapid gas expulsion a fraction

$$f_{\rm b} = \frac{M_{\rm b}}{M_{\rm ecl}} \tag{7.4}$$

of the initial stellar cluster mass $M_{\rm ecl}$ remains in the re-virialised cluster. In star cluster simulations with gas expulsion it is found that stars which are lost during gas expulsion originate from the outer parts of the pre-gas expulsion star cluster (Marks et al., 2008). Thus, the radius, $r_{\rm b}$, beyond which all stars are lost is defined by the integration over the spatial IMF to be equal to the bound mass

$$M_{\rm b} = 4\pi \int_0^{r_{\rm b}} \int_{m_{\rm low}}^{m_{\rm max}} m\ \xi_3(m, r)\ r^2\ dm\ dr, \tag{7.5}$$

All stars within the sphere of radius $r_{\rm b}$ contribute to the new effective IMF, $\xi_{\rm eff}(m)$, of the post-gas-expulsion star cluster,

$$\xi_{\rm eff}(m) = 4\pi \int_0^{r_{\rm b}} \xi_3(m, r)\ r^2\ dr. \tag{7.6}$$

An expression for the spatial IMF, $\xi_3(m)$, before gas expulsion can be extracted from Brandl et al. (1996): They examined the massive-star content of the young star cluster R136 in the LMC. The radial surface number density of stars is described by the analytical King-profile (King, 1962),

$$I_{m_{\rm th}}(r) = k(m_{\rm th}) \left[\frac{1}{\sqrt{1 + \left(\frac{r}{r_{\rm c}(m_{\rm th})}\right)^2}} - \frac{1}{\sqrt{1 + \left(\frac{r_{\rm t}}{r_{\rm c}(m_{\rm th})}\right)^2}} \right]^2 \tag{7.7}$$

considering only stellar masses above a varying threshold mass, $m_{\rm th}$. The core radii, $r_{\rm c}(m_{\rm th})$, for different mass thresholds, $m_{\rm th}$, of R136 derived by Brandl et al. (1996) are

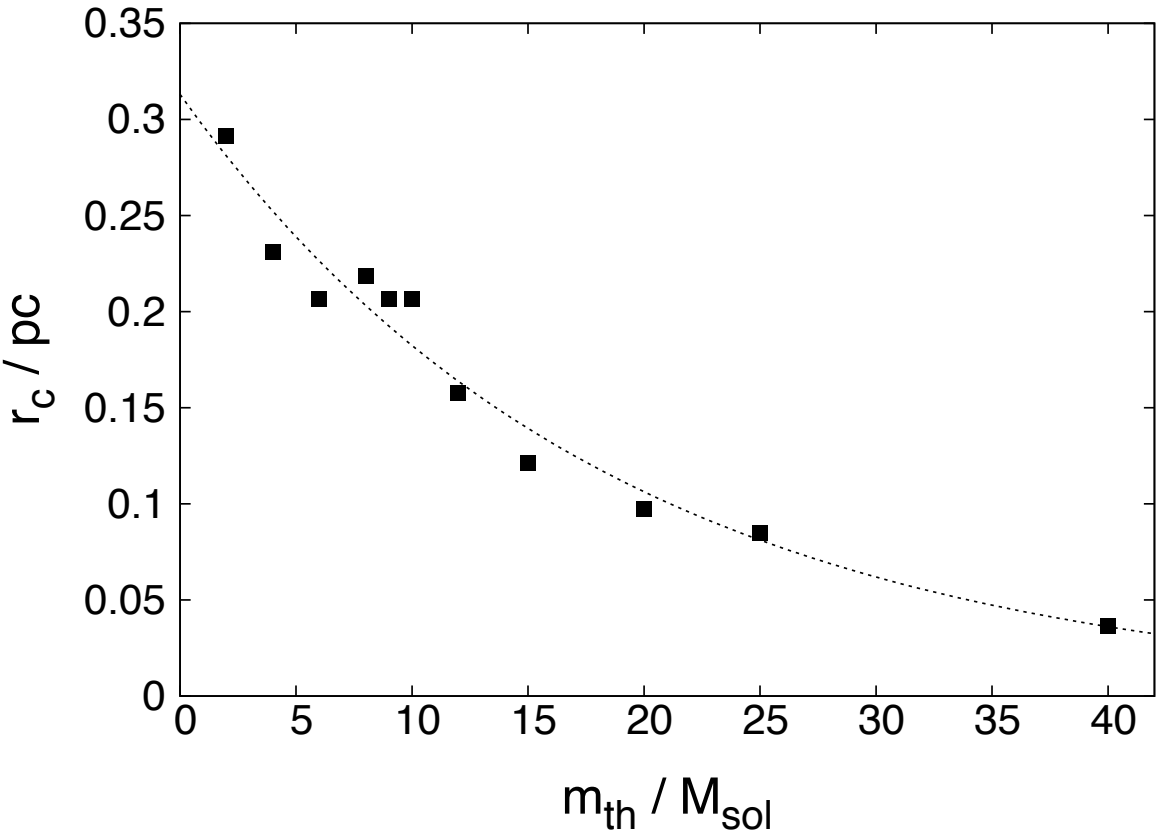

Figure 7.1: Observed core radii of the fitted King-profiles from Brandl et al. (1996) for different threshold masses in R136 after converting the radii measured in arcsec into pc for an adopted distance of the LMC of 50.1 kpc (Freedman et al., 2001). The observed core radii can be interpolated by eq. 7.8 with $r_{\rm c} = 0.313$ pc and $n = 0.054$ (dotted line).

plotted in Figure 7.1. It can be seen that the most massive stars are most concentrated and therefore R136 is mass segregated. For comparison, if R136 would not be mass segregated then the core radii for different threshold masses would be identical.

The observed relation between the core radii and the mass threshold can be described by an exponential law,

$$r_{\rm c}(m_{\rm th}) = r_{\rm c}\, e^{-n\, m_{\rm th}/M_{\rm sol}} \ . \tag{7.8}$$

The larger n is the stronger mass segregation is pronounced. The case of no mass segregation corresponds to $n = 0$. The best fitting parameters for R136 are

$$n_{\rm R136} = 0.054 \quad \text{and} \quad r_{\rm c} = 0.313 \text{ pc} \tag{7.9}$$

and are shown as the dotted line in Figure 7.1.

To get the radial spatial number density, $\rho_{m_{\rm th}}(r)$, of stars above the threshold mass $m_{\rm th}$ the radial surface number density profile, $I_{m_{\rm th}}$, in eq. 7.7 can be deprojected (King,

1962). The mass dependent constant, $k(m_{\rm th})$, in eq. 7.7 is determined by the integral over the radial spatial density, $\rho_{m_{\rm th}}(r)$, to give the same total number of stars with masses above $m_{\rm th}$ as the integral over the total cluster IMF, $\xi(m)$,

$$\int_{m_{\rm th}}^{m_{\rm max}} \xi(m)\, dm = 4\pi \int_0^{\infty} \rho_{m_{\rm th}}(r)\, r^2\, dr\ . \tag{7.10}$$

Now, the spatial three dimensional IMF, $\xi_3(m,r)$, which is required for the calculation of the effective IMF, $\xi_{\rm eff}$, after gas expulsion in eq. 7.6, follows from the integral expression

$$\int_{m_{\rm th}}^{m_{\rm max}} \xi_3(m,r)\, dm = \rho_{m_{\rm th}}(r) \tag{7.11}$$

after differentiating,

$$\xi_3(m,r) = -\frac{\partial \rho_{m_{\rm th}}(r)}{\partial m_{\rm th}}\ . \tag{7.12}$$

For each set of the parameters $f_{\rm b}$, n, and $r_{\rm c}$ a corresponding effective IMF, $\xi_{\rm eff}$, can be calculated.

For precise calculations full N-body simulations with pre-gas-expulsion mass segregation are required. But these simulations are very time consuming and, thus, this simple analytical approach is very efficient and allows a fast and wide parameter study. The algorithm presented here is straightforward and the calculations will be done soon.

Chapter 8

Ejection of massive stars from galaxies

Although massive stars have the shortest life times they can explode in a supernova far away from their birth sites due to the ejection processes described in Chapters 1 and 5.

To get a first estimation of the vertical supernova distribution in a disk galaxy we assume that all O stars have a mean velocity component, $v_{\rm O}$, in the vertical direction and have a time-of-flight from their ejection to the point where they explode in a supernova, $\tau_{\rm f}$. Their time-of-flight should be comparable to their mean life-time, $\tau_{\rm O}$, as ejections of massive stars from young star clusters can only occur while the local stellar number density is very high. The stellar number density of a young star cluster decreases rapidly because the star cluster immediately expands due to gas expulsion after the massive stars have ignited. Because the gas expulsion time scale is of the order of $\approx$1 Myr, the massive stars can only be ejected from young star clusters in the early stage of their life.

We now define the number density rate of massive-star birth,

$$\rho_{\rm b}(z) = \frac{dN_{\rm b}}{dV\ dt}\ , \tag{8.1}$$

which gives the number of massive stars born at the vertical galactic position, z, per volume element, dV, and per time interval, dt. Neglecting the galactic potential for the moment, all massive stars born at the vertical position z contribute to the supernova rate density, $\rho_{\rm SN}(z\prime)$, at the positions $z\prime = z + v_{\rm O}\tau_{\rm O}$ and $z\prime = z - v_{\rm O}\tau_{\rm O}$ with $\frac{1}{2}\ \rho_{\rm b}(z)$ at each position. The vertical supernova rate density,

$$\rho_{\rm SN}(z) = \frac{dN_{\rm SN}}{dV\ dt}\ , \tag{8.2}$$

defines the number of supernovae type II, $dN_{\rm SN}$, at the vertical galactic position, z, per volume element, dV, and per time interval, dt.

Thus, in the equilibrium case the vertical supernova rate density can be estimated by

$$\rho_{\rm SN}(z) = \frac{1}{2}\ (\rho_{\rm b}(z + v_{\rm O}\tau_{\rm O}) + \rho_{\rm b}(z - v_{\rm O}\tau_{\rm O}))\ . \tag{8.3}$$

Gies & Bolton (1986) found in a sample of O-star runaway candidates that 10–25 per cent are runaway stars with radial peculiar velocities larger than 30 km s^{-1}. In a more general analysis Stone (1991) decomposed the radial velocity spectrum of O stars into two Gaussian distributions with a velocity dispersion of $\sigma_{\rm L}$=7.7 km s^{-1} and a number fraction of 54 per cent for the low-velocity component, and $\sigma_{\rm H}$=28.2 km s^{-1} and a number fraction of 46 per cent for the high-velocity component. If an isotropic velocity distribution is assumed then these Gaussian distributions in line-of-sight directions correspond to two Maxwellian distributions of the absolute velocity with the same velocity dispersions. The corresponding mean velocities of the Maxwellian dispersions are

$$\bar{v} = \sqrt{\frac{8}{\pi}}\ \sigma\ , \tag{8.4}$$

being 12.2 km s^{-1} for the low-velocity component and 45.0 km s^{-1} for the high velocity component. In order to estimate a "lower" limit of the vertical supernova distribution we follow a very conservative approach and set the vertical mean velocity to $v_{\rm O}$=10 km s^{-1}. The true vertical supernova distribution can only be wider. The mean stellar life time of supernova type II progenitors can be set to $\tau_{\rm O}$=10 Myr (Köppen et al., 1995).

The vertical birth rate density of massive stars, $\rho_{\rm b}$, can be estimated by the vertical molecular gas distribution combined with a Kennicutt-Schmidt-type (KS) star formation law, which links the local gas density to the local star formation rate density. The vertical density distribution of molecular gas is given, for the Galaxy, in Cox (2005),

$$n_{\rm mol} = 0.58\ {\rm cm}^{-3}\ e^{-(z/81\ {\rm pc})^2}\ . \tag{8.5}$$

The star formation rate density, $\rho_{\rm SF}$, is then given by a KS-type law,

$$\rho_{\rm SF} = A\ \rho_{\rm mol}^n\ . \tag{8.6}$$

The original KS-law links surface densities with each other. We here assume that the relation between the spatial densities has the same functional form, a power-law, with the same exponent $n = 1.4$ (Kennicutt, 1998).

The vertical birth rate density of massive stars, $\rho_{\rm O}$, can be calculated as

$$\rho_{\rm b} = B\ \rho_{\rm SF}\ , \tag{8.7}$$

where the constant B is the number fraction of massive stars in the IMF. As we consider in the following estimation vertical densities, which are normalised to their $z = 0$ value

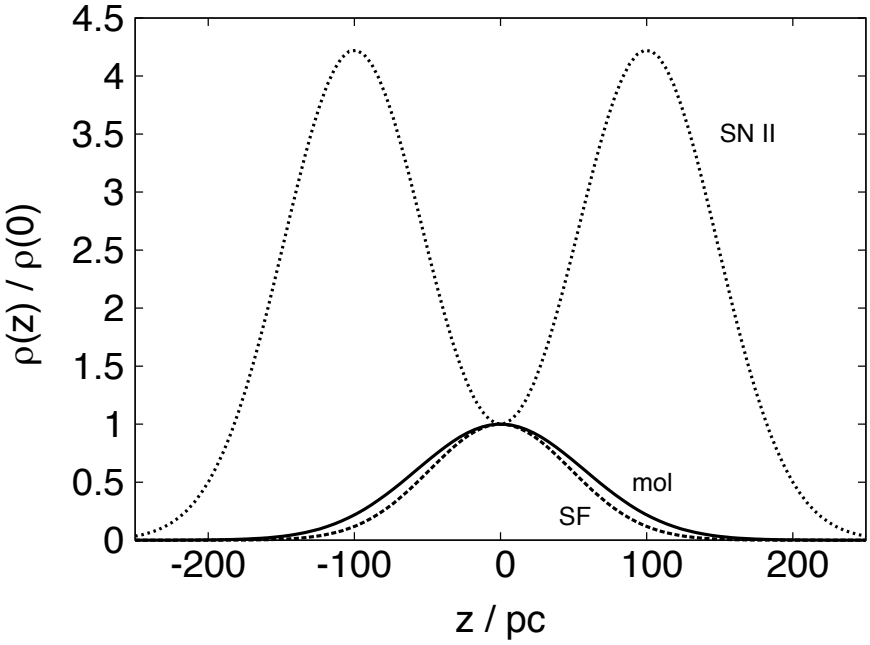

Figure 8.1: The vertical distributions normalised to the $z = 0$ value of the molecular gas density (mol), the star formation rate density (SF, for $n = 1.4$), and the resulting supernova type-II rate density (SN II).

($\rho_{\rm SN}(z)/\rho_{\rm SN}(0)$, $\rho_{\rm SF}(z)/\rho_{\rm SF}(0)$, and $n_{\rm mol}(z)/n_{\rm mol}(0)$) the coefficients A in eq. 8.6 and B in eq. 8.7 cancel out.

For the above stated values $v_{\rm O}$=10 km s^{-1} and $\tau_{\rm O}$=10 Myr the resulting estimated vertical SN-II distribution (eq. 8.3) is plotted in Fig. 8.1. In this simplified one-dimensional model the very thin star formation disk of the Milky Way is sandwiched by two supernova layers. A large fraction of energy feedback by supernovae and the metal release might occur outside the star forming disk. This effect of non-local energy feedback and metal enrichment on galactic evolution has to be investigated in future galaxy evolution models.

In this on-going project the vertical supernova rates will be numerically calculated by performing Monte-Carlo simulations. Individual massive stars with random velocities drawn from an O-star velocity distribution function (Stone, 1991) will be calculated as test particles in the Milky Way gravitational potential (Allen & Santillan, 1991; Dehnen & Binney, 1998). As life times of supernova type II progenitors are of the order of a few Myr the supernova rates will reach an equilibrium within a few tens of Myr. Over this short time scale the Galactic potential can be considered to be constant.

The vertical SN-II distribution has been derived indirectly from the distribution and the kinetic properties of pulsars (Narayan & Ostriker, 1990; Ferrière, 2001),

$$N_{\rm SN}(z) = \frac{50}{\rm kpc\ Myr}\ 0.79\ e^{-(z/212\ {\rm pc})^2} + 0.21\ e^{-(z/636\ {\rm pc})^2}\ . \qquad (8.8)$$

It can be possible that the two-component structure of the O-star velocity spectrum (Stone, 1991) can be in agreement with the indirectly derived SN-II distribution (Narayan & Ostriker, 1990; Ferrière, 2001). This will be explored in this on-going project.

In current galaxy evolution models it is already included that star formation follows gas, but it must additionally be taken into account that feedback from massive stars does not follow the star formation distribution exactly. It is another aim of this on-going project to quantify the spatial galactic SN-distributions and to provide easy-to-handle fitting functions for the usage in galaxy evolution models. An application of this work to star-forming dwarf galaxies is planned.

References

Aarseth, S. J. 1999, PASP, 111, 1333

Aarseth, S. J. 2003, Gravitational N-Body Simulations (Gravitational N-Body Simulations, by Sverre J. Aarseth, pp. 430. ISBN 0521432723. Cambridge, UK: Cambridge University Press, November 2003.)

Allen, C. & Poveda, A. 1974, in IAU Symp. 62: Stability of the Solar System and of Small Stellar Systems, ed. Y. Kozai, 239–246

Allen, C. & Santillan, A. 1991, Revista Mexicana de Astronomia y Astrofisica, 22, 255

Bahcall, J. N., Flynn, C., & Gould, A. 1992, ApJ, 389, 234

Baumgardt, H. & Kroupa, P. 2007, MNRAS, 380, 1589

Baumgardt, H., Kroupa, P., & Parmentier, G. 2008, MNRAS, 384, 1231

Baumgardt, H., Makino, J., Hut, P., McMillan, S., & Portegies Zwart, S. 2003, ApJ, 589, L25

Bedin, L. R., Piotto, G., Anderson, J., et al. 2004, ApJ, 605, L125

Bienayme, O., Robin, A. C., & Creze, M. 1987, A&A, 180, 94

Binney, J. & Tremaine, S. 1987, Galactic dynamics (Princeton, NJ, Princeton University Press, 1987, 747 p.)

Blaauw, A. 1961, Bull. Astron. Inst. Netherlands, 15, 265

Blaauw, A. 1991, in NATO ASIC Proc. 342: The Physics of Star Formation and Early Stellar Evolution, ed. C. J. Lada & N. D. Kylafis, 125–+

Boissier, S., Gil de Paz, A., Boselli, A., et al. 2007, ApJS, 173, 524

Böker, T., Sarzi, M., McLaughlin, D. E., et al. 2004, AJ, 127, 105

Bondi, H. 1952, MNRAS, 112, 195

Bonnell, I. A. & Davies, M. B. 1998, MNRAS, 295, 691

Brandl, B., Sams, B. J., Bertoldi, F., et al. 1996, ApJ, 466, 254

Brown, A. G. A., Blaauw, A., Hoogerwerf, R., de Bruijne, J. H. J., & de Zeeuw, P. T. 1999, in NATO ASIC Proc. 540: The Origin of Stars and Planetary Systems, ed. C. J. Lada & N. D. Kylafis, 411–+

Brown, A. G. A., de Geus, E. J., & de Zeeuw, P. T. 1994, A&A, 289, 101

Chabrier, G. 2003, PASP, 115, 763

Chevalier, R. A. 1974, ApJ, 188, 501

Clarke, C. J. & Pringle, J. E. 1992, MNRAS, 255, 423

Cox, D. P. 2005, ARA&A, 43, 337

Dabringhausen, J., Hilker, M., & Kroupa, P. 2008, MNRAS, 386, 864

D'Antona, F. & Caloi, V. 2004, ApJ, 611, 871

De Marchi, G., Paresce, F., & Pulone, L. 2007, ApJ, 656, L65

de Wit, W. J., Testi, L., Palla, F., Vanzi, L., & Zinnecker, H. 2004, A&A, 425, 937

de Wit, W. J., Testi, L., Palla, F., & Zinnecker, H. 2005, A&A, 437, 247

Decressin, T., Meynet, G., Charbonnel, C., Prantzos, N., & Ekström, S. 2007, A&A, 464, 1029

Dehnen, W. & Binney, J. 1998, MNRAS, 294, 429

Dejonghe, H. & Hut, P. 1986, LNP Vol. 267: The Use of Supercomputers in Stellar Dynamics, 267, 212

Djorgovski, S. G., Gal, R. R., McCarthy, J. K., et al. 1997, ApJ, 474, L19+

Egusa, F., Sofue, Y., & Nakanishi, H. 2004, PASJ, 56, L45

Elmegreen, B. G. 2000, ApJ, 530, 277

Elmegreen, B. G. & Scalo, J. 2006, ApJ, 636, 149

Fabian, A. C. 2003, MNRAS, 344, L27

Fellhauer, M., Kroupa, P., & Evans, N. W. 2006, MNRAS, 372, 338

Ferrière, K. M. 2001, Reviews of Modern Physics, 73, 1031

Figer, D. F. 2005, Nature, 434, 192

Forbes, D. A., Lasky, P., Graham, A. W., & Spitler, L. 2008, MNRAS, 389, 1924

Freedman, W. L., Madore, B. F., Gibson, B. K., et al. 2001, ApJ, 553, 47

Freeman, K. C. & Rodgers, A. W. 1975, ApJ, 201, L71+

Fuentes-Carrera, I., Jablonka, P., Sarajedini, A., et al. 2008, A&A, 483, 769

Georgiev, I. Y., Hilker, M., Puzia, T. H., Goudfrooij, P., & H., B. 2009a, MNRAS, – in press

Georgiev, I. Y., Puzia, T. H., Hilker, M., & Goudfrooij, P. 2009b, MNRAS, 392, 879

Gies, D. R. & Bolton, C. T. 1986, ApJS, 61, 419

Goodman, J., Heggie, D. C., & Hut, P. 1993, ApJ, 415, 715

Goodwin, S. P., Kroupa, P., Goodman, A., & Burkert, A. 2006, Protostars and Planets V., in press

Graff, D. S., Gould, A. P., Suntzeff, N. B., Schommer, R. A., & Hardy, E. 2000, ApJ, 540, 211

Gualandris, A., Portegies Zwart, S., & Eggleton, P. P. 2004, MNRAS, 350, 615

Gvaramadze, V. V. & Bomans, D. J. 2008, A&A, 490, 1071

Haşegan, M., Jordán, A., Côté, P., et al. 2005, ApJ, 627, 203

Hartmann, L. 2003, ApJ, 585, 398

Heggie, D. & Hut, P. 2003, The Gravitational Million-Body Problem: A Multidisciplinary Approach to Star Cluster Dynamics (The Gravitational Million-Body Problem: A Multidisciplinary Approach to Star Cluster Dynamics, by Douglas Heggie and Piet Hut. Cambridge University Press, 2003, 372 pp.)

Heggie, D. C. 1980, in Globular Clusters, ed. D. Hanes & B. Madore, 281–+

Herbig, G. H. & Terndrup, D. M. 1986, ApJ, 307, 609

Hilker, M. & Richtler, T. 2000, A&A, 362, 895

Hillenbrand, L. A. 1997, AJ, 113, 1733

Hillenbrand, L. A. & Hartmann, L. W. 1998, ApJ, 492, 540

Hoffer, J. B. 1983, AJ, 88, 1420

Hoogerwerf, R., de Bruijne, J. H. J., & de Zeeuw, P. T. 2000, ApJ, 544, L133

Hoogerwerf, R., de Bruijne, J. H. J., & de Zeeuw, P. T. 2001, A&A, 365, 49

Hut, P., Makino, J., & McMillan, S. 1995, ApJ, 443, L93

Iben, I. J. & Tutukov, A. V. 1997, ApJ, 491, 303

Isobe, S. & Sesaki, G. 1982, PASJ, 34, 241

Jones, B. F. & Walker, M. F. 1988, AJ, 95, 1755

Kaisin, S. S. & Karachentsev, I. D. 2008, A&A, 479, 603

Karachentsev, I. D. & Kaisin, S. S. 2007, AJ, 133, 1883

Kennicutt, Jr., R. C. 1998, ApJ, 498, 541

Kennicutt, Jr., R. C., Tamblyn, P., & Congdon, C. E. 1994, ApJ, 435, 22

King, I. 1962, AJ, 67, 471

Koen, C. 2006, MNRAS, 365, 590

Köppen, J., Theis, C., & Hensler, G. 1995, A&A, 296, 99

Köppen, J., Weidner, C., & Kroupa, P. 2007, MNRAS, 375, 673

Kroupa, P. 2001, MNRAS, 322, 231

Kroupa, P. 2002, Science, 295, 82

Kroupa, P. 2004, New Astronomy Review, 48, 47

Kroupa, P. 2005, in ESA SP-576: The Three-Dimensional Universe with Gaia, ed. C. Turon, K. S. O'Flaherty, & M. A. C. Perryman, 629–+

Kroupa, P., Aarseth, S., & Hurley, J. 2001, MNRAS, 321, 699

Kroupa, P. & Bouvier, J. 2003, MNRAS, 346, 343

Kroupa, P. & Gilmore, G. F. 1994, MNRAS, 269, 655

Kroupa, P., Petr, M. G., & McCaughrean, M. J. 1999, New Astronomy, 4, 495

Kroupa, P., Tout, C. A., & Gilmore, G. 1993, MNRAS, 262, 545

Kuijken, K. & Gilmore, G. 1989, MNRAS, 239, 651

Kustaanheimo, P. & Stiefel, E. 1965, J. Reine Angew. Math., 218

Lada, C. J. & Lada, E. A. 2003, ARA&A, 41, 57

Lee, J. C., Gil de Paz, A., Tremonti, C., et al. 2009, ApJ, 706, 599

Lehnert, M. D., Bell, R. A., & Cohen, J. G. 1991, ApJ, 367, 514

Leonard, P. J. T. 1991, AJ, 101, 562

Lin, D. N. C. & Murray, S. D. 2007, ApJ, 661, 779

Makino, J. 1991, ApJ, 369, 200

Marks, M., Kroupa, P., & Baumgardt, H. 2008, MNRAS, 386, 2047

Martel, H., Evans, II, N. J., & Shapiro, P. R. 2006, ApJS, 163, 122

Mathews, W. G. & Brighenti, F. 2003, ARA&A, 41, 191

Matthews, L. D. & Gallagher, III, J. S. 2002, ApJS, 141, 429

McKee, C. F. 1995, in Astronomical Society of the Pacific Conference Series, Vol. 80, The Physics of the Interstellar Medium and Intergalactic Medium, ed. A. Ferrara, C. F. McKee, C. Heiles, & P. R. Shapiro, 292–+

McLaughlin, D. E. & van der Marel, R. P. 2005, ApJS, 161, 304

Megeath, S. T., Flaherty, K. M., Hora, J., et al. 2005, in IAU Symposium, ed. R. Cesaroni, M. Felli, E. Churchwell, & M. Walmsley, 383–388

Meurer, G. R., Wong, O. I., Kim, J. H., et al. 2009, ApJ, 695, 765

Meylan, G., Sarajedini, A., Jablonka, P., et al. 2001, AJ, 122, 830

Mieske, S. & Baumgardt, H. 2007, A&A, 475, 851

Mikkola, S. 1983, MNRAS, 203, 1107

Mikkola, S. 1984, MNRAS, 207, 115

Mikkola, S. & Aarseth, S. J. 1990, CeMDA, 47, 375

Mikkola, S. & Aarseth, S. J. 1993, CeMDA, 57, 439

Miller, G. E. & Scalo, J. M. 1979, ApJS, 41, 513

Milone, A. P., Bedin, L. R., Piotto, G., et al. 2007, ArXiv e-prints, 709

Milosavljević, M. 2004, ApJ, 605, L13

Morgan, S. & Lake, G. 1989, ApJ, 339, 171

Narayan, R. & Ostriker, J. P. 1990, ApJ, 352, 222

Oey, M. S. & Clarke, C. J. 2005, ApJ, 620, L43

Olczak, C., Pfalzner, S., & Eckart, A. 2008, A&A, 488, 191

Palla, F., Randich, S., Flaccomio, E., & Pallavicini, R. 2005, ApJ, 626, L49

Parker, R. J. & Goodwin, S. P. 2007, MNRAS, 380, 1271

Parriott, J. R. & Bregman, J. N. 2008, ApJ, 681, 1215

Pflamm-Altenburg, J. & Kroupa, P. 2006, MNRAS, 373, 295

Pflamm-Altenburg, J. & Kroupa, P. 2007, MNRAS, 375, 855

Pflamm-Altenburg, J. & Kroupa, P. 2009a, MNRAS, 397, 488

Pflamm-Altenburg, J. & Kroupa, P. 2009b, ApJ, 706, 516

Pflamm-Altenburg, J. & Kroupa, P. 2009c, MNRAS– submitted

Pflamm-Altenburg, J., Weidner, C., & Kroupa, P. 2007, ApJ, 671, 1550

Pflamm-Altenburg, J., Weidner, C., & Kroupa, P. 2009, MNRAS, 395, 394

Plummer, H. C. 1911, MNRAS, 71, 460

Poveda, A., Ruiz, J., & Allen, C. 1967, Boletin de los Observatorios Tonantzintla y Tacubaya, 4, 86

Preibisch, T., Brown, A. G. A., Bridges, T., Guenther, E., & Zinnecker, H. 2002, AJ, 124, 404

Prince, P. J. & Dormand, J. R. 1981, JCAM, 7, 67

Ramspeck, M., Heber, U., & Edelmann, H. 2001, A&A, 379, 235

Recchi, S., Calura, F., & Kroupa, P. 2009, A&A, 499, 711

Recchi, S. & Danziger, I. J. 2005, A&A, 436, 145

Ree, C. H., Yoon, S.-J., Rey, S.-C., & Lee, Y.-W. 2002, in ASP Conf. Ser. 265: Omega Centauri, A Unique Window into Astrophysics, ed. F. van Leeuwen, J. D. Hughes, & G. Piotto, 101–+

Reid, I. N., Gizis, J. E., & Hawley, S. L. 2002, AJ, 124, 2721

Renzini, A. 2008, accepted by A&A, 808

Richter, P., Hilker, M., & Richtler, T. 1999, A&A, 350, 476

Sacco, G. G., Randich, S., Franciosini, E., Pallavicini, R., & Palla, F. 2007, A&A, 462, L23

Sarajedini, A. & Layden, A. C. 1995, AJ, 109, 1086

Schaerer, D., Meynet, G., Maeder, A., & Schaller, G. 1993, A&AS, 98, 523

Selman, F., Melnick, J., Bosch, G., & Terlevich, R. 1999, A&A, 347, 532

Seth, A. C., Blum, R. D., Bastian, N., Caldwell, N., & Debattista, V. P. 2008, ApJ, 687, 997

Seth, A. C., Dalcanton, J. J., Hodge, P. W., & Debattista, V. P. 2006, AJ, 132, 2539

Shustov, B. M. & Wiebe, D. S. 2000, MNRAS, 319, 1047

Skillman, E. D., Côté, S., & Miller, B. W. 2003, AJ, 125, 593

Spitzer, L. 1987, Dynamical evolution of globular clusters (Princeton, NJ, Princeton University Press, 1987, 191 p.)

Sterzik, M. F. & Durisen, R. H. 1998, A&A, 339, 95

Stone, R. C. 1991, AJ, 102, 333

Strom, K. M. & Strom, S. E. 1993, ApJ, 412, L63

Tan, J. C., Krumholz, M. R., & McKee, C. F. 2006, ApJ, 641, L121

Valtonen, M. J. 1974, in IAU Symp. 62: Stability of the Solar System and of Small Stellar Systems, 211–223

van Altena, W. F., Lee, J. T., Lee, J.-F., Lu, P. K., & Upgren, A. R. 1988, AJ, 95, 1744

Ventura, P. & D'Antona, F. 2008, A&A, 479, 805

Vine, S. G. & Bonnell, I. A. 2003, MNRAS, 342, 314

Walcher, C. J., van der Marel, R. P., McLaughlin, D., et al. 2005, ApJ, 618, 237

Warren, Jr., W. H. & Hesser, J. E. 1978, ApJS, 36, 497

Weidner, C. & Kroupa, P. 2004, MNRAS, 348, 187

Weidner, C. & Kroupa, P. 2006, MNRAS, 365, 1333

Weidner, C., Kroupa, P., & Bonnell, I. 2009, MNRAS – in press

Weidner, C., Kroupa, P., & Larsen, S. S. 2004, MNRAS, 350, 1503

Wünsch, R., Tenorio-Tagle, G., Palouš, J., & Silich, S. 2008, ApJ, 683, 683

Yoon, S.-J., Joo, S.-J., Ree, C. H., et al. 2008, ApJ, 677, 1080

Zwicky, F. 1957, Morphological astronomy (Berlin: Springer, 1957)

Publications

Publications/work preceded by a $*$ are part of the PhD project and presented in this thesis.

Accepted

1. **Pflamm-Altenburg, Jan** & Kroupa, Pavel, 2009, **ApJ**, 706, 516 — *The Fundamental Gas Depletion and Stellar-mass Buildup Times of Star-Forming Galaxies*

$*$ 2. **Pflamm-Altenburg, Jan** & Kroupa, Pavel, 2009, **MNRAS**, 397, 488 — *Recurrent gas accretion by massive star clusters, multiple stellar populations and mass thresholds for spheroidal stellar systems* ⟶ Chap. 4

3. **Pflamm-Altenburg, Jan**, Weidner, Carsten & Kroupa, Pavel, 2009, **MNRAS**, 395, 394 — *Diverging UV and Hα fluxes of star-forming galaxies predicted by the IGIMF theory*

4. **Pflamm-Altenburg, Jan** & Kroupa, Pavel, 2008, **Nature**, 455, 641 — *Clustered star formation as a natural explanation of the Hα cut-off in disk galaxies*

5. **Pflamm-Altenburg, Jan**, Weidner, Carsten & Kroupa, Pavel, 2007, **ApJ**, 671, 1550 — *Converting Hα Luminosities into Star Formation Rates*

$*$ 6. **Pflamm-Altenburg, Jan** & Kroupa, Pavel, 2007, **MNRAS**, 375, 855 — *Captured older stars as the reason for apparently prolonged star formation in young star clusters* ⟶ Chap. 3

$*$ 7. **Pflamm-Altenburg, Jan** & Kroupa, Pavel, 2006, **MNRAS**, 373, 295 — *A highly abnormal massive star mass function in the Orion Nebula cluster and the dynamical decay of trapezium systems* ⟶ Chap. 2

Submitted

8. **Pflamm-Altenburg, Jan**, Weidner, Carsten & Kroupa, Pavel, 2009, *MNRAS* — *The IMF in galaxies*

∗ 9. **Pflamm-Altenburg, Jan** & Kroupa, Pavel, 2008, *MNRAS* — *Two step ejection of massive stars and the issue of their formation in isolation* ⟶ Chap. 5

To be submitted / in preparation

10. **Pflamm-Altenburg, Jan** & Hensler, Gerhard, — *Accretion regulated star formation*

11. Weidner, C., Kroupa, P. & **Pamm-Altenburg, Jan**, — *Top-heavy IGIMFs in starbursts*

∗12. **Pflamm-Altenburg, Jan** & Kroupa, Pavel, — *Multiple stellar populations in R136?* ⟶ Chap. 6

∗13. **Pflamm-Altenburg, Jan** & Kroupa, Pavel, — *Ejection of massive stars from galaxies* ⟶ Chap. 8

14. **Pflamm-Altenburg, Jan** & Kroupa, Pavel, — *The star formation rate in the local universe*

∗15. **Pflamm-Altenburg, Jan** & Kroupa, Pavel, — *Producing effectively-top heavy IMFs* ⟶ Chap. 7

16. **Pflamm-Altenburg, Jan**, Weidner, Carsten & Kroupa, Pavel, — *A varying WR-RSG number ratio among star forming galaxies*

Talks, posters & press releases

Talks

- Galaxy Metabolism: Galaxy Evolution near and far, 22–26 June 2009, Sydney, Australia —
  Consequences of clustered star formation for the astrophysics of disk galaxies
- Tidal Dwarf Galaxies: Ghosts from structure formation, 25-29 May 2009, Bad Honnef, Germany —
  On the star-formation efficiencies of dwarf galaxies
- From Taurus to the Antennae, 4–8 August 2008, Sheffield, UK —
  Consequences of clustered star formation for the astrophysics of disk galaxies
- SPP1177-meeting, 9.–12. Oktober 2007, Bad Honnef, Germany —
  The determination of star formation rates of dwarf galaxies
- 22. Graduiertenkolleg 787 Meeting, 7th/8th December 2006, Bad Honnef, Germany —
  Multiple stellar populations in star clusters
- Utrecht-Bonn meeting, 26th Januar 2006, Utrecht, The Netherlands —
  Gas accretion by compact massive star clusters
- MOdeling DEnse STellar systems (MODEST)-6a, 12–15 December, 2005, Lund, Sweden —
  Star cluster cores as stellar accelerators
- Rhine Stellar Dynamics Network (RSDN) meeting, 25–27 November 2005, Hoher List, Germany —
  Older stars captured in the ONC by cloud collapse
- 21. Graduiertenkolleg 787 Meeting, 17th/18th November 2005, Bad Honnef, Germany —
  Older stars captured in the ONC by cloud collapse

- Herbsttagung der Astronomischen Gesellschaft, 26th September 2005 – 1st October 2005, Cologne, Germany — *Why is the Orion Trapezium still there?*
- 20. Graduiertenkolleg 787 Meeting, 02th/03th June 2005, Bad Honnef, Germany — *An Overview of Direct Methods in N-Body Simulations The decay of massive cores of young star clusters*
- Rhine Stellar Dynamics Network (RSDN) meeting, 15th/16th October 2004, Hoher List, Germany —
  The decay of massive cores of young star clusters
- Splinter Meeting of the Annual Meeting of the Astronomical Society (AG)Prague: The Formation of Massive Stars, 20–25 September 2004, Prague, Czech Republic —
  The decay of massive cores of young star clusters
- 17. Graduiertenkolleg 787 Meeting, 26th November 2004, Bochum, Germany — *On the dynamics of the Orion Nebular Cluster Trapezium System*

Posters

- IAUS 254: The Galaxy Disk in Cosmological Context, 9–13 June 2008, Copenhagen, Danmark —
  Consequences of clustered star formation for the astrophysics of disc galaxies
- Next Generation of Computational Models of Baryonic Physics in Galaxy Formation: From Protostellar Cores to Disk Galaxies, 17-21 September 2007, Zurich, Switzerland —
  Converting Halpha-Luminosity into SFRs
- IAUS 246: Dynamical Evolution of Dense Stellar Systems, 5–9 September 2007, Capri, Italy —
  The origin of complex stellar populations in compact star clusters
- The Milky Way Halo - Stars and Gas: Locations, Motions, Origins, 29 May – 2 June 2007, Bonn, Germany —
  Determination of SFRs of dwarf galaxies
- Pathways Through an Eclectic Universe, 23–27 April, 2007, Teneriffe, Spain — *Converting Hα luminosities into star formation rates*
- Herbsttagung der Astronomischen Gesellschaft, 26th September 2005 – 1st October 2005, Cologne, Germany — *Older stars captured in the ONC by cloud collapse*

- IAUS 227: Massive Star Birth: A Crossroads of Astrophysics, 16–20 May 2005, Acireale, Italy —
  The dynamical decay of massive cores of young star clusters

Press releases

- in prep: Sternentstehung im Verborgenen – *Vorhersage Bonner Astronomen durch amerikanische Sternentstehungsstudie besttigt*,
  `(tbd)` —
  based on: Pflamm-Altenburg, Jan & Kroupa, Pavel, 2009, ApJ, 706, 516
  Pflamm-Altenburg, Jan, Weidner, Carsten & Kroupa, Pavel, 2009, MNRAS, 395, 394

- 06.07.2009: Nimmersatte Sternhaufen – *Bonner Studie zeigt, warum manche Sternhaufen immer wieder Nachwuchs bekommen*,
  `(http://www3.uni-bonn.de/Pressemitteilungen/207-2009)` —
  based on: Pflamm-Altenburg, Jan & Kroupa, Pavel, 2009, MNRAS, 397, 488

- 01.10.2008: More star births than astronomers have calculated – *Bonn study in "Nature" explains the discrepancy*,
  `(http://www3.uni-bonn.de/Press-releases/119_2008)` —
  based on: Pflamm-Altenburg, Jan & Kroupa, Pavel, 2008, Nature, 455, 641

Appendix A

CATENA[1]

Pflamm-Altenburg, J., Kroupa, P., 2006, **MNRAS**, 373, 295 (Chapter 2)

This appendix presents the manual page of the CATENA *code which has been developed for the numerical integration of few-body systems.*

CATENA(1) Orbit Integrator CATENA(1)

NAME

catena - orbit integrator

SYNOPSIS

catena {in=input} [out=output] [view=view_output] [OPTIONS]

DESCRIPTION

Catena integrates the orbits of an ensemble of stars for which initial configurations are specified in an extra input file. The output is written formatted and in binary mode, appropriate for an orbit visualization program (OrbitView).

Catena uses the chain-regularisation method (Mikkola & Aarseth, 1990, 1993), to avoid errors resulting from close encounters which are frequent in compact few-body systems, combined with an embedded Runge-Kutta integration method of 9(8)th order (Prince & Dormand, 1981).

Catena is Latin for chain and can be read as an acronym standing for ChAin inTEgrator for Numerous Applications.

[1]Catena is freely available via the Downloads page at the AIfA: http://www.astro.uni-bonn.de/~webaiub/german/downloads.php

OPTIONS

in=<input file>
The initial orbit configuration in the INPUT format from 'input file'. The input file must be specified. Otherwise CATENA exits. Initial conditions can be created with MakeCluster.

out=<output file>
The output is written formatted in constant time intervals in the format OUTPUT_F to 'output file'.

view=<binary output file>
The output is written in format VIEW to 'binary output file' at constant time intervals appropriate for an orbit viewer (OrbitView).

tu=<unit>
Time unit: available are Myr, yr, s. DEFAULT: see option –default.

su=<unit>
Space unit: available are pc, ly, AU, m. DEFAULT: see option –default.

mu=<unit>
Mass unit: available are M_sun, kg. DEFAULT: see option –default.

t_end=<value>
The total physical time in tu. If t_end is negative then CATENA integrates backwards in time. DEFAULT: see option –default.

dt_out=<value>
Time interval in tu between two outputs. If dt_out is negative than CATENA integrates backwards in time. DEFAULT: see option –default.

t_max=<value>
Maximum run time in sec. DEFAULT: see option –default.

ctrl=<value>
Control parameter for calculating the time-step. DEFAULT: see option – default.

ctrl_out=<value>
To write output at a certain physical time the regularised time step must be chosen appropriately. If the output time lies within a window of plus/minus ctrl_out given in tu around t_out, output is written. DEFAULT: see option –default.

a=<value>
Coefficient for the kinetic energy in the time transformation function g = 1/(a*T-b*U). DEFAULT: see option –default.

b=<value>
Coefficient for the potential energy in the time transformation function g = 1/(a*T-b*U). DEFAULT: see option –default.

–f_out_cms
Formatted output is written in the centre of mass reference frame, i.e. the cms is at rest at the origin. DEFAULT: see option –default.

–f_no_out_cms
Formatted output is written in the original reference frame. DEFAULT: see option –default.

–v_out_cms
Output for the orbit viewer is written in the center of mass reference frame, i.e. the cms is at rest at the origin. DEFAULT: see option –default.

–v_no_out_cms
Output for the orbit viewer is written in the original reference frame. DEFAULT: see option –default.

–trt
CATENA provides a time reversal test. The initial configuration is integrated forward in time, stops at t_end, and integrates backward in time to 0. A message containing the initial and final values of the positions and velocities and their displacements is printed. Negative values for t_end and dt_out are ignored. DEFAULT: see option –default.

–time_reversal_test
See option –trt.

–no_trt
No time reversal test. See option –trt.

–no_time_reversal_test
No time reversal test. See option –trt.

–no_nb
The system will not be scaled internally to general N-body units. It is only scaled to ensure G=1. Output is written in the specified units. DEFAULT: see option –default.

–nb
If the total energy is negative, then the system will be scaled internally to general N-body units: G=1, M=1, E=-0.25. Output is written in the specified units. DEFAULT: see option –default.

–help
Print help message to stdout.

-h
Print help message to stdout.

–version
Print version message to stdout.

-v
Print version message to stdout.

–default
Print the default values.

-d
Print the default values.

STATUS MESSAGE

CATENA handles the signal USR1 by printing the actual status of the simulation. This is not the last output. Find out the process ID of the running executable by

ps -e

Then type in

kill -10 <PID of CATENA>

The signal is forwarded by the kernel to the executable and the signal handler installed forces CATENA to write a message of the actual status.

FILE FORMATS

Values are given in tu, su, and mu and are separated by spaces, lines are completed by EOL (end of line, \n in C).

INPUT

<number of stars>\n
<m1> <x1> <y1> <z1> <vx1> <vy1> <vz1>\n
<m2> <x2> <y2> <z2> <vx2> <vy2> <vz2>\n
...
<mn> <xn> <yn> <zn> <vxn> <vyn> <vzn>\n

The line specifying the number of stars can be omitted. CATENA then determines the number of stars automatically. The input file can also contain some comments. Each line of comments must have one of the following characters at its first position: '#', '%' or '!'.

OUTPUT_F

Each line consists of the whole phase space configuration at a certain time:

<t> <m1> <x1> <y1> <z1> <vx1> <vy1> <vz1> <m2> <x2> <y2> <z2>
...
<mn> <xn> <yn> <zn> <vxn> <vyn> <vzn>\n

VIEW

This file format consists of a header, specifying the number of stars, the time step and the masses, and a body containing the phase space information. All entries are in binary format.

Header:

<number of stars, integer>
<delta_t_out dt, double>
<m1, double>
...
<mn, double>

Body:

<x1 at t0, double><y1 at t0, double><z1 at t0, double>
...
<xn at t0, double><yn at t0, double><zn at t0, double>
<x1 at t0+dt, double><y1 at t0+dt, double><z1 at t0+dt, double>
...
<xn at t0+dt, double><yn at t0+dt, double><zn at t0+dt, double>
...

PHYSICAL UNITS

Different units are available for time, space and mass:

time: Myr, yr, s; where 1 yr = 60 * 60 * 24 * 365.25 s; DEFAULT: see option –default.

space: pc, ly, AU, m; DEFAULT: see option –default.

mass: M_sun, kg; DEFAULT: see option –default.

The gravitational constant G is implemented in SI-units by

$$G = 6.6726\text{e-}11\ m^3 / (kg * s^2)$$

NBODY UNITS

After reading the initial configuration, the system is transformed such that the centre of mass is at rest at the origin. Space, time and mass are then scaled again into N-body units, i.e. the gravitational constant G, the total CMS-energy E, and the total mass M have dimensionless values.

Let t, m, r, v, E, G, M be the physical quantities, t˜, m˜, ... the quantities scaled to arbitrary N-body units, and f_t, f_r, f_v, ... the corresponding scaling factors:

t = f_t * t˜; m = f_m * m˜; r = f_r * r˜; ...

By setting G˜, M˜, and E˜one gets three linked equations which specify f_t, f_m, and f_r. The other scaling factors are expressed in terms of these three basic units:

f_m = M / M˜

f_r = (G*E˜*M²) / (G˜*E*M˜²)

f_t = sqrt((E˜³*M³*G²)/(E³*M˜³*G˜²))

f_v = f_r / f_t

f_a = f_r / f_t²

f_E = f_m * f_r² / f_t²

Catena has fixed N-body units:

E < 0:

Scaling is done to satisfy the conditions:

M˜= 1 ; G˜= 1 ; E˜= -1/4

E >= 0:

Scaling is done to satisfy the condition:

G˜= 1

Output is written in the specified units, not in N-body units.

TIME TRANSFORMATION FUNCTION

The regularisation is based on a time and space transformation to remove the singularities in the equations of motion. In the Hamiltonian formulation of regularisation the space transformation is the so-called KS-transformation, and the time transformation is usually an expression of the energies (proportional to R, the closest two-body separation, as R→0). Catena uses as time transformation

g = 1./(a*T-b*U) ,

which gives for a = 1 and b = 1 the Lagrangian. NOTE: In the formulation of Mikkola & Aarseth the Lagrangian is defined by L = T + U and the Hamiltonian by H = T - U. Therefore their gravitational potential contains no minus sign.

OUTLOOK

CATENA will be extended by the following features soon: external potential (Plummer), handling an arbitrary number of very close binaries (principle of adiabatic invariance), physical collisions, other regularisation methods (global, wheel-spoke, TTL) to integrate special configurations efficiently .

AUTHOR

Written by Jan Pflamm-Altenburg at the Sternwarte Bonn, Germany.

LAST UPDATE

12th November 2008

REPORTING BUGS

Please report any bug or mistake to <jpflamm@astro.uni-bonn.de>.

COPYRIGHT

Mikkola, S., Aarseth, S. J., 1993, CeMDA, 57, 439

Mikkola, S., Aarseth, S. J., 1990, CeMDA, 57, 375

Pflamm-Altenburg, J., Kroupa P., 2006, MNRAS, 373, 295

E.g., this can be done by including a sentence like: These results are obtained with the code CATENA (Pflamm-Altenburg & Kroupa, 2006) based on the CHAIN-regularisation method by Mikkola & Aarseth (1990, 1993).

THANKS

Sverre Aarseth: reported bug in the command-line-parsing-routine; (Dec 3rd, 2005) - fixed

Sverre Aarseth: suggestions concerning manpage (Jan 26th, 2006)

REFERENCES

Aarseth, S. J., 2003, Gravitational N-Body Simulations, Cambridge University Press

Mikkola, S., Aarseth, S. J., 1990, CeMDA, vol. 47, no. 4, p. 375-390. - A Chain Regularization Method for the Few-Body Problem

Mikkola, S., Aarseth, S. J., 1993, CeMDA, vol. 57, no. 3, p. 439-459 - An Implementation of N-Body Chain Regularization

Pflamm-Altenburg, J., Kroupa P., 2006, MNRAS, 373, 295 - A highly abnormal massive-star mass function in the Orion Nebula cluster and the dynamical decay of trapezia systems

Prince, P. J., Dormand, J. R., 1981, JCAM, 7, 67 - High order embedded Runge-Kutta formulae

SEE ALSO

OrbitView(1)

catena March 2005 CATENA(1)

Appendix B

A practical numerical formulation of the IMF

Pflamm-Altenburg, J., Kroupa, P., 2006, **MNRAS**, 373, 295 (Chapter 2)

This appendix presents a convenient and general mathematical description of the stellar IMF, discusses its normalisation to a real physical system and its discretisation.

B.1 The general IMF

When doing research using the IMF a multi-power-law,

$$\xi(m) = k \begin{cases} \left(\frac{m}{m_{\rm H}}\right)^{-\alpha_0} & ,m_{\rm low} \leq m \leq m_{\rm H} \\ \left(\frac{m}{m_{\rm H}}\right)^{-\alpha_1} & ,m_{\rm H} \leq m \leq m_0 \\ \left(\frac{m_0}{m_{\rm H}}\right)^{-\alpha_1} \left(\frac{m}{m_0}\right)^{-\alpha_2} & ,m_0 \leq m \leq m_1 \\ \left(\frac{m_0}{m_{\rm H}}\right)^{-\alpha_1} \left(\frac{m_1}{m_0}\right)^{-\alpha_2} \left(\frac{m}{m_1}\right)^{-\alpha_3} & ,m_1 \leq m \leq m_{\rm max} \end{cases} , \tag{B.1}$$

with exponents for its canonical form,

$$\begin{array}{rcl} \alpha_0 = +0.30 & , & 0.01 \leq m/M_\odot \leq 0.08, \\ \alpha_1 = +1.30 & , & 0.08 \leq m/M_\odot \leq 0.50, \\ \alpha_2 = +2.30 & , & 0.50 \leq m/M_\odot \leq 1.00, \\ \alpha_3 = +2.35 & , & 1.00 \leq m/M_\odot \leq +\infty, \end{array} \tag{B.2}$$

(Kroupa et al., 1993; Reid et al., 2002; Kroupa, 2001; Weidner & Kroupa, 2004) requires many if-statements in code implementations. Note however that the canonical IMF parametrisation constitutes a two-part power-law IMF in the stellar regime: $\alpha_1 = 1.3$ for

$m \leq 0.5\ M_\odot$ and $\alpha_{2,3} = 2.3$ for $m \geq 0.5\ M_\odot$. Here we present a general formulation for an IMF that avoids these difficulties with IF-statements and allows any number of mass segments and types of interpolating functions. Complicated code constructions containing if-statements are replaced by two easy loops. The described method is realised by some very handy functions implemented in a shared C-library, and is available on request or at the AIfA homepage[1]. The formulation described below can be applied to any arbitrary distribution functions for any purpose.

Due to historical reasons multi-power-law IMFs start indexing intervals and slopes at zero instead of one. For simplicity we here index n intervals from 1 up to n.

Consider an arbitrary IMF with n intervals fixed by the mass array $[m_0, \ldots, m_n]$ and the array of functions $f_1, \ldots, f_n$. So on the i-th interval $[m_{i-1}, m_i]$ the IMF is described by the function f_i. For the case of a multi-power law the functions may be chosen to be

$$f_i(m) = m^{-\alpha_i} \ . \tag{B.3}$$

To make this power-law description correspond to the multi-power-law given above the IMF-slope indices above need to be shifted by one.

The following general IMF-description does not require power-laws for the functions f_i, but also any kind of function is allowed. This includes log-normal IMFs (Miller & Scalo, 1979; Chabrier, 2003).

With the two Θ-mappings

$$\Theta_{[\ ]}(x) = \begin{cases} 1 & x \geq 0 \\ 0 & x < 0 \end{cases} \tag{B.4}$$

and

$$\Theta_{]\ [}(x) = \begin{cases} 1 & x > 0 \\ 0 & x \leq 0 \end{cases} \ , \tag{B.5}$$

the function

$$\Gamma_{[i]}(m) = \Theta_{[\ ]}(m - m_{i-1})\Theta_{[\ ]}(m_i - m) \tag{B.6}$$

can be defined. It is unity on the interval $[m_{i-1}, m_i]$ and zero otherwise. The complete IMF can be conveniently formulated by

$$\xi(m) = k \prod_{j=1}^{n-1} \Delta(m - m_j) \sum_{i=1}^{n} \Gamma_{[i]}(m)\ \Psi_i\ f_i(m) \ , \tag{B.7}$$

where k is a normalisation constant and the array $(\Psi_1, \ldots, \Psi_n)$ is to ensure continuity at the interval boundaries. They are defined recursively by

$$\Psi_1 = 1 \quad , \quad \Psi_i = \Psi_{i-1}\ \frac{f_{i-1}(m_{i-1})}{f_i(m_{i-1})} \ . \tag{B.8}$$

[1] `http://www.astro.uni-bonn.de`

For a given mass m the $\Gamma_{[\mathrm{i}]}$ makes all summands zero except the one in which m lies. Only on the inner interval-boundaries do both adjoined intervals give the same contribution to the total value. The product over

$$\Delta(x) = \begin{cases} 0.5 & x = 0 \\ 1 & x \neq 0 \end{cases} \tag{B.9}$$

halves the value due to this double counting at the interval-boundaries. In the case of n equals one (one single power law), the empty product has, by convention, the value of unity.

An arbitrary integral over the IMF is evaluated by

$$\int_a^b \xi(m)\,\mathrm{d}m = \int_{m_0}^b \xi(m)\,\mathrm{d}m - \int_{m_0}^a \xi(m)\,\mathrm{d}m\ , \tag{B.10}$$

where the primitive of the IMF is given by

$$\begin{aligned} \int_{m_0}^a \xi(m)\,\mathrm{d}m = {} & k \sum_{\mathrm{i}=1}^{\mathrm{n}} \Theta_{]\,[}(a - m_{\mathrm{i}})\ \Psi_{\mathrm{i}} \int_{m_{\mathrm{i}-1}}^{m_{\mathrm{i}}} f_{\mathrm{i}}(m)\,\mathrm{d}m \\ & + k \sum_{\mathrm{i}=1}^{\mathrm{n}} \Gamma_{[\mathrm{i}]}(a)\ \Psi_{\mathrm{i}} \int_{m_{\mathrm{i}-1}}^{a} f_{\mathrm{i}}(m)\,\mathrm{d}m\ . \end{aligned} \tag{B.11}$$

The expressions for the mass content, i.e. $m\,\xi(m)$, and its primitive are easily obtained by multiplying the above expressions in the integrals by m.

B.2 The individual cluster IMF

B.2.1 Normalising the IMF

The IMF denotes the number of stars per mass interval. Therefore the normalisation depends on the cluster mass. Here we follow the normalisation strategy by Weidner & Kroupa (2004). This method requires two further masses. $m_{\mathrm{max}*}$ is the maximum physically possible stellar mass and m_{max} is the expected maximum stellar mass in a given cluster of mass M_{cl}. With $\xi = k\ \xi_k(m)$ two equations defining $m_{\mathrm{max}*}$ and m_{max} result:

$$M_{\mathrm{cl}} = k \int_{m_0}^{m_{\mathrm{max}}} m\ \xi_k(m)\,\mathrm{d}m, \tag{B.12}$$

$$1 = k \int_{m_{\mathrm{max}}}^{m_{\mathrm{max}*}} \xi_k(m)\,\mathrm{d}m. \tag{B.13}$$

To solve these two equations for k and $m_{\max}$ they can be divided by each other leading to an expression for the cluster mass as a function of $m_{\max}$

$$M_{\rm cl} = \int_{m_0}^{m_{\max}} m\ \xi_k(m)\ {\rm d}m / \int_{m_{\max}}^{m_{\max *}} \xi_k(m)\ {\rm d}m. \tag{B.14}$$

As a function of $m_{\max}$ it is continuous and strictly monotonically increasing and its image is $\mathcal{R}_{\geq 0}$. Therefore the existence of a solution $m_{\max}$ is concluded by a connectivity argument and the uniqueness follows from the strict monotony. This solution can be gained using any equation-solving method.

Above $m_{\max}$ no stars can be found and the IMF in a star cluster can be expressed by

$$\xi_{\rm cl}(m) = \Theta_{[\ ]}(m_{\max} - m)\ \xi(m)\ . \tag{B.15}$$

B.2.2 Dicing stars – the mass-generating function

When doing research on the IMF using Monte Carlo simulations or in setting-up star clusters for N-body simulations a finite set of random masses distributed according to the IMF have to be diced. A random number X is drawn from a constant distribution and then transformed into a mass m. The mass segments transformed into the X-space are fixed by the array $\lambda_0,\ldots,\lambda_n$ defined by

$$\lambda_i = \int_{m_0}^{m_{\rm i}} \xi_{\rm cl}(m)\ {\rm d}m. \tag{B.16}$$

If $P(X)$ denotes a constant distribution between 0 and $\lambda_{\rm n}$, both functions are related by

$$\int_{m_0}^{m(X)} \xi_{\rm cl}(m')\ {\rm d}m' = \int_0^X P(X')\ {\rm d}X' = X \tag{B.17}$$

for a uniform distribution $P(X)$. The solution of this equation for m is given by

$$m = \sum_{\rm i=1}^{\rm n} {}_{\lambda}\Gamma_{\rm [i]} F_{\rm i}^{-1} \left(\frac{X - \lambda_{i-1}}{k\ \Psi_{\rm i}} + F_{\rm i}(m_{\rm i-1}) \right) \cdot \prod_{\rm j=1}^{\rm n-1} \Delta(X - \lambda_{\rm i}) \tag{B.18}$$

where $F_{\rm i}$ is the primitive of $f_{\rm i}$, $F_{\rm i}^{-1}$ is the primitive's inverse mapping and ${}_{\lambda}\Gamma_{\rm i}$ are mappings which are unity between $\lambda_{\rm i-1}$ and $\lambda_{\rm i}$ and zero otherwise.

Appendix C

Finding the number of expected OB-stars in the ONC

Pflamm-Altenburg, J., Kroupa, P., 2006, **MNRAS**, 373, 295 (Chapter 2)

The observed total stellar mass of the ONC may be less than the initial one if OB-stars have been ejected. The total stellar mass $M_{\rm cl}$ is related to the IMF by

$$M_{\rm cl} = M_{<5} + \int_5^{m_{\rm max}} m\ \xi(m)\ {\rm d}m, \tag{C.1}$$

where $M_{<5}$ is the observed mass in stars less massive than 5 $M_\odot$. For a total mass for the ONC of 1800 - 3300 $M_\odot$ the expected maximum mass $m_{\rm max}$ lies in the range 50 - 63 $M_\odot$ (Weidner & Kroupa, 2006). If 5 $M_\odot < m_{\rm max}$, which is the case, the IMF can be normalised directly by

$$M_{<5} = k\ \int_{m_0}^{5} m\ \xi_k(m)\ {\rm d}m, \tag{C.2}$$

where $m_0 = 0.01\ M_\odot$ is the opacity-limited minimum fragmentation mass. The maximum stellar mass is then determined in the second step solving

$$1 = \int_{m_{\rm max}}^{m_{\rm max*}} \xi(m)\ {\rm d}m, \tag{C.3}$$

which means there exists one most massive star in the cluster (Weidner & Kroupa, 2004). The expected number of OB stars is then given by

$$N_{\rm OB} = \int_5^{m_{\rm max}} \xi_{\rm cl}\ {\rm d}m. \tag{C.4}$$

Appendix D

LIBIMF[1]

Pflamm-Altenburg, J., Kroupa, P., 2006, **MNRAS**, 373, 295 (Chapter 2)

This appendix presents the manual page of the LIBIMF C-library for discretising and working with the IMF of App. B.

IMF(3) IMF(3)

NAME

imf - Programming functions for the initial stellar mass function (IMF)

SYNOPSIS

All functions of the imf library are preceded by 'imf_ 'and all functions referring to a certain cluster are followed by the suffix '_cl'.

General:

#include <imf.h>

IMF imf;

Fixed-implemented general IMFs:

int imf_init_kroupa_2001(IMF *imf);

int imf_init_weidner_kroupa_2004(IMF *imf);

int imf_init_ktg_1993(IMF *imf);

int imf_init_salpeter_1955(IMF *imf);

int imf_init_chabrier_2003(IMF *imf);

[1]The IMF-library LIBIMF is freely available via the Downloads page at the AIfA: http://www.astro.uni-bonn.de/~webaiub/german/downloads.php

int imf_init_miller_scalo_1979(IMF *imf);

int imf_init_kennicutt_1983(IMF *imf);

Creating user defined general IMFs:

int imf_init_multi_power(IMF *imf, int n, double *m, double *x);

int imf_init_user(IMF *imf, char *imf_string);

int imf_shift_left(IMF *imf, double left);

int imf_shift_right(IMF *imf, double right);

Getting values and integrals of an initialized general IMF:

double imf_xi(IMF *imf, double m);

double imf_mxi(IMF *imf, double m);

double imf_int_xi(IMF *imf, double left, double right);

double imf_int_mxi(IMF * imf, double left, double right);

Normalize an IMF for an individual cluster:

int imf_norm_cl(IMF *imf, double m_cl, double m_phy_max);

int imf_norm_wk04_cl(IMF *imf, double m_cl, double m_phy_max);

Getting values and integrals of a normalized IMF for an individual cluster:

double imf_xi_cl(IMF *imf, double m);

double imf_mxi_cl(IMF *imf, double m);

double imf_int_xi_cl(IMF *imf, double left, double right);

double imf_int_mxi_cl(IMF *imf, double left, double right);

Dicing stars with respect to a normalized IMF for an individual clus- ter:

double imf_dice_star_cl(IMF *imf, double x);

Included segment functions

double imf_power(double m, double *a);

double imf_prim_power(double m, double *a);

double imf_inv_prim_power(double x, double *a);

double imf_log_normal(double m, double *a);

double imf_prim_log_normal(double m, double *a);

double imf_inv_prim_log_normal(double x, double *a);

double imf_mlog_normal(double m, double *a);

double imf_prim_mlog_normal(double m, double *a);

link with -limf

DESCRIPTION

struct IMF is the basic data element of all IMF-functions. It contains at least the following members:

```
unsigned short n;                /* number of segments */
double m_max_physical;           /* maximum physical stellar mass */
double m_cl;                     /* total cluster mass */
double m_max;                    /* expected maximum stellar mass
                                    for a given cluster mass*/
double k;                        /* normalization constant */
double *m;                       /* mass array defining the segment
                                    boundaries */
double *psi;                     /* coefficients array to ensure continuity
                                    on the segment boundaries */
double *lamda;
double (**f)(double,double *);
double (**a_f);
double (**mf)(double,double *);
double (**a_mf);
double (**F)(double,double *);
double (**a_F);
double (**mF)(double,double *);
double (**a_mF);
double (**invF)(double,double *);
double (**a_invF);
```

n indicates the number of segments. The masses run from m_0 to m_n. The IMF is zero outside the entire interval from m_0 to m_n. To choose an infinite mass use the macro IMF_MASSINF which is the maximum value for the data type double.

IMF_MASSINF is a macro to express an infinite stellar mass. IMF_MASSINF is the maximum value for the data type double and set by the DBL_MAX macro from float.h.

IMF

The IMF is an abbreviation of the initial mass function. It has been introduced by Salpeter (1955). The IMF describes the number of stars per mass interval. There exist two different but corresponding definitions. The original by Salpeter (1955):

xi(log10 m) := dN / dlog10 m

and the non-logarithmic form (Scalo, 1986)

xi(m) := dN / dm

where the mass unit is always M_sol. These two definitions correspond by

xi(log10 m) = m * ln(10) * xi(m)

These correspondence is trivial but one has to be careful with the explicit values of power-slopes. Throughout the whole library and this manpage the non-logarithmic definition is used:

xi(m) := dN / dm

Currently two types of functions are used to describe the IMF piece-wisely: a power-law and a log-normal form. The specified parameters of the fixed-implemented IMFs (see section FIXED IMFs) refer to the following definitions of the segment functions:

power-law

The power-law has the advantage that it transforms into a straight line in a double-logarithmic plot and it therefore can be fitted to data easily. It has the general form:

xi(m) ~ m^x

log-normal The log-normal form is a parabola in the log-log plot and has the transformed form:

xi(m) ~ m^(-1) * exp(- (log10(m) - log10(m_c)) / (2*sigma^2))

IMF-ALGORITHM These library functions are based on a general description of the IMF handling an arbitrary number of segments. See Pflamm-Altenburg & Kroupa (2006) for further information.

FIXED IMFs

The libimf contains some fixed-implemented IMFs frequently used in astrophysical science. These fixed IMFs refer to certain publications in which the IMF is described on a certain mass range. Outside these original mass range the IMF in these functions is set zero. E.g. the original Salpeter IMF has a power-slope of -1.35 in the logarithmic description on the mass range from -0.4 <= log10 (m/M_sol) <= +1.0, which means a slope of -2.35 in the non-logarithmic description on the mass range 0.40 <= m / M_sol <= 10.0. To apply these IMF tn different star clusters with a wider mass range many authors extrapolate the narrow Salpeter IMF to lower and larger mass limits. To do this an IMF struture has to be initialized first. Then the mass limits must be shifted using the functions imf_shift_left() and imf_shift_right(). See section EXAMPLES. As some authors have defined different IMFs the name of the fixed-implemented IMF functions contains the year of the publication. For reference see the section REFERENCE. The following definitions have not the original form but they are transformed into the non-logarithmic description (see section IMF):

imf_init_salpeter_1955() inits a one-segment power-law IMF:

x = -2.35 ; 0.40 <= m/M_sol <= 10.0

imf_init_kroupa_2001() inits a four-segment-power-law IMF described in Kroupa (2001, MNRAS).

x_1 = -0.30 ; 0.01 <= m/M_sol <= 0.08
x_2 = -1.30 ; 0.08 <= m/M_sol <= 0.50
x_3 = -2.30 ; 0.50 <= m/M_sol <= 1.00
x_4 = -2.30 ; 1.00 <= m/M_sol < +infinite

imf_init_weidner_kroupa_2004() inits a four-segment-power-law IMF described in Weidner & Kroupa (2004, MNRAS).

x_1 = -0.30 ; 0.01 <= m/M_sol <= 0.08
x_2 = -1.30 ; 0.08 <= m/M_sol <= 0.50
x_3 = -2.30 ; 0.50 <= m/M_sol <= 1.00
x_4 = -2.35 ; 1.00 <= m/M_sol < +infinite

imf_init_miller_scalo_1979() inits a three-segment-power-law IMF described in Miller & Scalo (1979, ApJS).

x_1 = -1.40 ; 0.10 <= m/M_sol <= 1.00
x_2 = -2.50 ; 1.00 <= m/M_sol <= 10.00
x_3 = -3.30 ; 10.00 <= m/M_sol < +infinite

imf_init_chabrier_2003() inits a two-segment IMF described by Chabrier (2003). The first segment is described by a log-normal form:

m_c = 0.079 & sigma = 0.69 ; 0.01 <= m/M_sol <= 1.0

The second segment is described by a power-law:

x = -2.30 ; 1.0 <= m/M_sol < +infinite

imf_init_ktg_1993() inits a three-segment-power-law IMF described in Kroupa, Tout & Gilmore (1993, MNRAS).

x_1 = -1.30 ; 0.08 <= m/M_sol <= 0.50
x_2 = -2.20 ; 0.50 <= m/M_sol <= 1.00
x_3 = -2.70 ; 1.00 <= m/M_sol < +infinite

NORMALIZATION

To apply the IMF to a true star cluster, the general IMF has to be normalized with respect to the total stellar mass of the cluster, m_cluster. This library currently supports two different normalization methods. They are using the parameter m_max_physical, which is the maximum physical upper stellar mass limit. This upper limit is expected to be approximately 150 M_sol (Weidner & Kroupa, 2004; Figer, 2005).

imf_norm_cl(): The normalization constant k of the IMF is chosen so that the mass integral over the IMF ranging from m[0] to m_max, where m_max is the minimum of m[n], m_max_physical and m_cluster, is m_cluster:

m_cluster = int_m[0]^m_max m * xi(m) dm

imf_norm_wk04(): This normalization introduces a new parameter m_max, the maximum stellar mass in a cluster with the mass m_cluster (Weidner & Kroupa, 2004). The two unknown variables, the normalization constant k and the maximum stellar mass m_max, are defined by two equations. The mass integral from m[0] to m_max gives the total cluster mass m_cluster and the IMF integral from m_max to m_max_physical gives one star. m_max_physical is the minimum of m_max_physical and m_cluster:

m_cluster = int_m[0]^m_max m * xi(m) dm

1 = int_m_max^m_max_physical xi(m) dm

DICING STARS

Stars can be drawn randomly from an IMF with the function **imf_dice_star_cl()**. It requires a random number x, drawn from a uniform distribution between 0 and 1. It returns a random mass obtained from an IMF specified by imf. The required transformations of the distribution functions is described in Pflamm-Altenburg & Kroupa (2006).

SEGMENT FUNCTIONS

The structure "struct IMF" contains pointers to function arrays storing the used functions on each segment: f, the IMF segment function, mf, the IMF mass-segment function, F, the primitive of the IMF segment function, mF, the primitive of the IMF mass segment function and inv_F, the inverse of the primitive of the IMF segment function. To allow the usage of parametrized functions all segment functions are of the form:

double f(double x, double *a);

EXAMPLES

1. Calculate the number of stars heavier than 10 M_sol in a star cluster with 2200

M_sol using a Kroupa IMF. The maximum physical stellar mass is 150 and the IMF should be normalized classically:

```
IMF imf;
double n_stars;
imf_init_kroupa_2001(&imf);
imf_norm_cl(&imf,2200,150);
n_stars = imf_int_xi_cl(&imf,10,IMF_MASSINF);
```

2. Create a new power-law IMF with 3 segments: from 0.6 to 1.2, from 1.2 to 8.5, and from 8.5 to 10.3 having the slopes -1.4, -2.6, and -3.4:

```
IMF imf;
double m[4] = 0.6,1.2,8.5,10.3;
double a[3] = -1.4,-2.6,-3.4;
imf_init_multi_power(&imf,3,m,a);
```

3. Create a mixed IMF with a log-normal form from 0.015 to 1.23 M_sol with m_c = 0.055 and sigma = 0.721 and a power-law from 1.23 to 75.3 M_sol with x = -2.64 and a power-law above 75.3 M_sol with x = -3.55.

```
IMF imf;
imf_init_manual(&imf,
   "0.015(log-norm:0.055:0.721)1.23(pow:-2.64)75.3(pow:-3.55)inf");
```

4. Dice 10000 stars from a Kroupa-IMF, normalized classically for a 5000 M_sol star cluster with a upper stellar mass limit of 150:

```
IMF imf;
int i;
double x;
double m[10000];
imf_init_kroupa_2001(&imf);
imf_norm_cl(&imf,5000,150);
for(i=0;i<10000;i++){
   x = rand()/(1.+RAND_MAX);
   m[i] = imf_dice_star_cl(&imf,x);
}
```

AUTHOR

Jan Pflamm-Altenburg at the Sternwarte of Bonn University.

COPYRIGHT

BUGS

Report any bugs, mistakes, ... to <jpflamm@astro.uni-bonn.de>

REFERENCES

Chabrier, G., 2003, ApJ, 586, 133L – The Galactic Disk Mass Function: Reconciliation of the Hubble Space Telescope and Nearby Determinations

Chabrier, G., 2003, PASP, 115, 763 – Galactic Stellar and Substellar Initial Mass Function

Figer, D. F., 2005, Nature, 434, 192 – An upper limit to the masses of stars

Kennicutt, R. C., Jr., 1983, ApJ, 272, 54 – The rate of star formation in normal disk galaxies

Kroupa, P., 2001, MNRAS, 322, 231 – On the variation of the initial mass function

Miller, G. E., Scalo, J. M., 1979, ApJS, 41, 513 – The initial mass function and stellar birthrate in the solar neighborhood

Pflamm-Altenburg, J., Kroupa, P., 2006, MNRAS, 373, 295 – A highly abnormal massive-star mass function in the Orion Nebula cluster and the dynamical decay of trapezia systems

Salpeter, E. E., 1955, ApJ, 121, 161 – The Luminosity Function and Stellar Evolution

Scalo, J. M., 1986, FCPh, 11, 1 – The stellar initial mass function

Weidner, C., Kroupa, P., 2004, MNRAS, 348, 187 - Evidence for a fundamental stellar upper mass limit from clustered star formation

SEE ALSO

MakeCluster(1)